

10-4-2007

The Characterization of tRNA Modifying Enzymes S-adenosylmethionine : tRNA Ribosyltransferase-isomerase (QueA) and a novel Type I GTP cyclohydrolase

Shilah Amal Bonnett
Portland State University

Follow this and additional works at: https://pdxscholar.library.pdx.edu/open_access_etds

 Part of the [Chemistry Commons](#)

Let us know how access to this document benefits you.

Recommended Citation

Bonnett, Shilah Amal, "The Characterization of tRNA Modifying Enzymes S-adenosylmethionine : tRNA Ribosyltransferase-isomerase (QueA) and a novel Type I GTP cyclohydrolase" (2007). *Dissertations and Theses*. Paper 6180.

This Dissertation is brought to you for free and open access. It has been accepted for inclusion in Dissertations and Theses by an authorized administrator of PDXScholar. Please contact us if we can make this document more accessible: pdxscholar@pdx.edu.

THE CHARACTERIZATION OF tRNA MODIFYING ENZYMES S-
ADENOSYLMETHIONINE:tRNA RIBOSYLTRANSFERASE-ISOMERASE
(QUEA) AND A NOVEL TYPE I GTP CYCLOHYDROLASE

by

SHILAH AMAL BONNETT

A dissertation submitted in partial fulfillment of the
requirements for the degree of


DOCTOR OF PHILOSOPHY
in
CHEMISTRY

Portland State University
2007

DISSERTATION APPROVAL

The abstract and dissertation of Shilah Amal Bonnett for the Doctor of Philosophy in Chemistry were presented October 4, 2007, and accepted by the dissertation committee and the doctoral program.

COMMITTEE APPROVALS:


Dirk Kwata-Reuyl, Chair



Niles Lehman


Scott Reed


Michael Bartlett


Kenneth Stedman
Representative of the Office of Graduate Studies

DOCTORAL PROGRAM APPROVAL:


Kevin Reynolds, Director
Chemistry Ph.D. Program

ABSTRACT

An abstract of the dissertation of Shilah Amal Bonnett for the Doctor of Philosophy in Chemistry presented October 4, 2007.

Title: The Characterization of tRNA Modifying Enzymes S-Adenosylmethionine:tRNA Ribosyltransferase-Isomerase (QueA) and A Novel Type I GTP Cyclohydrolase

Queuosine is a hypermodified nucleoside located in the wobble position of bacterial and eukaryotic tRNAs coding for Asp, Tyr, His and Asn. The biosynthesis involves the participation of S-adenosyl-methionine:tRNA ribosyltransferase-isomerase (QueA) and a GTP cyclohydrolase-I. QueA catalyzes the transfer and isomerization of the ribosyl moiety from AdoMet to preQ₁ modified tRNA. Substrate analogs of AdoMet were used to elucidate important substrate-enzyme interactions and to test key steps in the proposed chemical mechanism. Replacing AdoMet with SeAdoMet had little effect upon substrate binding but exhibited 30-fold reduction in k_{cat} , consistent with deprotonation at C-5' as the first catalytic step. 7-deazaAdoMet failed to function as a substrate of QueA, but exhibited a K_i that was only slightly higher than the K_m for AdoMet, suggesting that N-7 is critical for catalysis but not substrate binding. Neither the 2'- or 3'-deoxyAdoMet exhibited activity with QueA, however both analogs had a K_i of only 2-fold higher than the K_m of AdoMet.

Reported here is the identification and characterization of the COG1469 protein family as a novel Type-I GTP cyclohydrolase (GCYH) that catalyzes the conversion of GTP to 7,8-dihydroneopterin-triphosphate in ~20% of bacteria and most archaea. The COG1469 proteins and the genes that encode them were renamed GCYH-IB and *folE-2*, respectively, whereas the canonical cyclohydrolase, was renamed GCYH-IA. *B. subtilis* and *N. gonorrhoeae* GCYH-IB are homotrimers that were maximally active in the presence of manganese. GDP also functioned as a substrate; however the removal of the γ -phosphate resulted in a ~30-fold decrease in k_{cat}/K_m . Inhibition analysis with *N. gonorrhoeae* GCYH-IB demonstrated that 8-oxoGTP functioned as a potent inhibitor with a K_i 45-fold lower than the K_m for GTP. Although the 7-deazaGTP did not function as a substrate for GCYH-IB, it exhibited a K_i 7-fold higher than the K_m for GTP. The K_i for 2'-deoxyGTP was 24-fold higher than the K_m of GTP. H245 of *N. gonorrhoeae* GCYH-IB was believed to function analogous to that of H179 of *E. coli* FolE which facilitates the elimination of C-8 from GTP. However, H245 mutants were still able to catalyze the elimination of C-8, suggesting that H245 is not involved in the deformylation of GTP.

Dedication

This work is dedicated to Professor Dirk Iwata-Reuyl to whom I am grateful for giving me the opportunity to work in his research group and for his ongoing support of my development as a research biochemist. I would also like to dedicate this work to my partner, Deb Kovarik, family and friends who have supported me in my pursuit towards a degree in chemistry.

Acknowledgements

Professor Niles Lehman for advice and guidance.

Professor Scott Reed for his generosity in allowing me to utilize his fluorometer.

Dr. Manal Swairjo for protein crystallography analysis and her insightful discussions concerning the research project.

Dr. Debra Decker for DNA sequencing of plasmid constructs.

Dr. Robert Perkins for taking the time to help me in the ICP-MS analysis.

Dr. Andrea DeBarber and Jenny Luo at the OHSU BSR/PKCore facility in their participation in the LC-MS analysis of the reaction products.

Dr. Todd Link and Dr. Steven Van Lanen for advice and guidance concerning the research projects.

Table of Contents

Acknowledgements.....	ii
List of Tables.....	iv
List of Figures.....	v
List of Abbreviations.....	ix
Introduction.....	1
Experimental Procedures.....	15
Results.....	60
Discussion.....	82
References.....	184
Appendix A. Plasmids and proteins.....	194
Appendix B. Primer sequence.....	195
Appendix C. Buffer designation and components.....	196

List of Tables

Table 1. Michealis and inhibition constants for QueA.....	103
Table 2. Effect of metals upon <i>N. gonorrhoeae</i> COG1469 activity.....	104
Table 3. Effect of metals upon <i>B. subtilis</i> COG1469 activity.....	105
Table 4. COG1469 activity prior to excess metal removal.....	106
Table 5. ICP-MS results for COG1469 metal content.....	107
Table 6. Effect of DTT upon COG1469 activity	108
Table 7. Michealis constants for COG1469	109
Table 8. Inhibition constants and patterns for COG1469.....	110
Table 9. Radiochemical analysis of <i>N. gonorrhoeae</i> H245 mutant.....	111
Table 10. UV-vis analysis of <i>N. gonorrhoeae</i> mutants.....	112
Table 11. Type I fluorescence analysis of <i>N. gonorrhoeae</i> H245 mutants.....	113
Table 12. Type II/III fluorescence analysis of <i>N. gonorrhoeae</i> H245 mutants....	114
Table 13. Phylogenetic distribution of <i>folE</i> and <i>folE2</i>	115

List of Figures

Figure 1. Structures of archaeosine and queuosine.....	116
Figure 2. Biosynthetic pathway of archaeosine and queuosine	117
Figure 3. Reaction catalyzed by QueA.....	118
Figure 4. Proposed kinetic mechanism of QueA.....	119
Figure 5. Proposed chemical mechanism of QueA.....	120
Figure 6. Reactions catalyzed by type I, II and III GTP cyclohydrolases.....	121
Figure 7. Biosynthetic pathway of BH ₄	122
Figure 8. Reactions catalyzed by YgcM.....	123
Figure 9. Proposed chemical mechanism for GCYH-I.....	124
Figure 10. Reaction catalyzed by GCYH-I and metabolic Fate of H ₂ NTP.....	125
Figure 11. Physical clustering of folate and queuosine biosynthetic genes.....	126
Figure 12. Physical clustering of COG1469.....	127
Figure 13. Chemical structures of AdoMet and AdoMet analogs.....	128
Figure 14. Structures of COG1469 inhibitors.....	129
Figure 15. Purification of tRNA on BND-cellulose.....	130
Figure 16. Purification of tRNA on NACS Column.....	131
Figure 17. Enzymatic synthesis of ATP.....	132
Figure 18. SDS-PAGE gel of APRTase, PRPP synthetase, EcMAT and MjMAT.	133
Figure 19. HPLC purification of ATP.....	134
Figure 20. MAT catalyzed reaction.....	135
Figure 21. HPLC purification of AdoMet and SeAdoMet.....	136

Figure 22. HPLC purification of 3'dAdoMet and 7-deazaAdoMet.....	137
Figure 23. HPLC purification of 2'dAdoMet.....	138
Figure 24. SDS-PAGE gel of purified QueA His ₆ -tag.....	139
Figure 25. SDS-PAGE gel of purified QueA-GST.....	140
Figure 26. Dowex analysis.....	141
Figure 27. QueA activity with SeAdoMet.....	142
Figure 28. Substrate kinetic plot of QueA with SeAdoMet.....	143
Figure 29. QueA inhibition with substrate analogs.....	144
Figure 30. Time dependent inhibition of QueA with SeAdoMet.....	145
Figure 31. Enzymatic synthesis of GTP.....	146
Figure 32. SDS-PAGE gel of HGPRase purification.....	147
Figure 33. HPLC purification of GTP.....	148
Figure 34. SDS-PAGE gel of COG1469 proteins.....	149
Figure 35. Radiochemical GCYH-I and II activity assay.....	150
Figure 36. UV-vis GCYH-I activity assay.....	151
Figure 37. Oxidation of H ₂ NTP to neopterin triphosphate.....	152
Figure 38. Fluorescence GCYH-I activity assay.....	153
Figure 39. HPLC GCYH-I activity assay.....	154
Figure 40. HPLC analysis of COG1469 products.....	155
Figure 41. Temperature dependence of COG1469.....	156
Figure 42. COG1469 pH profile.....	157
Figure 43. Effect of buffers upon COG1469 activity.....	158

Figure 44. Effect of buffer strength upon COG1469 activity.....	159
Figure 45. COG1469 activity as a function of Mn ²⁺ and Zn ²⁺ concentration.....	160
Figure 46. Effect of Zn ²⁺ upon Mn ²⁺ stimulated COG1469 activity.....	161
Figure 47. Gel filtration standard plot.....	162
Figure 48. Molecular weight HPLC chromatograms of COG1469 proteins.....	163
Figure 49. COG1469 activity as a function of time and enzyme concentration....	164
Figure 50. Substrate kinetic plots of <i>N. gonorrhoeae</i> COG1469.....	165
Figure 51. Substrate kinetic plots of <i>B. subtilis</i> COG1469.....	166
Figure 52. COG1469 inhibition with substrate analogs.....	167
Figure 53. SDS-PAGE gel of purified COG1469 His 245 mutant proteins.....	168
Figure 54. UV-vis GCYH-I activity assay of COG1469 His 245 mutants.....	169
Figure 55. Fluorescence: GCYH-I activity assay of COG1469 His 245 mutant...	170
Figure 56. Derivatization of FAPy and APy.....	171
Figure 57. Fluorescence GCYH-II/III activity assay of COG1469 His245 mutant	172
Figure 58. Alternate QueA chemical mechanism.....	173
Figure 59. Plausible QueA reactions with SeAdoMet.....	174
Figure 60. COG1469 complementation studies.....	175
Figure 61. Structure of cyclic-neopterin monophosphate.....	176
Figure 62. Primary sequence alignment of GCYH-I and COG1469.....	177
Figure 63. Primary and tertiary structural alignment of GCYH-I and GCYH-IB...	179
Figure 64. T-fold domain.....	179
Figure 65. Structures of T-fold proteins.....	180

Figure 66. Substrate binding of T-fold proteins.....	181
Figure 67. Organization of the T-fold domain in COG1469 proteins.....	182
Figure 68. Keto-Enol tautomerization of 8-oxoGTP.....	183

List of Abbreviations

A	Adenosine
AdoMet	SAM, S-adenosyl-L-methionine
AnRNR	Anaerobic class III ribonucleotide reductase
APRTase	Adenine phosphoribosyltransferase
APy	2,5-diamino-6-hydroxy-4-(5-phosphoribosylamino)pyrimidine
ArcTGT	Archaeal tRNA guanine transglycosylase
Asp	Aspartic acid
Asn	Asparagine
ATP	Adenosine 5'-triphosphate
BacTGT	Bacterial tRNA guanine transglycosylase
BH ₄	(6R)-L-erythro-5,6,7,8-tetrahydrobiopterin
BND	Benzoylated-Napthoylated Diethylaminoethyl
<i>B. subtilis</i>	<i>Bacillus subtilis</i>
C	Competitive
CFE	Cell-free extract
COG	Cluster of Orthologous Groups of proteins
COG1469	GCYH-IB
cps	counts per second, units to describe fluorescence
Cys	Cysteine
D	Aspartic Acid
2'dAdoMet	2'-deoxy- S-adenosyl-L-methionine

3'-dAdoMet	3'-deoxy- S-adenosyl-L-methionine
2'-dATP	2'-deoxy-adenosine 5'-triphosphate
3'-dATP	2'-deoxy-adenosine 5'-triphosphate
DEAE	Diethylaminoethyl cellulose
7-deazaAdoMet	7-deaza- S-Adenosyl-L-Methionine
DEPC	Diethylpyrocarbonate
DHPS	Dihydropteroate Synthase
DNA	Deoxyribonucleic Acid
DPM	Disintegration per minute; units to express radioactivity
dT	deoxythymidine
DTT	Dithiothreitol
<i>E. coli</i>	<i>Escherichia coli</i>
EcMAT	S-adenosylmethionine Synthetase from <i>E. coli</i>
EDTA	Ethylenediaminetetraacetate
FAPy	2-amino-5-formylamino-6-ribosylamino-4(3H)pyrimidione
FoIE-1	GTP cyclohydrolase IA
FoIE-2	GTP cyclohydrolase IB
G	Guanosine
G*	Archeosine, 2-amino-4,7-dihydro-4-oxo-7-β-D-ribofuranosyl- 1H-pyrrolo(2,3-d)pyrimidiine-5-carboximidamide
galQ	Galactosyl modified Q-tRNA
GCYH	GTP Cyclohydrolase

GDP	Guanosine 5'-diphosphate
Gln	Glutamine
Glu	Glutamic Acid
GMP	Guanosine 5'-monophosphate
GTP	Guanosine 5'-triphosphate
h	hour
H	Histidine
HGPRTase	Hypoxanthine-guanine phosphoribosyl transferase
His	Histidine
His ₆	hexahistidine
H ₂ NMP	7,8-dihydroneopterin monophosphate
H ₂ NTP	7,8-dihydroneopterin triphosphate
HPLC	High performance liquid chromatography
HPPK	6-Hydroxymethyl-7,8-dihydropterin pyrophosphokinase
ICP-MS	Inductively Coupled Plasma Mass Spectroscopy
IPTG	Isopropyl-β-D-thiogalactopyranoside
K	Lysine
Kan	Kanamycin
LB	Luria broth
LC-MS	Liquid Chromatography Mass Spectroscopy
<i>L. donovani</i>	<i>Leishmania donovani</i>
manQ	Mannosyl modified Q-tRNA

MAT	S-Adenosylmethionine synthetase; ATP:L-methionine S-adenosyltransferase; methionine adenosyltransferase
MES	4-morpholineethanesulfonic acid
MetK	S-adenosyl-L-methionine synthetase
min	minute
<i>M. jannaschii</i>	<i>Methanococcus jannaschii</i>
MjMAT	S-adenosylmethionine synthetase from <i>M. jannaschii</i>
mRNA	messenger ribonucleic acid
MS	Mass Spectroscopy
N	Asparagine
NADH	Nicotinamide Adenine Dinucleotide, Reduced Form
NAD ⁺	Nicotinamide Adenine Dinucleotide, Oxidized Form
NADP ⁺	Oxidized Nicotinamide Adenine Dinucleotide Phosphate
NADPH	Reduced Nicotinamide Adenine Dinucleotide Phosphate
<i>N. gonorrhoeae</i>	<i>Neisseria gonorrhoeae</i>
NMR	Nuclear Magnetic Resonance Spectroscopy
nt	Nucleotide
OD	optical density
oQ	epoxy-queuosine, 7-{5-[(2,3-epoxy-4,5-dihydroxycyclopent-1-yl)amino]methyl}-7-deazaguanosine
PAGE	Polyacrylamide Gel Electrophoresis
PCR	Polymerase Chain Reaction

PMSF	Phenylmethanesulfonyl fluoride
PreQ ₀	7-cyano-7-deazaguanine, 2-amino-5-cyanopyrrolo[2,3-d]pyrimidine-4-one
PreQ ₁	7-aminomethyl-7-deazaguanine, 2-aminomethylpyrrolo[2,3-d]pyrimidin-4-one
PRPP synthetase	phosphoribosylpyrophosphate synthetase
PTP	6-pyruvoyl tetrahydropterin
PTPS	6-pyruvoyl tetrahydropterin synthase
Q	queuosine or (glutamine with respect to amino acid mutagenesis)
QueA	S-adenosylmethionine:tRNA ribosyltransferase-isomerase
QueD	Bacterial 6-pyruvoyl tetrahydropterin synthase ortholog
QueF	NADPH:7-cyano-7-deazaguanine oxidoreductase
RibA	GTP cyclohydrolase II
RNA	Ribonucleic acid
SAM	AdoMet, S-Adenosyl-L-methionine
SDS-PAGE	Sodium Dodecyl Sulfate Polyacrylamide Gel Electrophoresis
SeAdoMet	S-Adenosyl-L-selenomethionine
sec	second
SR	Sepiapterin reductase
TCA	Trichloroacetic acid
TGT	tRNA-guanine transglycosylase

THF	Tetrahydrofolic acid
<i>T. maritima</i>	<i>Thermotoga maritima</i>
tRNA	Transfer ribonucleic acid
tRNA ^{Asn}	Asparagine-specific transfer ribonucleic acid
tRNA ^{Asp}	Aspartate-specific transfer ribonucleic acid
tRNA ^{His}	Histidine-specific transfer ribonucleic acid
tRNA ^{Tyr}	Tyrosine-specific transfer ribonucleic acid
Tubercidin	7-deazaguanosine
TubMet	S-7-deazaadenosyl-L-selenomethionine
Tyr	Tyrosine
UV-vis	Ultraviolet-visible
YgcM	<i>E. coli</i> 6-pyruvoyl tetrahydropterin synthase ortholog
YkvM	NADPH:7-cyano-7-deazaguanine oxidoreductase
YkvK	<i>B. subtilis</i> 6-pyruvoyl tetrahydropterin synthase ortholog

Introduction

Transfer RNA (tRNA)

Transfer RNA (tRNA) plays a crucial role in biology; it participates in the translation of the genetic code and functions by delivering the specified amino acid to the growing peptide chain. It is a small RNA molecule composed of 75-90 nt that has a well defined secondary (cloverleaf) and tertiary (3D L-shaped) structure. A common feature of all tRNAs are the presence of three stem-loop moieties; the D-loop which often contains a dihydrouridine; T-loop which contains a conserved T ψ C sequence (ribothymidine (T), pseudouridine (ψ), and cytosine(C)); and the anticodon stem-loop, which contains the three nucleotide sequence involved in the recognition and translation of the corresponding 3-nucleotide codon region of the mRNA.

A fascinating aspect of tRNA is the occurrence modified nucleosides which are an integral part of tRNA maturation. Modifications take place post-transcriptionally through the action of various enzymes. To date, more than a 100 distinct modified nucleosides have been characterized in RNA from all domains of life [1, 2]. tRNA contains proportionally more modified nucleosides than any other nucleic acid within the cell [3]. Approximately 1% of bacterial genomes code for enzymes involved in tRNA modification [4]. On average 10%, and in some cases up to 25%, of the nucleosides of a particular tRNA are modified [2]. While some modifications are conserved across the three domains, the occurrence, location and distribution of

modified nucleosides varies depending upon the domain, species, and specificity of the tRNA [2].

Modified nucleosides are derived from the four common nucleosides adenosine (A), guanosine (G), cytosine (C) and uridine (U). The nature of tRNA modification varies considerably, from the simple introduction of chemical substituents in the base or ribose moiety to extensive modification (hypermodification) of the canonical base resulting in the formation of a structurally complex base or nucleoside. While the former is typically mediated by a single enzyme, the latter entails radical structural changes of the base and can require multiple enzymatic steps [2].

Except for a few cases, most of the modified nucleosides found in tRNA are not well characterized with respect to the overall biosynthetic pathway and physiological function. In general, it is believed that modifications located outside the anticodon region influence the structural integrity of the tRNA, while modifications occurring within and/or around the anticodon region are thought to influence the efficiency and fidelity of translation [5, 6].

7-Deazaguanine Derivatives: Archaeosine and Queuosine

In terms of chemistry and structure, archaeosine (G*) [7] and queuosine (Q) [8] are two of the most complex hypermodified nucleosides identified in tRNA (Figure 1). While both modified nucleosides share the unusual 7-deazaguanosine core structure in

which the N-7 atom of the base is replaced with a carbon, queuosine contains an aminomethyl cyclopentendiol side chain at position 7, whereas archaeosine contains a formamidino side chain. Archaeosine is present exclusively in archaeal tRNAs containing a genetically encoded G at position 15 of the D-loop, a site not modified in any other tRNA outside this domain (Figure 1) [9]. While the exact physiological role of archaeosine is unclear, its location at the critical D-loop and T-stem interface suggests a role in maintaining the structural integrity of the tRNA molecule.

Queuosine and its derivatives, in contrast, are found exclusively in bacteria and eukaryotes, with the exception of yeast (*Saccharomyces cerevisiae*) and *Mycoplasma*, at position 34 (the wobble position) in the anticodon of tRNAs coding for asparagine, aspartic acid, histidine and tyrosine (Figure 1) [10, 11]. The physiological role of queuosine has yet to emerge, but it is known to have an influence on translational frameshift events essential for retroviral protein synthesis [12-14], the ability of pathogenic bacteria to invade and proliferate in human tissue [15], tyrosine biosynthesis in mammals [16], eukaryotic cell proliferation and development [17, 18], neoplastic transformation [19-21], hypoxic stress management [22], and signal transduction pathways [19, 23-26] and most importantly the modulation of translational fidelity which is consistent with its location in the anticodon (codon-anticodon interaction) [5].

Biosynthesis of Archaeosine and Queuosine

The *de novo* biosynthesis of archaeosine and queuosine by archaea and bacteria, respectively, is only partially understood (Figure 2). While the biosynthetic pathway has primarily been studied with respect to queuosine, given the fact that both archaeosine and queuosine share an unusual 7-deazaguanosine core structure, the presence of *ykvJKL* homologs in both domains, and the structural similarity of the preQ₀ (7-cyano-7-deazaguanine) intermediate to archaeosine, the steps leading up to preQ₀ are identical in both pathways. Early studies had shown that GTP was the metabolic precursor to queuosine which is converted to the precursor preQ₀ through a number of enzymes [27], three of which have been recently identified, YkvJKL (QueCDE) [28]. While the fate of N-7 has yet to be determined, the transformation involves the loss of C-8 from guanine suggesting GTP cyclohydrolase like chemistry [27]. In archaea, preQ₀ is directly incorporated into the appropriate tRNA replacing the genetically encoded guanine in a reaction catalyzed by the enzyme tRNA guanine transglycosylase (ArcTGT; EC 2.4.2.29) [29, 30]. Once incorporated, preQ₀ is further modified with the addition of ammonia to the nitrile group of preQ₀ to give archaeosine, a step catalyzed by an unidentified enzyme. In bacteria, preQ₀ is reduced to preQ₁ (7-aminomethyl-7-deazaguanine) in an NADPH dependent reaction catalyzed by YkvM (QueF, NADPH:7-cyano-7-deazaguanine oxidoreductase) and subsequently inserted into the wobble position of the appropriate tRNA by a bacterial TGT (BacTGT; EC 2.4.2.29) [31]. Once incorporated, preQ₁ is further modified to oQ (epoxyqueuosine-tRNA) in an S-adenosylmethionine (AdoMet, SAM) dependent step

catalyzed by the enzyme S-adenosylmethionine:tRNA ribosyltransferase-isomerase (QueA) [32, 33]. Finally, oQ is reduced to Q-tRNA (queuosine-tRNA) by an unidentified enzyme [34].

Unlike bacteria, eukaryotes lack the ability to synthesize queuosine *de novo*. Instead, eukaryotes obtain free queuine base from the diet and intestinal flora [35]. Once acquired the queuine base is directly inserted into the appropriate tRNA in a transglycosylation reaction catalyzed by eukaryotic tRNA-guanine transglycosylase (TGT) [36]. In some mammalian queuosine containing tRNAs, queuosine can be further modified in a tRNA-queuine glycosyltransferase catalyzed glycosylation reaction between D-mannose or D-galactose with the C-5' hydroxyl group of the cyclopentendiol moiety to generate manQ and galQ, respectively (Figure 1). ManQ is present in tRNAs coding for aspartic acid, whereas galQ is found in tyrosyl specific tRNA [37]. Recently, a truncated glutamyl-tRNA synthetase (mini-GluRS; YadB) was discovered in bacteria to activate and attach a glutamate residue onto the queuine base of tRNA coding for aspartic acid [38].

QueA

QueA catalyzes the penultimate step in the biosynthesis of queuosine; the unprecedented transfer and isomerization of the ribosyl moiety from AdoMet to preQ₁-tRNA to give epoxyqueuosine modified tRNA (oQ-tRNA) (Figure 3). The reaction is accompanied by the rearrangement of the ribosyl moiety and the

elimination of methionine and adenine from AdoMet [32, 33]. An unusual feature of the QueA catalyzed reaction is the nature of the ribosyl donor [32, 33]. AdoMet is a known essential metabolite in many biological systems and functions as a methyl donor in various methylation reactions involving DNA, RNA, lipids, proteins, and various small molecules [39]; as well as a precursor of the aminopropyl group in polyamines and as a precursor of glutathione (GSH) in trans-sulfuration reactions [40]. AdoMet is also involved in the formation of substrate or protein radicals in the newly identified Radical SAM class of enzymes [41, 42].

Recent kinetic analysis has reported that QueA follows an ordered sequential bi-ter mechanism in which preQ₁-tRNA binds to the enzyme followed by AdoMet forming a ternary complex. The formation of the ternary complex is followed by reaction and the release of products in the following order: adenine, methionine and oQ-tRNA (Figure 4) [43]. A chemical mechanism has been proposed for the reaction catalyzed by QueA and is consistent with the kinetic mechanism and biochemical studies carried out to date (Figure 5) [44]. The first step of the proposed chemical mechanism involves the deprotonation of AdoMet at C-5' to give the sulfonium ylide **I**. The subsequent opening of the ribose ring and the subsequent elimination of adenine generates the vinyl sulfonium **II**. Nucleophilic attack of the preQ₁ methylamine at C-4' generates the sulfonium ylide **III** which subsequently attacks the C-1' aldehyde to give the alkoxy-carbocycle **IV**. Intramolecular S_N2 attack of the alkoxy oxygen on the

adjacent carbon results in the formation of oQ-tRNA and the elimination of methionine.

GTP Cyclohydrolase

Early biochemical studies suggests the involvement of a GTP cyclohydrolase like enzyme in the first step of the queuosine biosynthetic pathway [11, 27]. The basis of this conjecture stems from early labeling experiments in which *Salmonella typhimurium* was administered [2-¹⁴C] guanine and [8-¹⁴C] guanine [11, 27]. In these studies, incorporation of the isotope was observed with [2-¹⁴C] guanine but not with [8-¹⁴C] guanine suggesting that C-8 was eliminated in the process, an observation reminiscent to the biosynthesis of pterins, folic acids, flavins [45] and antibiotics toyocamycin [46, 47] and tubercidin [48].

There are three known classes of GTP cyclohydrolase (GCYH; Figure 6), each of which catalyzes the cleavage of the C8-N9 bond of the guanine ring. GTP cyclohydrolase-III (GCYH-III) has recently been discovered in archaea, and catalyzes not only the hydrolysis of the guanine ring but the release of pyrophosphate to give the monophosphorylated N-formyl product, 2-amino-5-formylamino-6-ribosylamino-4(3H)-pyrimidinone (FAPy) (Figure 6) [49]. The physiological role of GCYH-III in archaea has yet to emerge [49]. GTP cyclohydrolase-II (GCYH-II; RibA; EC 3.5.4.25), encoded by *ribA*, catalyzes the conversion of GTP to 2,5-diamino-6-hydroxy-4-(5-phosphoribosylamino)-pyrimidine (APy), a precursor to flavins

(riboflavin and deazariboflavin) (Figure 6). Not only does it catalyze the hydrolysis of the guanine ring but the elimination of C-8 as formate followed by the release of pyrophosphate to give the monophosphorylated product [50]. GTP cyclohydrolase-I (GCYH-I; FolE; EC 3.5.4.16), encoded by *folE*, catalyzes the conversion of GTP to dihydroneopterin triphosphate (H₂NTP; 6-D-*threo*-1',2',3'-hydroxypropyl-7,8-dihydroneopterin 3'-triphosphate), a precursor to folates and pterins (Figure 6). The conversion involves the hydrolysis and removal of C-8 as formate followed by the rearrangement of the ribosyl moiety to give the pterin system [51-53]. Theoretically GCYH-I or GCYH-II could catalyze the first step in the biosynthesis of archaeosine and queuosine, however GCYH-II is an unlikely candidate because it has been demonstrated that an *E. coli* GCYH-II (*ribA*) mutant still generated queuosine modified tRNA [54]. On the other hand, a distinct cyclohydrolase-like enzyme may be responsible for the initial conversion of GTP in the biosynthesis of archaeosine and queuosine.

Until recently, *tgt* and *queA* were the only known genes involved in the biosynthesis of queuosine that had been identified, cloned and the proteins encoded by them characterized. Using comparative genomics techniques de Crécy-Lagard and co-workers (Department of Microbiology and Cell Science, University of Florida) identified four previously uncharacterized bacterial gene families, *ykvJKLM*, encoding enzymes involved in the biosynthesis of queuosine [28]. Based on its sequence homology to FolE, YkvM was initially depicted as a GTP cyclohydrolase-like enzyme

and was therefore hypothesized to catalyze the first step in the biosynthesis of queuosine. Upon biochemical analysis it was discovered that YkvM did not contain GTP cyclohydrolase activity, instead it catalyzes the NADPH dependent reduction of preQ₀ to preQ₁. These findings lead us to reexamine all sequenced genomes by comparative genomic analysis in search for an uncharacterized gene that may encode a cyclohydrolase-like enzyme and to evaluate the potential involvement of GCYH-I in the biosynthesis of queuosine.

Insight into the early steps of the queuosine pathway was provided by the fact that the YkvK homolog in *E. coli* (YgcM, QueD) was annotated as a 6-pyruvoyl tetrahydropterin synthase (PTPS), an essential enzyme that catalyzes the second step of the BH₄ pathway, the conversion of H₂NTP to PTP (Figure 7). Although glycosidic forms of BH₄ have been identified in cyanobacteria and *Chlorobium* [55-57], bipterins and derivatives thereof have no known function in bacteria and archaea. Furthermore, those organisms that contain an YkvK homolog lack a sepiapterin reductase (SR), which catalyzes the final step in the BH₄ pathway. YgcM has been reported to catalyze the conversion of H₂NTP to BH₄ in the presence of SR, suggesting the formation of PTP (Figure 8). However in absence of SR, YgcM was shown to catalyze the cleavage of the C6 side chain of H₂NTP and sepiapterin generating 7,8-dihydropterin (Figure 8). These findings not only support the early biochemical studies but suggest the involvement of GCYH-I in queuosine biosynthesis.

GCHY-I catalyzes the formation of dihydroneopterin triphosphate and formate from GTP through a mechanistically complex ring expansion reaction (Figure 9). A chemical mechanism has been proposed and is consistent with crystallography and biochemical studies, including mutagenesis, NMR analysis and transient state kinetics [52, 58-61]. The conversion of GTP to dihydroneopterin triphosphate is initiated with the reversible hydrolysis of GTP at C8-N9 via a nucleophilic attack of a zinc activated water molecule to form an N-formyl intermediate, FAPy (Figure 9, compound 4), which undergoes a 2nd hydrolysis reaction with the subsequent loss of C-8 as formate to generate APy (Figure 9, compound 6). The ribosyl moiety undergoes ring opening and an Amadori rearrangement followed by cyclization to give the pterin ring.

In most bacteria, fungi and plants GCYH-I catalyzes the first and rate limiting step in the de novo biosynthesis of tetrahydrofolate (THF) (Figure 10) [62]. Homologs of GCYH-I have been observed in higher eukaryotes including mammals and catalyzes the first and rate limiting step in the biosynthesis of tetrahydrobiopterins (BH₄; [6R]-[L-erythro-1',2'-dihydroxypropyl]-2-amino-4-hydroxy-5,6,7,8-tetrahydropteridine), a compound ubiquitous in higher animals (vertebrates and insects) (Figure 10) [62]. It has been demonstrated that a type I GTP cyclohydrolase catalyzes the first committed step in the biosynthesis of methanopterin in archaea, however, no genes have been identified in any archaeal genome to encode a GCYH-I [63].

Folates are essential cofactors involved in one carbon transfer reactions in the biosynthesis of purines, formylmethionyl-tRNA, thymidylate, panthothenate, glycine, serine and methionine in all domains of life [52]. While folate is essential for normal growth and development, animals lack the ability to synthesize THF *de novo* and must acquire folate from a dietary source [64]. Since the genes encoding enzymes involved in folate biosynthesis have not been found in mammals they constitute an attractive target for antimicrobial chemotherapy [65-67]. The biosynthesis of tetrahydrofolate involves the dephosphorylation of dihydroneopterin triphosphate, a reaction proposed to be catalyzed by specific and non-specific pyrophosphatase and phosphorylase [68]. It has been demonstrated that dihydroneopterin triphosphate can be chemically converted to the monophosphorylated species in the presence of divalent metal ions, such as Mg^{2+} or Ca^{2+} [69], however, the concentrations utilized in those studies were well above the physiological concentrations. Regardless of the underlying means in the dephosphorylation of dihydroneopterin triphosphate, the resulting product, 7,8-dihydroneopterin, is converted to THF by the enzymes encoded by *folBKPCA* in *E. coli*.

Tetrahydrobiopterin is an essential cofactor for nitric oxide synthases [70], glycerol ether monooxygenases [71] and various aromatic amino acid hydroxylases such as phenylalanine hydroxylase, tyrosine hydroxylase and tryptophan hydroxylase [52, 72-74]. Dihydroneopterin triphosphate is converted to tetrahydrobiopterin (BH_4) by the sequential action of 6-pyruvoyl tetrahydropterin synthase (PTPS; E.C. 4.6.1.10) and

sepiapterin reductase (SR; E.C. 1.1.1.153) (Figure 7) [75]. While the participation of a type I GTP cyclohydrolase in the biosynthesis of folates and pterins has been well established, its involvement in the biosynthesis of queuosine remains unclear.

To determine if the participation of GCYH-I in the biosynthesis of queuosine was a viable hypothesis a comparative genomic analysis was conducted by de Crécy-Lagard. All sequenced genomes were analyzed in which two genes of the *de novo* folate biosynthetic pathway, *folP* and *folK*, which encode dihydropteroate synthase (DHPS) and 6-hydroxymethyl-7,8-dihydropterin pyrophosphokinase (HPPK), respectively, were utilized as signature genes. Since metabolic intermediates in the conversion of H₂NTP to 7,8-dihydrohydroxymethylpterin pyrophosphate are not transported in bacteria, all organisms containing both the *folP* and *folK* genes should contain a *folE* homolog that encodes a GCHY-I [76]. Since clustering of genes of a common pathway is frequently observed in bacterial genomes, a gene clustering and distribution analysis was conducted. The analysis revealed that *folE* clustered with known queuosine biosynthesis genes in a number of organisms (Figure 11). However, *folE* was absent in a large number of bacteria genomes that contain both queuosine *ykvJKLM*, and more importantly other folate biosynthesis genes, *folBKPCA*. Based on these findings it was predicted that another unidentified protein family was responsible for conversion of GTP to H₂NTP in those organisms lacking *folE*.

Utilizing the newly developed SEED database, which allows the identification of protein families that follow a defined phylogenetic distribution profile, all sequenced genomes were searched for protein families that were present in those organisms that lacked a *folE* homolog and were absent in *E. coli*, which contains *folE*. The search resulted in the identification of five protein families that followed the defined phylogenetic criteria. Of the 5, only COG1469 was of unknown function that clustered with folate or queuosine biosynthetic genes in a number of organisms (Figure 12). Based on this analysis we proposed that COG1469 genes would encode the missing GCYH-I enzyme in those organisms lacking *folE*.

The scope of my research entails the further characterization of QueA and the biochemical analysis of COG1469 proteins. In order to gain further insight into QueA catalysis, experiments were designed to elucidate important substrate-enzyme interactions and to test key steps in the proposed chemical mechanism by utilizing the following AdoMet analogs; 2'-dAdoMet, 3'-dAdoMet, SeAdoMet, and 7-deazaAdoMet (TubMet) (Figure 13). Reported here are the results from the substrate and inhibition studies utilizing the AdoMet analogs and their mechanistic and structural implications on catalysis are discussed.

The work presented here also describes the cloning, purification, and characterization of COG1469 proteins from *T. maritima*, *N. gonorrhoeae*, and *B. subtilis*. In addition to the functional identification of the COG1469 proteins, biochemical characterization

including divalent metal analysis, steady-state kinetics, and site directed mutagenesis was conducted. Inhibition analysis with COG1469 from *N. gonorrhoeae* was also carried out with the following substrate analogs; 8-oxoGTP, 7-deazaGTP and 2'dGTP (Figure 14). Presented here are the results from these studies and their mechanistic and structural implications upon catalysis are discussed.

Experimental Procedures

Chemicals and Reagents

All reagents, salts and buffers were of the highest quality grade, and were purchased from Sigma unless otherwise noted. Millipore ultrapure water was used for all solutions. Ampicillin, DTT, kanamycin sulfate and isopropyl-1-thio-B-D-galactopyranoside (IPTG) were purchased from RPI Corporation. [U-¹⁴C]Glucose, L-[1C-¹⁴C] methionine, and [8-¹⁴C]-guanine were purchased from Moravек.

Benzoylated-naphthoylated DEAE-cellulose (BND-cellulose), DEAE-cellulose, activated charcoal, Dowex-50WX4, and Sephadex-G25 were purchased from Sigma. NACs[™] resin was from BRL Life Technologies, Inc. Chelex-100 was purchased from BioRad. Nickel agarose affinity resin (Ni-NTA) was purchased from Qiagen. Glutathione Sepharose 4B was purchased from Amersham Biosciences. POROS chromatography resins were from PerSeptive Biosystems. Whatman GF-B and Whatman P81 filter disks were purchased from Fisher. Centriprep YM-30, Centricon YM-10, Centricon YM-3, and Amicon Ultra YM-10 centrifugal devices, Amicon Ultra-MC spin filters, and HA filters were from Millipore. Dialysis was performed in Slide-A-Lyzer cassettes or mini dialysis units from Pierce. Buffers used in work involving RNA were prepared with DEPC-treated water and filtered through Cameo 25ES nitrocellulose filters from Osmonics, Inc. Anti-RNase was from Ambion. Ultra pure grade 2'-deoxyGTP, GTP, GMP and GDP were from Ameresco or Sigma. Protein concentrations were based on the Bradford dye binding procedure (Bio-Rad). Adenine, methionine, 2'-deoxyATP, 3'-deoxyATP, ATP, AMP, S-adenosyl-L-

methionine (AdoMet, SAM), neopterin, L-sepiapterin, ribose-5-phosphate, phospho(enol)pyruvate trisodium salt (PEP), NADH, NAD, NADPH, 7-deazaadenosine (Tubercidin), and 3-deazaadenosine were from Sigma. 7,8-dihydro-D-neopterin and 7,8-dihydro-L-biopterin were from Axxora. D-neopterin-3'-monophosphate and 7,8-dihydro-D-neopterin-3'-monophosphate were purchased from Schircks Laboratories. Pterin was from MP Biomedicals. 8-oxo-GTP was purchased from Jena Bioscience. 7-deazaGTP and 7-deazaATP were purchased from Trilink Biotechnologies. 6-Phosphogluconate dehydrogenase type V from torula yeast and nucleoside monophosphate kinase was purchased from MP Biologics as an ammonium sulfate suspension. L-Glutamic dehydrogenase type I from bovine liver, pyruvate kinase type II from rabbit muscle, glucose-6-phosphate dehydrogenase type VII from baker's yeast, and myokinase from rabbit muscle were from Sigma as ammonium sulfate suspensions. Phosphoriboisomerase from torula yeast and hexokinase type F-300 from baker's yeast were from Sigma as lyophilized powders and were stored in 50% glycerol and the appropriate buffer at -80°C. Proteins utilized in gel filtration analysis were from Sigma. Ultraclean™ mini plasmid and Ultraclean™ 15 DNA purification kits were from MolBio. Oligodeoxynucleotides were from Integrated DNA Technologies. Linearized vector pET-30Xa/LIC PCR cloning kit was from Novagen. DNA from *E. coli* K12 was a generous gift from Dr. David Boone, Portland State University. Genomic DNA from *B. subtilis* JH642 (trpC2 pheA1) was a generous gift from Dr. Michiko Nakano, Oregon Graduate Institute of Science and Engineering. Genomic DNA from *N. gonorrhoeae* and *T. maritima* were

from ATCC. Bromophenol blue, blue dextran 2000 and DNP-aspartic acid were from Sigma. Econosafe scintillation counting cocktail is from RPI. Protein concentrations were determined by Bradford dye-binding analysis (BioRad).

All chemicals used in metal analysis were of high purity, analytical metal-free grade. All buffers and solutions utilized in metal analysis were prepared with Milli-Q water (18.2 M Ω) and treated with Chelex-100 (BioRad) to remove any contaminating metals. Divalent metals used were a minimum of 99.9% pure and prepared with Chelex-100 treated Milli-Q water. To minimize the leaching of metals into solution all plastic and glassware were soaked in 10% nitric acid followed by 1 mM EDTA (for glassware) and rinsed liberally with Chelex-treated Milli-Q water before use. To reduce enzyme activation due to metals leaching from the quartz cuvettes, the cuvettes were soaked in 1:1 nitric acid:sulfuric acid for 15 min and rinsed extensively with Chelex-treated Milli-Q water before use.

Instrumentation

PCR was carried out using a Perkin-Elmer 2400 thermocycler. Radioactivity was quantified by liquid scintillation counting utilizing a Beckman LS6500 Liquid Scintillation Counter. UV-vis spectrophotometry was conducted with a Varian Cary 100 Bio spectrophotometer. Fluorescence spectroscopy was carried out with either a PTI Time-Master fluorometer or a Gemini XPS microplate spectrofluorometer from Molecular Devices. HPLC analysis was performed on a Hitachi Model D-7000

System equipped with a L-7100 pump system and an L-4500A diode array detector. PAGE electrophoresis was conducted utilizing a Mini Protean III apparatus from BioRad. Sequence analysis was carried out using the Vector NTI software package. Centrifugation was performed with an Avanti J-20 XP centrifuge utilizing JA-25.50 and JA-10 rotors, an LE-80K ultracentrifuge using a Ti-60 rotor, or a TJ-6 swinging bucket centrifuge all from Beckman Coulter. A Molecular Dynamics Typhoon 9200 variable mode imager with ImageQuant 5.2 software was used for the fluorescence detection of ethidium bromide or SybrGreen-stained nucleic acids in PAGE and agarose gels. Mass spectrometry was done on an LCQ Advantage ion trap mass spectrometer (Thermo Electron, San Jose, CA) equipped with an electrospray ionization source at the BioAnalytical Shared Resource/Pharmacokinetics Core Facility in the Department of Physiology and Pharmacology at Oregon Health and Science University. The metal content of the proteins were analyzed by inductively coupled plasma mass spectroscopy (ICP-MS; HP-4500 ICP-MS) performed at the Trace Element Laboratory, Department of Geology, Portland State University (Portland, OR). DNA sequencing analysis was performed on a 3100 Avant Genetic Analyzer from Applied Biosystems at the Portland State University-Keck Genomic Facility (Portland, OR).

Bacterial Strains

E. coli strain DH5 α (F⁻, Φ 80*lacZ* Δ 15, Δ (*lacZYA-argF*)U169, *deoR*, *recA1*, *endA1*, *hsdR17*(r_K⁻,m_K⁻), *phoA*, *supE44*, λ , *thi-1*, *gyrA96*, *relA1*) was from Gibco BRL Life

Technologies. *E. coli* strain BL21 (DE3) (F⁻, *dcm*, *ompT*, *hsdS*(r_B, m_B) was from Stratagene. The *E. coli* *queA* deletion mutant K12QueA and the pGEX-QA plasmid were generous gifts from Helga Kersten, (Univeritat Erlangen, Erlangen, Germany). The *E. coli* strains, BL21(DE3), harboring the recombinant AdoMet synthetase (*MAT*) genes from *Methanococcus jannaschii* in plasmid pMJ1208 and *E. coli*, in plasmid pK8, respectively, were generous gifts from Dr. G. Markham (Fox Chase Cancer Center, Philadelphia, PA). Hypoxanthine-guanine phosphoribosyltransferase (HGPRTase) from *Leishmania donovani* was expressed from pBAC-HGPRTase-LB/SØS6, a generous gift from Dr. Buddy Ullman (Oregon Health and Science University, Portland, OR). The *E. coli* strain, B25, harboring the recombinant adenine phosphoribosyltransferase (APRTase) gene in plasmid pQEAPT1 was a generous gift from Dr. Milton Taylor (Indiana University). The *E. coli* strain DH5α, harboring the recombinant 5-phosphoribosyl-1-pyrophosphate (PRPP) synthetase gene from *Salmonella typhimurium* in plasmid pBRS11R was a generous gift from Dr. Vern L. Schramm (Albert Einstein College of Medicine, Bronx, NY).

Factor Xa Cleavage Reactions

The His₆-affinity fusion tag was cleaved from recombinant fusion proteins (20 mg) with 20 μg of Factor Xa protease (Novagen) in a reaction mixture consisting of 50 mM Tris-acetate (pH 8.0), 100 mM KCl, and 2 mM CaCl₂ in a final volume of 1 ml. After incubating for 20 h at room temperature the cleavage reactions were loaded onto a 2 ml Ni-NTA agarose column (Qiagen) equilibrated in 50 mM Tris-Acetate (pH

8.0), 300 mM KCl, and 10% glycerol (Buffer A). The cleaved proteins were eluted from the column with the addition of 10 column volumes of Buffer A. Uncleaved His₆-tagged protein was eluted with the addition of 10 column volumes of Buffer A containing 200 mM imidazole. Wild type protein was concentrated and dialyzed against 50 mM Tris-Acetate (pH 8.0), 50 mM KCl, and 10% glycerol. The proteins were analyzed by SDS-PAGE and concentration was determined by Bradford assay (BioRad) using bovine serum albumin as a standard.

Selenomethionine Proteins

Selenomethionine containing proteins utilized in structural crystallography were expressed according to methods of Doublet [77]. Transformed *E. coli* BL21(DE) cells were grown in M9 media supplemented with 50 mg of each amino acid (except methionine), 0.2% glucose, 2 mM MgSO₄, 0.1 mM CaCl₂, 1.5 mg thiamine, 1.5 mg biotin, 0.5 mg guanosine, 0.5 mg thymine, 0.5 mg uracil, 2 µl Maria's magic 1,000,000X micronutrients, 50 mg of selenomethionine and either 30 µg/ml kanamycin or 100 µg/ml ampicillin [77]. Cultures were incubated at 37 °C with shaking until an OD₆₀₀ 0.9-1.0 was attained. Protein expression was induced with the addition of IPTG to a final concentration of 0.1 mM 15 min after the addition of 50 mg lysine, 50 mg phenylalanine, 50 mg threonine, 25 mg leucine, 25 mg valine and 25 mg selenomethionine. Cells were allowed to grow overnight and harvested by centrifugation (5000 x g for 10 min). Selenomethionine proteins were purified identically to their non-selenomethionine containing counter-parts except all buffers

contained 10 mM β -mercaptoethanol and were degassed prior to use. The addition of a reductant and degassing the buffers prior to use was essential in the prevention of the oxidation of selenomethionine.

***In vivo* Overexpression of preQ₁-tRNA^{Tyr}**

An expression plasmid, pTrc99B-Tyr, was constructed previously, in which the synthetic gene for *E. coli* tRNA^{Tyr}(I) was ligated into a pTrc99B vector [78]. *E. coli* K12QueA competent cells (100 μ l) were transformed with 1 μ g of pTrc99B-Tyr expression plasmid and plated onto LB medium agar plates containing 100 μ g/ml ampicillin. A single colony was used to inoculate 3 ml of LB medium containing 100 μ g/ml ampicillin. After incubating for 12 h at 37 °C with shaking (250 rpm), a 1 ml aliquot was removed from the cultures and used to inoculate 100 ml of LB medium supplemented with 100 μ g/ml ampicillin. The culture was incubated for 12 h at 37 °C with shaking (250 rpm), then 5 ml aliquots were used to inoculate 7-2500 ml flasks, each containing 500 ml of LB medium supplemented with 100 μ g/ml ampicillin. The resulting cultures were incubated at 37 °C with shaking (250 rpm) until the OD₆₀₀ reached 0.9-1.0. Expression of preQ₁-tRNA^{Tyr} was induced by the addition of IPTG to a final concentration of 0.5 mM. Cells were harvested by centrifugation (5000 x g for 10 min at 4 °C) 13 h post induction, flash frozen in liquid nitrogen and stored at -80 °C until needed. Approximately 15 g of cells were obtained from 3.5 L of cell culture.

Isolation of preQ₁ enriched tRNA^{Tyr}

Bulk tRNA was extracted and isolated from *E. coli* cells utilizing the acid guanidium thiocyanate-phenol-chloroform method [79]. Twenty grams of cells were suspended in 40 ml of lysis buffer (4 M guanidine thiocyanate, 0.5% N-lauroylsarcosine, 100 mM 2-mercaptoethanol and 25 mM sodium citrate (pH 7.0)) and stirred for 1 h at 4 °C. A 4 ml solution of 2 M sodium acetate (pH 4.0) was added and the solution was stirred for an additional 5 min followed by the addition of 40 ml of water-saturated phenol. After stirring for 5 min, 8 ml of chloroform:isoamyl alcohol (49:1) was added and the solution was shaken vigorously for 10 sec. The aqueous phase was recovered after centrifugation (800 x g for 20 min) and the RNA was precipitated from solution with the addition of an equal volume of cold isopropanol. After storing at -20 °C for 2 h, the precipitated RNA was recovered by centrifugation (20,000 x g for 30 min) and washed twice with 70% ethanol.

To ensure complete removal of proteins a second round of extraction was conducted as described above except ¼ the original volumes were used. After suspending the RNA pellet in sterile DEPC treated water, an equal volume of 8 M lithium chloride was added and the resulting solution was stored -20 °C for 2 h, followed by centrifugation (20,000 x g for 30 min) to remove large RNAs. The tRNA was precipitated from the supernatant with the addition of an equal volume of cold isopropanol. After storing at -20 °C for 2 h, the tRNA was recovered by centrifugation (20,000 x g for 30 min), washed with 70% ethanol and suspended in 3

mM sodium citrate (pH 6.3). Total concentration of tRNA was determined by UV-vis spectroscopy ($\epsilon_{260} = 15$ units/mg/ml). Tyrosine-tRNA synthetase activity assay was used to determine the percentage of preQ₁-tRNA^{Tyr} from total tRNA that had been extracted from the cells [80].

Purification of preQ₁ containing tRNA^{Tyr}

PreQ₁-tRNA^{Tyr} was purified further by successive chromatography using BND-cellulose [81, 82] and NACsTM (trialkylamine ion exchange resin) [83, 84]. Crude tRNA (20 mg) was loaded onto a 12 ml BND-cellulose column equilibrated in Buffer B (20 mM sodium acetate (pH 4.5), 10 mM MgCl₂ and 0.5 M NaCl). The column was washed with 20 ml of Buffer B at a flow rate of 0.5 ml/min followed by an 80 ml salt gradient (0.5M-1.0M NaCl) in Buffer B from 20-100 ml. After washing the column with 10 ml of Buffer C (Buffer B containing 1 M NaCl), tyrosine specific tRNA was eluted from the column with a 40 ml ethanol gradient (0-20% v/v) in Buffer C.

Fractions (2 ml) were collected and analyzed by UV-vis at 260 nm. Those fractions containing preQ₁-tRNA^{Tyr}, as determined by QueA or tyrosine-tRNA synthetase activity assays, were pooled and the tRNA was precipitated from solution with the addition an equal volume of cold isopropanol. After storing at -20 °C for 2 h, the precipitated preQ₁-tRNA^{Tyr} was collected by centrifugation (20,000 X g for 30 min), washed twice with 70% ethanol and suspended in 3 mM sodium citrate (pH 6.3).

After dialyzing against 4 L of Buffer D (10 mM sodium acetate (pH 4.5), 10 mM $MgCl_2$ and 0.2 M NaCl) at 4 °C for 4 h, the enriched tRNA sample was applied to a column containing 10 ml NACsTM resin equilibrated in Buffer D. The column was washed with a 100 ml of Buffer D at a flow rate of 1 ml/min and tyrosyl-tRNA was eluted with a 400 ml salt gradient (0.2 M - 1M) in Buffer D. Fractions (2.5 ml) were collected and analyzed by UV-vis at 260 nm. Those fractions containing preQ₁-tRNA^{Tyr}, as determined by QueA or tyrosine-tRNA synthetase activity assays, were pooled and the tRNA was precipitated from solution with the addition an equal volume of cold isopropanol. After storing at -20 °C for 2 h, the precipitated RNA was collected by centrifugation (20,000 X g for 30 min), washed twice with 70% ethanol and suspended in 3 mM sodium citrate (pH 6.3). Removal of excess metal ions was achieved with the addition of EDTA to a final concentration of 5 mM followed by dialysis against 3 mM sodium citrate (pH 6.3) for 10 min at 80 °C. The sample was dialyzed further at 4 °C for 8 h against 2 exchanges of buffer (2 L). The concentration of tyrosyl-tRNA was determined spectrophotometrically at 260 nm ($\epsilon = 816,000 \text{ L mol}^{-1} \text{ cm}^{-1}$).

Expression and Purification of APRTase His₆-tag Fusion Protein

The expression and purification of recombinant APRTase was conducted according to the methods of Alfonzo [85, 86]. *E. coli* B25 competent cells (100 μ l) were transformed with 1 μ g of the APRTase expression plasmid, pQE-APT1, and plated on 2xYT medium agar plates containing 100 μ g/ml ampicillin and 25 μ g/ml kanamycin.

Isolated colonies were used to inoculate 3 ml of 2xYT medium containing 100 µg/ml ampicillin and 25 µg/ml kanamycin. After incubating for 12 h at 37 °C with shaking (250 rpm), a 1 ml aliquot was removed from the culture and used to inoculate 100 ml of 2xYT medium containing 100 µg/ml ampicillin and 25 µg/ml kanamycin. The culture was incubated for 12 h at 37 °C with shaking (250 rpm), then 5 ml aliquots were used to inoculate 7-2500 ml flasks containing 500 ml of 2xYT medium supplemented with 100 µg/ml ampicillin and 25 µg/ml kanamycin. The cultures were allowed to grow at 37 °C with shaking (250 rpm) until an OD₆₀₀ of 0.9-1.0 was attained. The expression of APRTase was induced by the addition of IPTG to a final concentration of 0.1 mM. After incubating the cultures for an additional 5 h at 37 °C with shaking (250 rpm), the cells were collected by centrifugation (5000 x g for 10 min at 4°C), flash frozen in liquid nitrogen and stored at -80 °C until needed. Approximately 12 g of cells were obtained from 3.5 L of cell culture.

Recombinant His₆-tag APRTase fusion protein was purified by suspending 10 g of frozen cells in lysis buffer (50 mM Tris-HCl (pH 7.5), 300 mM NaCl, 1 mM β-mercaptaethanol, 1 mM PMSF; 10% glycerol, and 1 mM MgCl₂) at a concentration of 250 mg/ml. Once the cells were completely suspended, DNase was added to a final concentration of 10 µg/ml and the cells were lysed by two passes through a French press. Cell debris was removed by centrifugation (15,000 x g for 30 min). The cell free extract was filtered with a low protein binding, 0.45 µm, syringe filter (Fisherbrand) and loaded onto a 10 ml Ni-NTA agarose column (Qiagen) equilibrated

with 10 column volumes of Buffer E (100 mM Tris-HCl (pH 7.5), 300 mM KCl, 2 mM β -mercaptoethanol, 1% Triton X-100, 1 mM PMSF and 10% glycerol). The column was sequentially washed with 5 column volumes of Buffer E, 5 column volumes of Buffer F (Buffer E containing 20 mM imidazole) and 5 column volumes of Buffer G (Buffer F without Triton X-100 and PMSF). The protein was eluted from the column with 7 column volumes of Buffer H (Buffer G containing 200 mM imidazole) and collected in 10 ml fractions. Fractions containing the protein were pooled, concentrated using an Amicon Ultra YM-10 centrifugal filter device (Millipore) and dialyzed against 50 mM Tris-HCl (pH 7.5), 50 mM KCl, and 2 mM DTT at 4 °C. The recombinant APRTase was greater than 90% homogeneous as determined by SDS-PAGE and stored as glycerol stocks at -80°C. Protein concentration was determined by Bradford assay (BioRad) using bovine serum albumin as a standard, and activity was measured by methods described by Hochstadt [87].

Expression and Purification of PRPP Synthetase

E. coli DH5 α competent cells (100 μ l) were transformed with 1 μ g of the PRPP synthetase expression plasmid, pBRS11R, and plated onto LB medium agar plates containing 100 μ g/ml ampicillin. An isolated colony was used to inoculate 3 ml of LB medium containing 100 μ g/ml ampicillin. After incubating for 12 h at 37 °C with shaking (250 rpm), a 1 ml aliquot was removed from the culture and used to inoculate 100 ml of LB medium containing 100 μ g/ml ampicillin. The culture was incubated for 12 h at 37 °C with shaking (250 rpm), then 5 ml aliquots were used to inoculate 7-

2500 ml flasks containing 500 ml of LB medium supplemented with 100 µg/ml ampicillin. Once the OD₆₀₀ reached 0.9-1.0, the cultures were incubated for an additional 4 h at 37 °C with shaking (250 rpm), cells were collected by centrifugation (5000 x g for 10 min), flash frozen in liquid nitrogen and stored at -80 °C until needed. Approximately 10 g of cells were obtained from 3.5 L of cell culture.

PRPP synthase was purified by suspending 10 g of frozen cells in lysis buffer (50 mM sodium phosphate (pH 7.5), 1 mM PMSF and 2 mM DTT) at a concentration of 250 mg/mL. The cells were lysed by the addition of lysozyme to a final concentration of 200 µg/ml. After incubating at 37 °C with rotation for 30 min, DNase was added to a final concentration of 10 µg/ml and the cell solution was incubated for an additional 30 min at 37 °C with rotation. Cell debris was removed by centrifugation (15,000 x g for 30 min) and the resulting cell free extract was filtered with a low protein binding, 0.45 µm syringe filter (Fisherbrand). PRPP synthetase was precipitated from solution upon the addition of ammonium sulfate to a final concentration of 15%. The protein was collected by centrifugation (15,000 X g for 30 min) and suspended in minimal amount of lysis buffer containing 10% glycerol. The protein sample was dialyzed against the lysis buffer containing 10% glycerol at 4°C and stored at -80 °C as a glycerol stock. The protein sample was approximately 60% pure as judged by SDS-PAGE analysis. Protein concentration was determined by Bradford assay (BioRad) using bovine serum albumin as a standard, and activity was measured by methods described by Braven [88].

Enzymatic synthesis of [U-*ribose*-¹⁴C]ATP

[U-*ribose*-¹⁴C]ATP was synthesized from [U-¹⁴C]-glucose in a modification of the multienzyme reaction described by Parkin and LoBrutto [89, 90]. The reaction was carried out in 50 mM phosphate (pH 7.5), 50 mM gly-gly (pH 7.8), 10 mM MgCl₂, 3 mM adenine, 10 mM α -ketoglutarate, 835 μ M ATP, 20 mM phosphoenol pyruvate, 1 mM NADP⁺, 1.2 mM [U-¹⁴C]glucose, 4.8 U glucose-6-phosphate dehydrogenase, 4.8 U 6-phosphogluconate dehydrogenase, 48 U myokinase, 48 U hexokinase, 48 U phosphoriboisomerase, 96 U pyruvate kinase, 0.6 mg PRPP synthetase, 150 μ g APRTase and 72 U glutamate dehydrogenase in a final volume of 6 ml. To minimize the inhibitory effects of excess ammonium ions all of the enzymes except for glutamate dehydrogenase were diluted to 15 ml with water and then concentrated by centrifugation to 500 μ l prior to use. The reaction was incubated for 4 h at 37 °C and terminated by heating at 95 °C for 3 min. Precipitated proteins were removed by centrifugation (14,000 X g for 30 min) and [U-*ribose*-¹⁴C]ATP was purified by reverse phase HPLC on a semipreparative Luna C18 column (250 mm X 10 mm, 5 μ M, Phenomenex) under isocratic conditions using a mobile phase of 83.3 mM triethylammonium acetate (pH 6.0) and 6% methanol at a flow rate of 4 ml/min. Fractions containing ATP were pooled, lyophilized to dryness and suspended in water. The concentration of ATP was determined by UV-vis spectroscopy (ϵ = 15.4 X 10³ M⁻¹cm⁻¹). Typical radiochemical yields were 65-80% after accounting for the loss of C-1 from glucose.

Expression and Purification of *E. coli* AdoMet Synthetase (EcMAT) Protein

E. coli DH5 α competent cells (100 μ l) were transformed with 1 μ g of the *E. coli* AdoMet synthetase expression plasmid, pk8, and plated onto LB medium agar plates containing 50 μ g/ml tetracycline. An isolated colony was used to inoculate 3 ml of LB medium containing 50 μ g/ml tetracycline. After incubating for 12 h at 37 °C with shaking (250 rpm), a 1 ml aliquot was removed from the cultures and used to inoculate 100 ml of LB medium supplemented with 50 μ g/ml tetracycline. The culture was incubated for 12 h at 37 °C with shaking (250 rpm), then 5 ml aliquots were used to inoculate 7-2500 ml flasks containing 500 ml of LB medium supplemented with 50 μ g/ml tetracycline. The cultures were allowed to grow at 37 °C with shaking (250 rpm) until an OD₆₀₀ of 0.9-1.0 was attained. The expression of EcMAT was induced by the addition of IPTG to a final concentration of 0.1 mM. After incubating the cultures for an additional 5 h at 37 °C with shaking (250 rpm) the cells were collected by centrifugation (5000 x g for 10 min), flash frozen in liquid nitrogen and stored at -80 °C until needed. Approximately 12 g of cells were obtained from 3.5 L of cell culture.

E. coli AdoMet synthetase was purified by suspending 10 g of frozen cells in Buffer I (50 mM Tris-HCl (pH 8.0), 1 mM PMSF, 1 mM DTT and 0.5 mM EDTA) at a concentration of 250 mg/ml. The cells were lysed by the addition of lysozyme to a final concentration of 200 μ g/ml. After incubating at 37 °C with rotation for 30 min, DNase was added to final concentration of 10 μ g/ml and the cell solution was

incubated for an additional 30 min at 37 °C. Cell debris was removed by centrifugation (15,000 x g for 30 min) and the resulting cell free extract was filtered with a low protein binding, 0.45 µm syringe filter (Fisherbrand). A fresh solution of streptomycin sulfate was added to a final concentration of 1% and the solution was centrifuged at 15,000 X g for 30 min. AdoMet synthetase was partially purified by the addition of ammonium sulfate to a final concentration of 65%. The precipitated protein was collected by centrifugation (15,000 X g for 30 min) and suspended in minimal amount of Buffer J (Buffer I containing 10% glycerol). The protein sample was dialyzed against the Buffer J at 4°C and stored -80°C as a glycerol stock. The protein sample was judged to be ~70% pure as judged by SDS-PAGE. Protein concentration was determined by Bradford assay (BioRad) using bovine serum albumin as a standard, and activity was measured by methods described by Markham [91].

Expression and Purification of *M. jannaschii* AdoMet Synthetase (MjMAT) His₆-tag Fusion Protein

E. coli BL21(DE) competent cells (100 µl) were transformed with 1 µg of the MjMAT expression plasmid, pMJ1208, and plated onto LB medium agar plates containing 100 µg/ml ampicillin. An isolated colony was used to inoculate 3 ml of LB medium containing 100 µg/ml ampicillin. After incubating for 12 h at 37 °C with shaking (250 rpm), a 1 ml aliquot was removed from the culture and used to inoculate 100 ml of LB medium containing 100 µg/ml ampicillin. The culture was incubated for 12 h at 37 °C with shaking (250 rpm), then 5 ml aliquots were used to inoculate 7-2500 ml flasks

containing 500 ml of LB medium supplemented with 100 µg/ml ampicillin. The cultures were incubated at 37 °C with shaking (250 rpm) until an OD₆₀₀ of 0.9-1.0 was attained. The expression of MjMAT was induced by the addition of IPTG to a final concentration of 0.1 mM. After incubating the cultures for an additional 5 h at 37 °C with shaking (250 rpm), the cells were collected by centrifugation (5000 x g for 10 min), flash frozen in liquid nitrogen and stored at -80 °C until needed. Approximately 12 g of cells were obtained from 3.5 L of cell culture.

Recombinant His₆-tag MjMAT fusion protein was purified by suspending 10 g of frozen cells in lysis buffer (50 mM Tris-HCl (pH 7.5), 300 mM NaCl, 1 mM β-mercaptaethanol, 1 mM PMSF; 10% glycerol and 1 mM MgCl₂) at a concentration of 250 mg/ml. Once the cells were completely suspended, DNase was added to a final concentration of 10 µg/ml and lysed by two passes through a French press. Cell debris was removed by centrifugation (15,000 x g for 30 min) and the cell free extract was filtered with a low protein binding, 0.45 µm syringe filter (Fisherbrand). The protein sample was loaded onto a 10 ml Ni-NTA agarose column (Qiagen) equilibrated with 10 column volumes of Buffer E (100 mM Tris-HCl (pH 7.5), 300 mM KCl, 2 mM β-mercaptoethanol, 1% Triton X-100, 1 mM PMSF and 10% glycerol). The column was sequentially washed with 5 column volumes of Buffer E, 5 column volumes of Buffer F (Buffer E containing 20 mM imidazole) and 5 column volumes of Buffer G (Buffer F without Triton X-100 and PMSF). The protein was eluted from the column with 7 column volumes of Buffer H (Buffer G containing 200 mM imidazole) and collected

in 10 ml fractions. Fractions containing protein were pooled, concentrated using an Amicon Ultra YM-10 centrifugal filter devices (Millipore) and dialyzed against 50 mM Tris-HCl (pH 7.5), 50 mM KCl, and 2 mM DTT at 4 °C. The recombinant MjAdoMet synthetase was greater than 90% homogeneous as determined by SDS-PAGE and stored at -80°C as glycerol stocks. Protein concentration was determined by Bradford assay (BioRad) using bovine serum albumin as a standard and activity was measured by methods described by Markham et.al. [92].

Enzymatic Synthesis of AdoMet and AdoMet Analogs

The enzymatic synthesis of [U-*ribosyl*-¹⁴C]AdoMet and AdoMet analogs (SeAdoMet, 3'-deoxyAdoMet and 7-deazaAdoMet) was achieved according to modified methods described by Park [93, 94]. Reactions involving the synthesis of [U-*ribosyl*-¹⁴C]AdoMet were carried out at 25°C in the presence of 100 mM Tris-HCl (pH 8.0), 50 mM KCl, 26 mM MgCl₂, 5 mM DTT, 20% acetonitrile, 0.2 mg/ml *E.coli* MAT (EcMAT), 1 mM [U-*ribosyl*-¹⁴C]ATP and 5 mM L-methionine. After 2 h the reaction was terminated with the addition of cold 50% TCA to a final concentration of 8% and the precipitated proteins were removed by centrifugation (15,000 x g for 30 min). The synthesis of [U-*ribosyl*-¹⁴C]SeAdoMet and SeAdoMet was achieved in a similar manner except with the substitution of selenomethionine in place of methionine. Due to the decreased stability of SeAdoMet, reactions were carried out for 1 h at 25 °C using 0.6 mg/ml of EcMAT. The synthesis of 3'-deoxyAdoMet and 7-deazaAdoMet was conducted according to the procedure described for [U-*ribosyl*-¹⁴C]AdoMet

except the reactions were carried out in the presence of 1 mM 3'-deoxyATP or 7-deazaATP (Tubercidin), and 0.5 mM [^{14}C]-methionine (55 mCi/mmol) or 5 mM methionine using 0.6 mg/ml EcMAT. The enzymatic synthesis of 2'-deoxyAdoMet was conducted according to methods described by Graham [95, 96]. Reactions were carried out at 55 °C for 1 h in 25 mM HEPES (pH 8.0), 50 mM KCl, 10 mM MgCl_2 , 5 mM DTT, 20% acetonitrile, 0.5 mM of [^{14}C]-methionine (55 mCi/mmol) or 5 mM methionine, 1 mM 2'-deoxyATP, and 0.6 mg/ml *M. jannaschii* AdoMet synthetase (MjMAT). AdoMet analogs were purified from unreacted substrate and decomposition products by HPLC on a semipreparative Luna C18 column (250 mm X 10 mm, 5 μM , Phenomenex) under isocratic conditions using a mobile phase of 20 mM ammonium acetate (pH 6.0) and 2% methanol at a flow rate of 3 ml/min. Fractions containing AdoMet analogs were pooled, lyophilized to dryness and dissolved in 10 mM H_2SO_4 . The concentration of the compounds were determined by UV-vis spectroscopy ($\epsilon = 14.9 \times 10^3 \text{ M}^{-1}\text{cm}^{-1}$ or $\epsilon = 9500 \text{ M}^{-1}\text{cm}^{-1}$ for 7-deazaAdoMet).

Expression and Purification of *Escherichia coli* QueA-GST Recombinant protein

E. coli DH5 α competent cells (100 μl) were transformed with 1 μg of the QueA-GST expression plasmid, pGEX-QueA, and plated on LB medium agar plates containing 100 $\mu\text{g}/\text{ml}$ ampicillin. A single colony used to inoculate 3 ml of LB medium containing 100 $\mu\text{g}/\text{ml}$ ampicillin. After incubating for 12 h at 37 °C with shaking (250 rpm), a 1 ml aliquot was removed from the cultures and used to inoculate 100 ml of

LB medium containing 100 µg/ml ampicillin. The culture was incubated for 12 h at 37 °C with shaking (250 rpm), then 5 ml aliquots were used to inoculate 7-2500 ml flasks containing 500 ml of LB medium supplemented with 100 µg/ml ampicillin. The cultures were incubated at 37 °C with shaking (250 rpm) until an OD₆₀₀ of 0.9-1.0 was attained. The expression of QueA-GST was induced by the addition of isopropyl-1-thio-B-D-galactopyranoside (IPTG) to a final concentration of 0.1 mM. Cells were harvested 4 h post induction by centrifugation (5000 x g for 10 min), flash frozen in liquid nitrogen and stored at -80 °C until needed. Approximately 10 g of cells were obtained from 3.5 L of cell culture.

Recombinant QueA-GST protein was purified by suspending 10 g of frozen cells in lysis buffer (50 mM Tris-HCl (pH 8.0), 10 mM EDTA and 50 mM KCl) at a concentration of 250 mg/ml and lysed by the addition of lysozyme to a final concentration of 250 µg/ml. After incubating at 37 °C with rotation for 30 min, DNase was added to final concentration of 10 µg/ml and the solution was incubated for an additional 30 min at 37 °C. Cell debris was removed by centrifugation (15,000 x g for 30 min) and the resulting cell free extract was filtered with a low protein binding, 0.45 µm, syringe filter (Fisherbrand). An equal volume of Buffer K (50 mM Tris-HCl (pH 7.8.0), 100 mM KCl, 10 mM MgCl₂, 2 mM DTT, 1 mM PMSF, 10% glycerol) was added and the cell free extract was centrifuged in a Beckman 50 Ti rotor at 33,000 rpm for 4 hours at 4 °C. Triton X-100 was added to a final concentration of 1% and the resultant solution was filtered with a low protein binding, 0.45 µm, syringe filter

(Fisherbrand). The cell free extract was loaded on to 10 ml of Glutathione-sepharose 4B (Pharmacia) equilibrated with 10 column volumes of Buffer L (Buffer K, containing 1 % Triton X-100, 2 mM PMSF). The column was sequentially washed with 10 column volumes of Buffer L and 10 column volumes of Buffer M (Buffer K containing 2 mM PMSF). The protein was eluted from the column with 5 column volumes of Buffer N (Buffer K containing 2 mM PMSF and 20 mM reduced glutathione) at 4 °C. Fractions containing QueA-GST were pooled and the pH adjusted to 8.6 with the addition of 1 M NaOH. The protein sample was concentrated using a Amicon Centriprep YM-30 ultracentrifugation device (Millipore) and dialyzed at 4 °C against Buffer K without PMSF.

QueA-GST was purified further by HPLC by loading 1 mg of protein onto a POROS HQ column (4.6 mm X 100 mm; PerSeptive Biosystems) equilibrated with Buffer O (20 mM Tris-HCl (pH 8.0), 10 mM MgCl₂, 2 mM DTT, and 10 % glycerol). The protein was eluted from the column with a linear salt gradient (0-1M NaCl) in Buffer O at a flow rate of 4 ml/min. The eluant was monitored at 280 nm and fractions containing QueA-GST were pooled and concentrated using an Amicon Ultra YM-30 centrifugation device (Millipore). The protein solution was dialyzed at 4 °C against Buffer K without PMSF. The recombinant QueA-GST was purified to near homogeneity as determined by SDS-PAGE and stored at -80 °C as a glycerol stock. Protein concentration was determined by Bradford assay (BioRad) using bovine serum albumin as a standard.

Expression and Purification of recombinant His₆-QueA from *E. coli*

The expression plasmid, pET30-EcHis₆-QueA, was transformed into *E. coli* BL21(DE) competent cells (100 µl) with 1 µg of expression plasmid and plated on LB medium agar plates containing 50 µg/ml kanamycin. An isolated colony was used to inoculate 3 ml of LB medium containing 50 µg/ml kanamycin. After incubating for 12 h at 37 °C with shaking (250 rpm), a 1 ml aliquots was used to inoculate 100 ml of LB medium supplemented with 50 µg/ml kanamycin. The culture were incubated for 12 h at 37°C with shaking (250 rpm), then 5 ml aliquots were used to inoculate 7-2500 ml flasks containing 500 ml of LB medium supplemented with 50 µg/ml kanamycin. The cultures were incubated at 37 °C with shaking (250 rpm) until an OD₆₀₀ of 0.9-1.0 was attained. Protein expression was induced by the addition of isopropyl-1-thio-B-D-galactopyranoside (IPTG) to a final concentration of 0.1 mM. Cells were harvested 4 h post induction by centrifugation (5000 x g for 10 min), flash frozen in liquid nitrogen and stored at -8 0°C until needed. Approximately 12 g of cells were obtained from 3.5 L of cell culture.

The recombinant His₆-tag QueA fusion protein was purified by suspending 10 g of frozen cells in lysis buffer (50 mM Tris-Acetate (pH 8.0), 50 mM KCl, 1 mM β-mercaptaethanol, 1 mM PMSF; 10% glycerol, and 1 mM MgCl₂) at a concentration of 250 mg/ml. The cells were lysed by the addition of lysozyme to a final concentration of 250 µg/ml. After incubating at 37 °C with rotation for 30 min, DNase was added to final concentration of 10 µg/ml and the cell solution was incubated for an additional

30 min at 37 °C. The solution was placed on ice for 10 min after the addition of 10 ml of Buffer P (200 mM Tris-acetate (pH 8.0), 1.2 M KCl, 8 mM β -mercaptaethanol, 4 mM PMSF and 40% glycerol) and clarified by centrifugation (15,000 x g for 30 min). The resulting cell free extract was filtered with a low protein binding, 0.45 μ m, syringe filter (Fisherbrand) and loaded onto 10 ml Ni-NTA agarose column (Qiagen), equilibrated with 10 column volumes of Buffer Q (100 mM Tris-Acetate (pH 8.0), 300 mM KCl, 2 mM β -mercaptoethanol, 1% Triton X-100, 1 mM PMSF and 10% glycerol). The column was sequentially washed with 5 column volumes of Buffer Q, 5 column volumes of Buffer R (Buffer Q containing 20 mM imidazole) and 5 column volumes of Buffer S (Buffer R without Triton X-100 and PMSF). The protein was eluted from the column with 7 column volumes of Buffer T (Buffer S containing 250 mM imidazole). Fractions containing the protein were pooled, concentrated with Amicon Ultra YM-10 centrifugal filtration device (Millipore) and dialyzed against 50 mM Tris-Acetate (pH 8.0), 50 mM KCl, and 2 mM DTT at 4 °C. The recombinant QueA-His proteins were purified to homogeneity as determined by SDS-PAGE and stored as a glycerol stock at -80 °C. The protein concentration was determined by Bradford assay (BioRad) using bovine serum albumin as a standard.

QueA Activity Assays

QueA activity was determined by following the radiochemical incorporation of the ribosyl moiety from either [U-*ribosyl*-¹⁴C]AdoMet or [U-*ribosyl*-¹⁴C]SeAdoMet into preQ₁-tRNA^{Tyr} according to established procedures described by Van Lanen et. al.

[78]. Assays were performed in 100 mM gly-gly (pH 8.7), 100 mM EDTA (pH 8.7), 100 mM KCl, 0.5 mM DTT, 0.2 μ M QueA, 20 μ M of preQ₁-tRNA^{Tyr}, and varying concentration of either [U-*ribosyl*-¹⁴C]SeAdoMet or [U-*ribosyl*-¹⁴C]AdoMet in a final volume of 50 μ l. The reaction mixtures were incubated at 37 °C under initial velocity conditions. Due to the instability of substrate under alkaline conditions, reactions were initiated upon the addition of AdoMet or SeAdoMet. Reactions were terminated with the addition of 3 volumes of cold 10% TCA to precipitate the tRNA and protein from solution. The precipitant was recovered on Whatman GF/B filters by vacuum filtration and washed with cold 5% TCA followed by 95% ethanol and dried. Radioactivity was determined by liquid scintillation counting.

The catalytic activity of QueA in the presence of AdoMet analogs in which the isotope is located in the methionine or adenine moiety, was measured using a chromatographic protocol to separate substrates and products [97]. Reactions were carried out as described above in the presence of varying concentrations of [1-methionine-¹⁴C]3'-deoxyAdoMet, [1-methionine-¹⁴C]2'-deoxyAdoMet, or [1-methionine-¹⁴C]7-deazaAdoMet. The reactions were terminated by decreasing the pH to 6.5 with the addition of acetic acid and the samples were subsequently loaded onto 250 μ l of Dowex 50WX4 (cation exchange resin) equilibrated in 0.1 N H₂SO₄, respectively. Methionine, adenine and AdoMet were sequentially washed from the column with the addition of 10 ml of 1N, 2N and 8N H₂SO₄. Fractions (1 ml) were collected and quantified by liquid scintillation counting. When applicable, kinetic parameters were

calculated from the average of minimally 4 duplicates with the Michaelis-Menten equation using the curve fitting software Kaleidagraph 4.0 (Synergy Software, Reading, PA).

QueA Inhibition Analysis

Inhibition analysis of QueA was conducted with varying concentration of [U-*ribosyl*-¹⁴C]AdoMet and various fixed concentrations of SeAdoMet, 3'dAdoMet, 2'dAdoMet and 7-deazaAdoMet. Reactions were carried out as described above and terminated with the addition of TCA. QueA activity was quantified by liquid scintillation counting. The data (average of minimally 4 duplicates) were fitted to the equation for competitive inhibition (eq. 1).

$$v = VS / (K_m(1 + I/K_i) + S) \quad (1)$$

Where S is the varied substrate concentration, I is the inhibitor concentration and K_i the inhibition constant.

Time Dependent Inhibition Analysis

Time dependent inactivation studies were conducted in which 2 μM QueA was preincubated in the presence of 300 μM SeAdoMet and 50 μM preQ₁-tRNA^{Tyr} in reaction Buffer U (100 mM gly-gly (pH 8.7), 100 mM EDTA (pH 8.7), 100 mM KCl, and 0.5 mM DTT) or reaction Buffer V (50 mM Tris-HCl (pH 8.0), 100 mM EDTA

(pH 8.0), 100 mM KCl, and 0.5 mM DTT). Aliquots of the preincubation mixture were taken at various times into standard QueA assay conditions containing 100 μ M [U-*ribosyl*- 14 C]AdoMet and 20 μ M preQ₁-tRNA^{Tyr}. The reaction assays were carried out as described above and terminated with the addition of 3 volumes of cold 10% TCA and worked up as described above.

QueA Activity Assay using Ni-NTA

Potential formation of an enzyme-substrate covalent adduct was analyzed by nickel affinity chromatography. Assays were performed in 100 mM gly-gly (pH 8.7), 25 mM sodium phosphate (pH 8.0), 100 mM KCl, 0.5 mM β -mercaptoethanol, 25-50 μ M QueA, 50 μ M preQ₁-tRNA^{Tyr}, and 200 μ M [U-*ribosyl*- 14 C]SeAdoMet or [U-*ribosyl*- 14 C]AdoMet in a final volume of 50 μ l. The reaction mixtures were incubated at 37 °C for 30 min and loaded onto 500 μ l Ni-NTA agarose equilibrated in Buffer W (100 mM Tris-HCl (pH 8.0) and 300 mM KCl). The column was washed with 25 ml of Buffer A followed by 6 ml of Buffer X (Buffer W containing 250 mM imidazole). One milliliter fractions were collected and quantified by liquid scintillation counting.

Expression and Purification of HGPRTase

The expression system, pBAC-HGPRTase-LD/SOS6, for the recombinant HGPRTase from *Leishmania donovani* was grown in a low phosphate media supplemented with 0.2% glucose, 1.5 μ M thiamine, 20 μ g/ml adenine, 75 μ g/ml ampicillin and 0.1% vitamin free casamino acids [98-101]. The cultures were allowed to grow until an

OD₆₀₀ of 1.4 was attained. Cells were collected by centrifugation (5000 x g for 10 min), washed two times with phosphate buffered saline solution, flash frozen in liquid nitrogen and stored at -80 °C until needed. Approximately 9 g of cells were obtained from 3.5 L of cell culture.

HGPRTase was purified by suspending 9 g of frozen cells in lysis buffer (20 mM Tris-HCl (pH 7.5), 5 mM MgCl₂, 1 mM PMSF, and 1 mM DTT) at a concentration of 250 mg/mL. The cells were lysed by the addition of lysozyme to a final concentration of 200 µg/ml and incubating at 37 °C with rotation for 30 min, DNase was added to a final concentration of 10 µg/ml and the cell solution was incubated for an additional 30 min at 37 °C. Cell debris was removed by centrifugation (15,000 x g for 30 min) and the resulting cell free extract was filtered with a low protein binding, 0.45 µm, syringe filter (Fisherbrand). HGPRTase was precipitated out of the solution upon the addition of ammonium sulfate to 40% saturation. The solution was clarified by centrifugation (15,000 x g for 30 min) and HGPRTase from precipitated from solution with the addition of ammonium sulfate to 80% saturation. The protein was collected by centrifugation (15,000 X g for 30 min) and suspended in minimal amount of lysis buffer containing 10% glycerol. The protein sample was dialyzed against the lysis buffer containing 10% glycerol at 4°C and stored at -80 °C as a glycerol stock. The purity of the protein sample was analyzed by SDS-PAGE analysis and found to be ~60% pure. Protein concentration was determined by Bradford assay (BioRad) using

bovine serum albumin as a standard, and activity was measured by methods described by Jardim and Ullman [101]

Enzymatic Synthesis of [8-¹⁴C]-GTP

The enzymatic synthesis of [8-¹⁴C]GTP from [8-¹⁴C] guanine was achieved in a similar fashion to that of [U-*ribosyl*-¹⁴C]ATP. The synthesis reaction was carried out at 37°C in 50 mM gly-gly (pH 7.8), 50 mM potassium phosphate (pH 7.5), 10 mM MgCl₂, 20 mM PEP, 0.25 mM ATP, 0.4 mM PRPP, 0.1 mM [8-¹⁴C]guanine, 8 U/ml myokinase, 16 U/ml pyruvate kinase, 0.5 mg/ml nucleoside monophosphate kinase, and 0.5 mg/ml hypoxanthine-guanine phosphoribosyltransferase (HGPRTase) in a final volume of 0.5 ml. After 2 h the reaction was terminated by heating at 95 °C for 2 min followed by centrifugation (14,000 X g for 30 min). ATP was removed from the mixture with the addition of EcMAT. The reaction was carried out in 20% acetonitrile, 10 mM MgCl₂, 5 mM methionine, 0.2 mg/ml EcMAT to a final volume of 0.7 ml. After incubating for 1 hr at room temperature the reaction was terminated with the addition cold 50% TCA to a final concentration of 8%. Precipitated proteins were removed by centrifugation (14,000 x g for 10 min), and [8-¹⁴C]GTP was purified by HPLC on a semipreparative LUNA C18 column (250 X 10 mm, 5 um, Phenomenex). Radiolabeled GTP eluted from the column under isocratic conditions using a mobile phase of 83.3 mM triethylammonium acetate (pH 6.0), and 5% methanol at a flow rate of 4 ml/min. Fractions containing GTP were pooled, lyophilized to dryness and

dissolved in water. Concentration was determined by UV-vis spectroscopy ($\epsilon = 12.5 \times 10^3 \text{ M}^{-1} \text{ cm}^{-1}$). Typical radiochemical yields were 50-60%.

Cloning and Construction of an Expression System for COG1469 proteins from *Thermotoga maritima*, *Neisseria gonorrhoeae* and *Bacillus subtilis*

The COG1469 genes from *Thermotoga maritima* (*tm0039*; GenBank accession number gi115642814), *Neisseria gonorrhoeae* (*ngo0387*; GenBank accession number gi159800831) and *Bacillus subtilis* (*ycaA*; GenBank accession number gi12632620) were amplified by PCR from genomic DNA. The following primers corresponding to the 5'- and 3'- regions of the gene were used for PCR amplification: *T. maritima* sense primer (5'-GGTATTGAGGGTCGCTTGAAGGATGTTTCAGAAC-3'), *T. maritima* antisense primer (5'-AGAGGAGAGTTAGAGCCTCATCCCTCCAGAACG-3'), *N. gonorrhoeae* sense primer (5'-GGTATTGAGGGTCGCATGAACGCCATTGCAG-3') and *N. gonorrhoeae* antisense primer (5'-AGAGGAGAGTTAGAGCCCTACGGGTAGGCGATATAG-3'), *B. subtilis* sense primer (5'-GGTATTGAGGGTCGCATGAATCAACATACGCTGCTCCCG-3') and *B. subtilis* antisense primer (5'-AGAGGAGAGTTAGAGCCTCATATTTTATCCAC-3'). The start codons are represented in boldface type and the Factor Xa cleavage site is underlined in the sense primer.

The PCR reaction contained 500 ng genomic DNA, 200 μM dNTPs, 50 pmol of the sense and antisense primers, 1x Pfu Ultra buffer (supplied by the manufacturer), and

2.5 units of Pfu Ultra DNA polymerase (Stratagene) in a final volume of 50 μ l. A three step PCR thermocycling protocol was utilized; (1) 94 °C for 1 min; (2) 30 cycles of denaturation at 94 °C for 1 min, annealing at 50 °C for 2 min, and extension at 72 °C for 1 min; (3) 72 °C for 4 min. The PCR product was purified from a 1% agarose gel containing ethidium bromide and cloned into a linearized pET-30 Xa/LIC expression vector according to manufacturer (Novagen). The primary structures of the cloned genes were confirmed by sequencing.

Expression and Purification of recombinant *T. maritima*, *N. gonorrhoeae* and *B. subtilis* COG1469 proteins

E. coli BL21(DE) competent cells (100 μ l) were transformed with 1 μ g of plasmid DNA harboring the COG1469 gene and plated on LB medium agar plates containing 50 μ g/ml kanamycin. An isolated colony was used to inoculate 3 ml of LB medium containing 50 μ g/ml kanamycin. After incubating for 12 h at 37 °C with shaking (250 rpm), a 1 ml aliquot was used to inoculate 100 ml of LB medium supplemented with 50 μ g/ml kanamycin. The culture was incubated for 12 h at 37 °C with shaking (250 rpm), then 5 ml aliquots were used to inoculate 7-2500 ml flasks containing 500 ml of LB medium supplemented with 50 μ g/ml kanamycin. The cultures were allowed to grow at 37 °C until an OD₆₀₀ of 0.9-1.0 was attained. Expression of the recombinant proteins was induced by the addition of IPTG to a final concentration of 0.1 mM. Cells were harvested 4 h post induction by centrifugation (5000 x g for 10 min), flash

frozen in liquid nitrogen and stored at -80 °C until needed. Approximately 10-15 g of cells was obtained from 3.5 L of cell culture.

The recombinant His₆-tag fusion proteins from *T. maritima*, *B. subtilis* and *N. gonorrhoeae* were purified by suspending 10 g of frozen cells in lysis buffer (50 mM Tris-Acetate (pH 8.0), 50 mM KCl, 1 mM β-mercaptaethanol, 1 mM PMSF and 10% glycerol) at a concentration of 250 mg/ml. The cells were lysed by the addition of lysozyme to a final concentration of 250 µg/ml and incubating at 37 °C with rotation for 30 min, DNase was then added to final concentration of 10 µg/ml and the cell solution was incubated for an additional 30 min at 37 °C. The solution was incubated on ice for 10 min after the addition of 10 ml of Buffer P (200 mM Tris-acetate (pH 8.0), 1.2 M KCl, 8 mM β-mercaptaethanol, 4 mM PMSF and 40% glycerol). Cell debris was removed by centrifugation (15,000 x g for 30 min) and the resulting cell free extract was filtered with a low protein binding, 0.45 µm syringe filter (Fisherbrand). The cell free extract was loaded onto a 10 ml Ni-NTA agarose column (Qiagen), equilibrated with 10 column volumes of Buffer Q (100 mM Tris-Acetate (pH 8.0), 300 mM KCl, 2 mM β-mercaptoethanol, 1% Triton X-100, 1 mM PMSF and 10% glycerol). The column was sequentially washed with 5 column volumes of Buffer 1, 5 column volumes of Buffer R (Buffer Q containing 20 mM imidazole) and 5 column volumes of Buffer S (Buffer R without Triton X-100 and PMSF). The protein was eluted from the column with 7 column volumes of Buffer T (Buffer S containing 250 mM imidazole). Fractions containing the protein were pooled,

concentrated with Amicon Ultra YM-10 centrifugal filtration device (Millipore) and dialyzed against 50 mM Tris-Acetate (pH 8.0), 50 mM KCl, and 2 mM DTT at 4 °C. The recombinant proteins were greater than 90% homogeneous as determined by SDS-PAGE and stored as glycerol stocks at -80 °C. The protein concentration was determined either by Bradford assay (BioRad) using bovine serum albumin as a standard or spectrophotometrically using the extinction coefficient calculated by the amino acid sequence of the denatured protein (6 M guanidine hydrochloride) [102].

Radiochemical Based Assay for GCYH-I and GTPCH-II Activity

COG1469 proteins were analyzed for type I and II GTP cyclohydrolase activity by monitoring the release of [¹⁴C] formate from [8-¹⁴C]-GTP [51, 103]. Assays were carried out in 100 mM Tris-HCl (pH 8.0), 100 mM KCl, 2 mM MgCl₂, 1 mM [8-¹⁴C]-GTP and 5 μM of enzyme in a total volume of 250 μl. Aliquots of 50 μl were taken at specific time points and terminated by the addition of 62.5 μl 0.5 M formic acid. After chilling on ice for 5 min the samples were loaded onto a column containing 250 μl of charcoal equilibrated in 50 mM Tris-HCl (pH 7.5). Radiolabeled formate was washed from the column with the addition of 50 mM Tris-HCl (pH 7.5). Five 2 ml fractions were collected and quantified by liquid scintillation counting.

Spectrophotometric Based Assay for GCYH-I Activity

GCYH-I activity of the COG1469 proteins were assayed spectrophotometrically by monitoring the increase in absorbance at 330 nm ($\epsilon = 6300 \text{ M}^{-1} \text{ cm}^{-1}$) due to the

formation of a dihydroneopterin chromophore [60, 104]. Assays were performed in 100 mM Tris-HCl (pH 8.0), 100 mM KCl, 2 mM MgCl₂, and either 20 μM *E. coli* FoIE or 40 μM COG1469 proteins in a total volume of 100 μl. Reactions were initiated upon the addition of GTP to a final concentration of 0.1 mM and incubated at 37 °C. The reactions were allowed to proceed for 60 min while monitoring the absorbance from 200-400 nm.

Fluorescence Based Assay for GTPCH-I Activity

GTYH-I activity of the COG1469 proteins were assessed by fluorescence according to methods of Nar [52]. Assays were performed in 100 mM Tris-HCl (pH 8.0), 100 mM KCl, 2 mM MgCl₂, and either 10 μM *E. coli* FoIE or 40 μM COG1469 proteins in a total volume of 100 μl. Reactions were initiated upon the addition of GTP to a final concentration of 1 mM and incubated at 37 °C (*E. coli* FoIE, *N. gonorrhoeae* and *B. subtilis* COG1469) or 75 °C (*T. maritima* COG1469). Dephosphorylation of the reaction product was achieved upon the addition of 5 units of alkaline phosphatase followed by a 30 min incubation at 37 °C. The suspected product, 7,8-dihydroneopterin, was oxidized to neopterin with the addition of 12 μl 1% I₂ (w/v) and 2% KI (w/v) in 1 M HCl followed by incubating in the dark at room temperature for 15 min. Excess iodine was reduced by the addition of 6 μl of 2% ascorbic acid (w/v) and the samples were analyzed by fluorescence (excitation 365 nm and emission at 446 nm; slit width of 4 nm) after centrifuging at high speed for 5 min. Fluorescence

based activity assays were also carried out in which the dephosphorylation of the reaction product, was eliminated.

HPLC Based Assay for GCYH-I Activity

Product formation was monitored by HPLC in reactions containing 100 mM Tris-HCl (pH 8.0), 100 mM KCl, 2 mM MgCl₂, 1 mM GTP and either 60 μM *E. coli* FoIE or 100 μM *B. subtilis* COG1469 protein. Reactions were incubated at 37 °C for 60 min in the dark followed by the addition of 5 units of alkaline phosphatase incubated for an additional 60 min at 37 °C. The proteins were removed from the solution using an YM-10 micron centrifugal device and the samples were analyzed by reversed phase HPLC on a Gemini C18 (Phenomenex; 250 X 3.90, 5 μm) column equilibrated in 25 mM ammonium acetate (pH 6.0), at a flow rate of 1 ml/min. The following solvent gradient was used to elute neopterin from the column: (time, % acetonitrile): 0 min, 0%, 10 min 0%, 30 min 4%, 35 min, 50% and 40 min, 0%. Assays were also performed by analyzing the products without dephosphorylation by alkaline phosphatase.

LC-MS Analysis of COG1469 Reaction Product

The preparation of dihydroneopterin triphosphate for LC-MS analysis was achieved in reaction mixtures containing 100 mM Tris-HCl (pH 8.0), 100 mM KCl, 2 mM MgCl₂, 1 mM GTP and either 20 μM *E. coli* FoIE or 40 μM *N. gonorrhoeae* COG1469 protein in a final volume of 500 μl. The reactions were carried out at 37°C for 3 h in the dark

and treated with activated charcoal according to modified methods of Yim [105]. After incubating in the presence of charcoal at 4°C for 30 min in the dark, the mixtures were filtered through a Millipore type HA (0.45 µm) filter. The filter which contains the charcoal was successively washed with 10 ml water, 10 ml 5% ethanol, 10 ml 50% ethanol containing 3.1% ammonium hydroxide (pH 8.0) and 5 ml 50% ethanol containing 3.1% ammonium hydroxide (pH 12) after which the filtrate from the final wash was quickly neutralized with acetic acid.

The fractions were immediately frozen in liquid nitrogen and lyophilized to dryness. The samples containing neopterin triphosphate were suspended in 20 mM ammonium acetate (pH 8.0), and 50% methanol and filtered through a Millipore Amicon ultrafree-MC spin filter. Samples were analyzed by an LCQ Advantage ion-trap mass spectrometer (Thermo Electron, San Jose, CA) equipped with an electrospray ionization (ESI) source. The ion interface was operated in the negative mode using the following settings; needle voltage of 4.5kV; sheath and auxiliary gas flow rates of 25 and 3.0 p.s.i., respectively; tube lens voltage of 50 V; capillary voltage of 3.0 V; and capillary temperature of 275 °C. An instrument method was created to scan the range m/z 50-1100. An isocratic LC mobile phase system consisted of methanol and water (pH 9.0) (1:1 v/v) at a flow rate of 0.4 ml/min. The injection volume was 20-50µl in aqueous 20mM ammonium acetate (pH 8.0).

Temperature and pH optima

The determination of optimal temperature for enzymatic activity of *B. subtilis*, *N. gonorrhoeae*, and *T. maritima* COG1469 proteins, was determined in reaction mixtures containing 100 mM phosphate (pH 7.5), 0.5 mM MnCl₂, 0.5 mM GTP and 2 μM protein in a final volume of 100 μl. After incubating at various temperatures in the dark for 30 min, the reactions were terminated and analyzed by fluorescence as described above.

The optimal pH of *B. subtilis* and *N. gonorrhoeae* COG1469 proteins were determined in a 3 component buffer system composed of Tris-MES-acetic acid (100-50-50 mM) over a pH range of 4.0-9.0. Buffers also contained 100 KCl, 0.5 mM MnCl₂, 2 mM DTT, 50 μM GTP and 1 μM protein in a final volume of 100 μl. After incubating at 37 °C in the dark for 30 min, the reactions were terminated and analyzed by fluorescence as described above.

Molecular Mass Determination

The molecular mass of native wild-type *B. subtilis* and *N. gonorrhoeae* COG1469 proteins were determined by HPLC on a BioSep-SEC-S4000 (300 mm X 7.8 mm, Phenomenex Inc.) gel filtration column. The proteins (100 μg) were eluted with 20 mM sodium phosphate (pH 7.2) and 100 mM NaCl at a flow rate of 0.5 ml/min. Ferritin (443 kDa), pyruvate kinase (237 kDa), alcohol dehydrogenase (150 kDa), BSA (65.4 kDa), ovalbumin (48.9 kDa), and carbonic anhydrase (30 kDa) were used

as molecular weight standards. The void and total column volume were determined from the elution volume of blue dextran and DNP-aspartate (299 Da). Elution of the proteins from the column was monitored by the absorbance at 280 nm. The analysis was also repeated with an elution buffer containing GTP and MnCl₂.

Buffer and Buffer Strength

The effect of buffer on activity was examined for *B. subtilis* and *N. gonorrhoeae* COG1469 proteins in reactions carried out at 37 °C for 20 min in 100 mM buffer (Tris-HCl, HEPES, Tricine and MOPS; pH 8.0), 100 mM KCl, 0.5 mM MnCl₂, 1 mM DTT, 50 µM GTP, and 0.5 µM protein in a final volume of 100 µl. Reactions were terminated and analyzed as described above for fluorescence based activity assays. Follow up studies were conducted with varying concentration of HEPES (pH 8.0) under conditions described above.

Apoenzyme Preparation

Removal of metal ions from COG1469 proteins was achieved by incubating the purified wild-type enzyme in the presence of 5 mM EDTA for 1 h at room temperature followed by dialysis against of 50 mM Tris-HCl (pH 8.0), 50 mM KCl, 5 mM EDTA, and a few grams of Chelex-100 for 4 h at room temperature. The protein sample was dialyzed for an additional 12 h at 4 °C with 3 exchanges of buffer (4 L each). EDTA was removed by dialyzing the resulting apoenzyme solution against 50 mM Tris-HCl (pH 8.0), 50 mM KCl and Chelex-100 for 16 h at 4 °C with three

exchanges of buffer (3 L each). Protein samples were then passed through Chelex-100 resin (5 ml protein solution per 3 ml resin) prior to activity assays or ICP-MS analysis. Protein concentrations were determined spectrophotometrically using the extinction coefficient calculated by the amino acid sequence of the denatured protein (6 M guanidine hydrochloride) [102].

Metal Activation Studies

The effects of metal ions on enzyme activity was examined by incubating the apoenzyme (2 μ M) in the presence of varying concentration (0.1 μ M-4 mM) of metal chlorides (MnCl₂, ZnCl₂, MgCl₂, NiCl₂, CaCl₂, CdCl₂, CoCl₂, CuCl₂, CoCl₃, FeCl₃) in 100 mM HEPES (pH 8.0) and 100 mM KCl for 10 min at 37 °C. Since iron(II) readily oxidizes in the presence of oxygen, all assays involving iron were conducted with Fe(SO₄)₂ under anaerobic conditions with buffers that had been degassed and sparged with nitrogen prior to use. Assays were initiated upon the addition of GTP to a final concentration of 0.1 mM and the reactions were allowed to proceed at 37 °C for 30 min in the dark. Reactions were terminated and analyzed as described above for fluorescence based activity assays.

Determination of Iron Content

The iron content of apo-forms of *N. gonorrhoeae* and *B. subtilis* COG1469 was determined by methods described by Fish [106] and Percival [107]. The proteins (0.5 mg) were precipitated from solution upon the addition of 30% trichloroacetic acid

solution to a final concentration of 5% and volume of 100 μ l. The samples were centrifuged for 5 min at high speed and the resulting supernatant was transferred to a clean 1.5 ml centrifuge tube. The following components were added to the samples in the following order: 0.04 ml of saturated ammonium acetate solution; 0.025 ml 0.12 M ascorbic acid; 0.025 ml 0.25 M FerroZine and milliQ water to 0.3 ml. The resultant mixture was incubated for 30 minutes at room temperature, centrifuged at a high speed, and the absorbance monitored at 562 nm in a 0.5 ml quartz cuvette. An external calibration curve generated from an iron atomic absorption standard solution was used to determine the iron concentration of the protein samples.

Reconstitution of Enzyme with Divalent Metals

Reconstitution of the enzymes was carried out by incubating the purified apoenzyme in the presence of 2-7 molar equivalents of $MnCl_2$ or $ZnCl_2$ in 100 mM HEPES (pH 8.0), 100 mM KCl, and 2 mM DTT for 60 min at 25 °C with gentle shaking. Prior to excess metal removal, the proteins were analyzed for activity as described above for the fluorescence based activity assay. The reconstituted protein was isolated from unbound metal either by: (1) dialyzing against 2 L Buffer Y (50 mM Tris-HCl, (pH 8.0), 50 mM KCl, and 1 mM DTT) for 4 hr at 4 °C (2 exchanges of buffer); (2) passing the protein solution over a Sephadex G-25 column; or (3) extensive dilution and concentration with Buffer Y using the Amicon YM-10 ultra-centrifugal device. The reconstituted proteins were assayed for activity by fluorescence and the metal content was analyzed by ICP-MS.

Metal Analyses by ICP-MS

The metal content of various protein samples was analyzed by ICP-MS. Protein samples (2 mg/ml) were prepared in metal free solutions and acidified below pH 2.0 with the addition of high purity nitric acid to release any protein bound metal ions into solution. The samples were analyzed for the following metal ions; Ni²⁺, Ca²⁺, Co²⁺, Mn²⁺, Zn²⁺ by ICP-MS. An external calibration curve was generated from the multielement calibration standard 2 (Spex CertiPrep). Each sample was prepared in triplicate.

The Effects of DTT upon COG1469 Activity

The effect of DTT on enzyme activity of COG1469 proteins from *B. subtilis* and *N. gonorrhoeae* was examined in UV-vis based assays by monitoring the increase in absorbance at 330 nm ($\epsilon = 6300 \text{ M}^{-1} \text{ cm}^{-1}$) [60, 104]. Assays were carried out at 37 °C in 100 mM HEPES (pH 8.0), 100 mM KCl, 0.5 mM MnCl₂, 10 µM protein, 0.1 mM GTP and varying concentration of DTT (0-12 mM) in a final volume of 110 µl. Absorbance readings from 200-400 nm were recorded for 30 min. The effect of DTT on COG1469 proteins from *B. subtilis* and *N. gonorrhoeae* activity was also monitored using fluorescence based assays performed in 100 mM HEPES (pH 8.0), 100 mM KCl, 0.5 mM MnCl₂, 0.5 µM protein, 50 µM GTP and varying concentration of DTT (0-12 mM) in a final volume of 100 µl. Reactions were incubated at 37 °C for 30 min in the dark and terminated as described above. Follow-up studies examined the effects of DTT on as-isolated and apoenzymes with and without 0.5 mM MnCl₂.

COG1469 Activity as a Function of Time and Enzyme Concentration

A time course analysis of *B. subtilis* and *N. gonorrhoeae* COG1469 activity was performed at 37 °C in 100 mM HEPES (pH 8.0), 100 mM KCl, 0.5 mM MnCl₂, 2 mM DTT, 30 μM GTP and 0.1 μM protein in a final volume of 100 μl. Reactions were terminated at specific time points and analyzed by fluorescence as described above. Enzyme activity was also investigated as a function of enzyme concentration. Reactions were performed as described above except in the presence of varying concentration of enzyme (0.1-2 μM). Reactions were terminated after 15 min and analyzed by fluorescence.

Substrate Specificity Analysis of *N. gonorrhoeae* COG1469 Protein

Substrate specificity of *N. gonorrhoeae* COG1469 was determined with various nucleosides in the presence of 100 mM HEPES, 100 mM KCl, and 0.5 mM MnCl₂. Reactions were incubated at 37 °C for 60 min. Substrate activity with 2'-dGTP, GMP, GTP and guanosine were monitored by fluorescence whereas 8-oxoGTP, 7-deazaGTP, 2'-dGTP, GTP and ATP were analyzed by HPLC.

Kinetic Studies of and *B. subtilis* and *N. gonorrhoeae* COG1469 Proteins

Steady-state kinetic measurements were conducted for *B. subtilis* and *N. gonorrhoeae* COG1469 proteins under initial velocity conditions with varying GTP (3-50 μM) or GDP (50-2000 μM) as substrate. Initial assays were carried out in 100 mM HEPES (pH 8.0), 100 mM KCl, 0.5 mM MnCl₂ and 2 μM of protein in a final volume of 100

μl at 37°C . Subsequent steady state studies were conducted under conditions described above except in the presence of 1 mM DTT and $0.5\ \mu\text{M}$ protein. Time course assays, up to 80 min, were conducted in order to determine initial velocity conditions. Reactions were terminated at various time points and analyzed by fluorescence. Kinetic parameters were calculated from the average of minimally 4 triplicates with the Michaelis-Menten equation using the curve fitting software Kaleidagraph 4.0 (Synergy Software, Reading, PA).

Inhibition Analysis of *N. gonorrhoeae* COG1469 Protein

Inhibition analysis for *N. gonorrhoeae* COG1469 protein was conducted with variable GTP ($3\text{-}50\ \mu\text{M}$) and various fixed concentration of 7-deazaGTP ($15\text{-}60\ \mu\text{M}$), 8-oxo-GTP ($0.1\text{-}0.5\ \mu\text{M}$) and 2'-d-GTP ($0\text{-}200\ \mu\text{M}$). Reactions were carried out as described above in the presence of 1 mM DTT and $0.5\ \mu\text{M}$ protein. The data (average of minimally 4 triplicates) were fitted to the equation for competitive inhibition (eq. 1)

$$v = VS / (K_m(1 + I/K_i) + S) \quad (1)$$

where S is the varied substrate concentration, I is the inhibitor concentration, K_i is the inhibition constant.

Mutagenesis of *N. gonorrhoeae* COG1469 Protein

The His 245 mutants of *N. gonorrhoeae* COG1469 protein were constructed using the QuikChange™ site-directed mutagenesis protocol from Stratagene. Primers were designed to mutate His 245 to Asp (CAC→GAC), Lys (CAC→AAG), Asn (CAC→AAC), Gln (CAC→CAG), Gly (CAC→GGC), Ala (CAC→GCC). The PCR reaction contained 500 ng plasmid DNA encoding the wild-type COG1469 protein from *N. gonorrhoeae*, 200 μM dNTPs, 50 pmol of the sense and antisense primers, 1x Pfu Ultra buffer (supplied by the manufacturer), and 2.5 units of Pfu Ultra DNA polymerase in a final volume of 50 μl. A three step PCR thermocycling protocol was utilized; (1) 95 °C for 1 min; (2) 12 cycles of denaturation at 95 °C for 30 s, annealing at 55 °C for 1 min, and extension at 68 °C for 10 min; (3) 68 °C for 15 min. The PCR reaction mixture was incubated with *DpnI* at 37 °C for 1 h to digest the methylated wild-type DNA template. The mutant plasmids were transformed into *E. coli* NovaBlue competent cells (Novagen) and plated. An isolated colony was used to inoculate 3 ml LB media supplemented with 30 μg/ml kanamycin. After growing the cultures for 12 h at 37 °C with shaking and the mutant plasmids were extracted from the cells. The primary structures of the cloned genes were confirmed by sequencing. The expression plasmid (1 μg) for each of the mutants were transformed into *E. coli* BL21(DE) (100 μl) competent cells and protein expression and purification was carried out according to procedures described for the wild-type protein.

Radiochemical Based Assay for GCYH-I and GTPCH-II Activity

Type I and II GTP cyclohydrolase activity for each of the mutants, with the wild-type *N. gonorrhoeae* COG1469 and *E. coli* RibA functioning as positive controls, were assessed by the release of ^{14}C formate from $[8\text{-}^{14}\text{C}]\text{-GTP}$ according to methods described by Burg [108] and Ferre [103]. Assays were carried out in 100 mM HEPES (pH 8.0), 100 mM KCl, 0.5 mM MnCl_2 , 50 μM $[8\text{-}^{14}\text{C}]\text{-GTP}$ and 50 μM of enzyme in a total volume of 50 μl . Reactions were allowed to proceed at 37 $^\circ\text{C}$ for 60 min and terminated by the addition of 62.5 μl of 0.5 M formic acid. After chilling on ice for 5 min the reaction mixtures were loaded onto a column containing 250 μl of charcoal equilibrated in 50 mM Tris-HCl (pH 7.5). Radiolabeled formate was washed from the column with the addition of 50 mM Tris-HCl (pH 7.5). Five 2 ml fractions were collected and quantified by liquid scintillation counting.

Spectrophotometric Based Assay for Mutant Activity

Each of the mutants were assayed spectrophotometrically, with wild-type *N. gonorrhoeae* COG1469 as a positive control, by monitoring the increase in absorbance at 330 nm ($\epsilon = 6300 \text{ M}^{-1} \text{ cm}^{-1}$) due to the formation of a dihydroneopterin chromophore [60, 104]. Assays were performed in 100 mM HEPES (pH 8.0), 100 mM KCl, 0.5 mM MnCl_2 , and 50 μM mutant *N. gonorrhoeae* COG1469 protein in a total volume of 150 μl . Reactions were initiated upon the addition of GTP to a final concentration of 0.1 mM and incubated at 37 $^\circ\text{C}$. The reactions were allowed to proceed for 2 h while recording the absorbance from 200-400 nm.

Fluorescence Based Assay for Type II and III GTPCH Activity

Reactions catalyzed by *N. gonorrhoeae* COG1469 mutants were analyzed for the potential formation of FAPy or APy according to procedures described by Bracher [59]. Wild-type *N. gonorrhoeae* COG1469 and *E. coli* RibA were utilized as controls. Assays were carried out at 37 °C for 1 h in 100 mM HEPES (pH 8.0), 100 mM KCl, 0.5 mM MnCl₂, 1 mM DTT 0.1 mM GTP and 2 μM enzyme. Reactions were terminated upon the addition of 100 μl of 1 M HCl followed by incubation at 90 °C for 5 min. After adjusting the pH to 8.5 with the addition of 1 M NaOH, butanedione in 1 M Tris-HCl (pH 8.5) was added to each of the assays to a final concentration of 0.5%. The reactions were incubated for 1 h at 90 °C and the formation of 6,7-dimethylpterin was analyzed by fluorescence (excitation 365 nm, emissions 460 nm).

Results

QueA PreQ₁-tRNA^{Tyr}

The expression plasmid, pTrc-Tyr, was expressed in *E. coli* K12QueA, a *queA* deletion mutant strain that produces preQ₁ containing tRNA instead of queuosine modified tRNA [33]. Total tRNA was extracted from the cells using the acid guanidinium thiocyanate/phenol/chloroform protocol [109], of which ~ 20-25% was determined to be preQ₁-tRNA^{Tyr} by tyrosine-tRNA synthetase activity assay.

Enrichment of preQ₁-tRNA^{Tyr} was achieved by mixed-mode chromatography using benzoylated-naphthoylated DEAE-cellulose (BND-cellulose) as described in Material and Methods [81, 82]. PreQ₁-tRNA^{Tyr} eluted from the column in the presence of 1M NaCl and ~10% ethanol (Figure 15). PreQ₁-tRNA^{Tyr} was enriched further by chromatography on a NACSTM (trialkylmethylammonium chloride anion exchange) column, with preQ₁-tRNA^{Tyr} eluting at ~750 mM NaCl (Figure 16) [83, 84]. PreQ₁-tRNA was then precipitated from solution, suspended in 3 mM citrate (pH 6.3) and dialyzed against EDTA to remove any metals. The preQ₁-tRNA^{Tyr} content was 80-90% based on tyrosine-tRNA synthetase activity assay.

[U-*ribosyl*-¹⁴C]ATP Synthesis

A multienzymatic synthesis reaction was used to produce [U-*ribosyl*-¹⁴C]ATP from [U-¹⁴C]glucose (Figure 17) [89, 110]. Seven of the enzymes (hexokinase, myokinase, glutamate dehydrogenase, glucose-6-phosphate dehydrogenase, phosphoriboisomerase and pyruvate kinase) were commercially available, 5 of which

were obtained as sulfate suspensions. Recombinant His₆-tag APRTase was purified in a single step to homogeneity by nickel metal affinity chromatography and appeared as a 25 kDa band on SDS-PAGE gel (Figure 18). PRPP was partially purified by ammonium sulfate precipitation, and appeared as a 34 kDa band on SDS-PAGE gel (Figure 18).

All of the necessary enzymes, excluding glutamate dehydrogenase, were pooled, diluted with Milli-Q water and concentrated by ultrafiltration prior to use. [U-*ribosyl*-¹⁴C]ATP was purified by C18 reverse phase HPLC under isocratic conditions using a mobile phase composed of 83.3 mM triethylammonium acetate (pH 6.0) and 6% methanol. Under these conditions [U-*ribosyl*-¹⁴C]ATP eluted at 24 min (Figure 19). Fractions containing [U-*ribosyl*-¹⁴C]ATP were pooled, lyophilized to dryness and dissolved in Milli-Q water. Typical radiochemical yields were approximately 70-80% after accounting for the loss of ¹⁴CO₂ from C-1 of glucose.

Enzymatic Synthesis of AdoMet and AdoMet Analogs

AdoMet and AdoMet analogs were prepared enzymatically from their respective NTP and methionine or selenomethionine in an AdoMet synthase (MAT) catalyzed reaction (Figure 20). AdoMet synthase from *E. coli* (EcMAT) was overproduced in *E. coli* and purified to 70-80% homogeneity by streptomycin sulfate and ammonium sulfate fractionation (Figure 18). Approximately 100 mg of protein was purified from 10 g of cells. AdoMet synthase from *M. jannaschii* (MjMAT) was expressed as a His₆-tag

fusion protein and purified in a single step by nickel metal affinity chromatography. Approximately 53 mg of MjMAT from 10 g of cells was purified to homogeneity as determined by SDS-PAGE (Figure 18).

EcMAT was utilized in the synthesis of [U-*ribosyl*-¹⁴C]AdoMet and [U-*ribosyl*-¹⁴C]SeAdoMet as well in the synthesis of [1C-methionine-¹⁴C]3'-dAdoMet and [1C-methionine-¹⁴C]7-deazaAdoMet. Since 2'-dATP does not function as a substrate for EcMAT the synthesis of [1C-methionine-¹⁴C]2'-dAdoMet was carried out in the presence of MAT from *M. jannaschii* (MjMAT). Due to the high temperature optimum of MjMAT, the synthesis of 2'-dAdoMet was needed to be carried out at 55°C. Unfortunately, the higher reaction temperatures promoted the decomposition of 2'-dAdoMet. Therefore, to maximize product formation and minimize the decomposition of the newly formed 2'-dAdoMet, reactions were allowed to proceed for 1 h instead of 2 in the presence of 0.6 mg/ml of MjMAT as opposed to 0.2 mg/ml.

AdoMet analogs were purified from their respective nucleoside triphosphates and decomposition products by reverse-phase HPLC under isocratic conditions, with a mobile phase composed of 20 mM ammonium acetate (pH 6.0) and 2% methanol. Under these conditions both [U-*ribosyl*-¹⁴C]-AdoMet and [U-*ribosyl*-¹⁴C]SeAdoMet eluted ~ 10 min (Figure 21), [1-methionine-¹⁴C]3'-dAdoMet and [1-methionine-¹⁴C]7-deazaAdoMet eluted at ~11.5 and 17 min, respectively (Figure 22). The HPLC chromatogram from the enzymatic synthesis of 2'-deoxyAdoMet displayed three

peaks eluting at 8, 12 and 26 min (Figure 23). Unreacted 2'-dATP eluted at 8 min while [1-methionine-¹⁴C]2'-dAdoMet eluted at 12 min, as determined from the amount of radioactivity associated with the peak. The peak at 26 min is probably due to the formation of 2'dMTA as a result of higher reaction temperatures. Typical radiochemical yields of [U-*ribosyl*-¹⁴C]AdoMet and [U-*ribosyl*-¹⁴C]SeAdoMet were 80 and 65%, respectively. The radiochemical yield for [1C-methionine-¹⁴C]-3'-dAdoMet, [1C-methionine-¹⁴C]7-deazaAdoMet and [1C-methionine-¹⁴C]2'-dAdoMet were approximately 70, 45 and 40%, respectively. Each of the samples were lyophilized to dryness and resuspended in 10 mM H₂SO₄.

QueA Expression and Purification

QueA from *E. coli* was expressed as an amino-terminal His₆-tag fusion protein and purified in a single step by nickel metal affinity chromatography. Approximately 120 mg of protein from 10 g of cells was purified to homogeneity as determined by SDS-PAGE (Figure 24). *E. coli* QueA was also expressed as an amino-terminal glutathione-S-transferase fusion protein that was partially purified by affinity chromatography utilizing Glutathione Sepharose 4B (Figure 25A). The protein was purified to 90% homogeneity after HPLC (Figure 25B). It has been demonstrated previously that the GST or the His-tag does not compromised QueA activity, therefore all substrate and inhibition analysis was conducted with the fusion proteins.

Assay Development for the Quantification of Methionine and Adenine

The development of a QueA assay which allows for the quantification of the reaction by methionine or adenine elimination was based on chromatographic procedures used to analyze the decomposition products of AdoMet [111]. To confirm the chromatographic resolution of substrate and products, isotopically labeled AdoMet, methionine and adenine were each analyzed. A QueA reaction with [1C-methionine-¹⁴C]AdoMet was also analyzed. Samples were loaded onto a column containing Dowex-50WX4 equilibrated with 0.1 N H₂SO₄ and the columns were washed with the successive addition of 0.1, 2, and 4 N H₂SO₄ and the eluant was quantified by liquid scintillation counting. Methionine and adenine eluted from the column with the addition of 1 and 2 N H₂SO₄, respectively, whereas AdoMet eluted from the column with the addition of 4 N H₂SO₄ (Figure 26A). Analysis of the QueA catalyzed reaction on Dowex-50WX4 resulted in the resolution of methionine and unreacted AdoMet (Figure 26B). The chromatographic method using Dowex was used in all QueA assays using AdoMet analogs in which methionine or adenine were isotopically labeled.

Substrate Analysis of QueA

SeAdoMet, 3'-dAdoMet, 2'-dAdoMet, and 7-deazaAdoMet were all tested as substrates of QueA under initial velocity conditions. Table 1 summarizes the results obtained from the substrate analysis. No activity was observed for QueA in the presence of 2'-dAdoMet, 3'-dAdoMet and 7-deazaAdoMet regardless of substrate

analog and enzyme concentration. These results suggest that 3'-dAdoMet, 2'-dAdoMet and 7-deazaAdoMet do not function as substrates for QueA.

Very little QueA activity was observed when assayed in the presence of varying concentration of SeAdoMet (Figure 27A). However, activity was observed when QueA concentration was varied (0.2-50 μM) while SeAdoMet was fixed at a 100 μM (Figure 27B). Steady state activity assays conducted in the presence of higher enzyme concentrations gave a K_m of $111 \pm 3 \mu\text{M}$ for SeAdoMet and k_{cat} of 0.0838 min^{-1} to give a k_{cat}/K_m of $0.75 \text{ min}^{-1}\text{nM}^{-1}$ (Figure 28).

Inhibition Analysis of QueA

2'-deoxyAdoMet, 3'-deoxyAdoMet, 7-deazaAdoMet and SeAdoMet were tested as inhibitors using [*U-ribosyl*- ^{14}C]AdoMet as substrate. Table 1 summarizes the results obtained from the inhibition analysis. All AdoMet analogs gave competitive inhibition patterns with respect to AdoMet (Figure 29). Inhibition constants, derived by fitting the data to the competitive inhibition equation, are 217.1 ± 7.3 , 224.4 ± 5.1 , 99.2 ± 2.9 and $138.4 \pm 3.5 \mu\text{M}$ for 2'-deoxyAdoMet, 3'-deoxyAdoMet, SeAdoMet and 7-deazaAdoMet, respectively.

Analysis of the Formation of a Covalent Adduct

Time dependent inactivation studies were conducted in which QueA was preincubated in the presence of SeAdoMet. Aliquots of the preincubation mixture were taken into

standard QueA assay conditions containing [U-*ribosyl*-¹⁴C]AdoMet at various times. Upon analysis, time-dependent inactivation was not observed, suggesting that the formation of a covalent adduct between QueA and SeAdoMet did not occur (Figure 30). To confirm these findings, follow up studies exploiting the presence of the N-terminal His₆-tag on QueA was conducted. The analysis entailed incubating 20-50 μM of QueA in the presence of 20-50 μM tRNA and 100-300 μM of [U-*ribosyl*-¹⁴C]SeAdoMet for 20 min. Samples were directly loaded onto 250 μl of nickel metal affinity resin and unreacted SeAdoMet and tRNA were washed from the column. QueA was then eluted and the eluant was analyzed by scintillation counting. No radioactivity was associated with the fractions containing QueA, demonstrating that QueA did not form a covalent adduct with SeAdoMet.

COG1469

[8-¹⁴C]GTP Synthesis

The enzymatic synthesis of [8-¹⁴C]GTP from [8-¹⁴C]-guanine was based on procedures used in the synthesis of [U-*ribosyl*-¹⁴C]ATP, as illustrated in Figure 31. Of the three enzymes two were commercially available; pyruvate kinase and nucleoside monophosphate kinase. Hypoxanthine-guanine phosphoribosyltransferase (HGPRTase) from *L. donovani* was expressed in a low phosphate media supplemented with the necessary growth factors [98-100] and was partially purified by ammonium sulfate precipitation (Figure 32). The progress of the [8-¹⁴C]GTP synthesis reaction was monitored by TLC over a 24 h period and showed that maximal product

formation was observed at 2 h, with further incubation resulting in a decrease in GTP yield. Therefore, all GTP synthesis reactions were terminated at two hours by the addition of EcMAT and methionine to remove ATP, and [8-¹⁴C]GTP was then purified by HPLC under isocratic conditions using a mobile phase composed of 83.3 mM triethylammonium acetate (pH 6.0), and 5% methanol. Under these conditions [8-¹⁴C]GTP eluted around 7 min (Figure 33). Fractions containing [8-¹⁴C]GTP were pooled, lyophilized to dryness and dissolved in water. Typical radiochemical yields were 50-60%.

Cloning and Expression, and Purification of *T. maritima*, *N. gonorrhoeae* and *B. subtilis* COG1469 proteins

The genes encoding COG1469 proteins from *N. gonorrhoeae* (*ngo0387*), *T. maritima* (*tm0039*) and *B. subtilis* (*ycaA*) were amplified by PCR from genomic DNA and cloned into a linearized pET-30 Xa/LIC expression vector (Novagen) containing an in-frame His₆ cassette allowing for nickel metal affinity purification. The expression constructs also contained a Factor Xa cleavage site immediately adjacent to the start Met to generate wild-type proteins. Each of the proteins were successfully overproduced in *E. coli* BL21(DE) as soluble N-terminal His₆-tag fusion proteins that were purified to homogeneity in a single step by nickel metal affinity chromatography. Recombinant proteins containing fractions from each of the purifications had a yellowish brown tint that disappeared after dialysis. Purified *N. gonorrhoeae*, *T. maritima*, and *B. subtilis* COG1469 His₆-tag proteins showed a major band on a coomassie stained SDS-PAGE gel (Figure 34) with a apparent molecular weights of

33.6, 35.2 and 39.7 kDa, respectively, which were consistent with the molecular masses calculated by the amino acid sequences plus the mass of the N-terminal fusion (Figure 34). Typical yields ranged from 70-110 mg protein per 10 g of cells.

Though the activities of the His₆-tag fusion proteins were comparable to that of the wild-type, all analysis was conducted with wild-type protein, which was obtained by incubating the His₆-tag fusion protein in the presence of Factor Xa followed by nickel metal affinity chromatography. Purified wild-type *N. gonorrhoeae*, *T. maritima* and *B. subtilis* COG1469 proteins showed a major band on a coomassie stained SDS-PAGE gel with apparent molecular masses of 28.7, 30.3 and 34.7 kDa consistent with the molecular masses calculated by the amino acid sequences (Figure 34).

Radiochemical Based Assay for GCYH-I and GCYH-II Activity

The use of radiolabeled GTP at C-8 allows the detection and quantification of enzyme activity by monitoring the elimination of C-8 as formate. Radiochemical analysis utilizing [8-¹⁴C]GTP with each of the COG1469 proteins along with *E. coli* FolE functioning as a positive control demonstrated the time dependent formation of [¹⁴C]-formate (Figure 35). The calculated specific activities for COG1469 proteins under conditions optimal for *E. coli* FolE were 4-10 fold lower than that of the *E. coli* FolE.

Spectrophotometric Based Assay for GCYH-I Activity

To determine if the release of formate was the result of GCYH-I activity, and not GCYH-II activity, enzyme assays were monitored directly by UV-vis spectroscopy to determine if dihydroneopterin was formed. The reactions catalyzed by COG1469 proteins from *B. subtilis* and *N. gonorrhoeae*, resulted in a time dependent decrease of the GTP peak at 252 nm with the concomitant increase of a new broad peak at 330 nm ($\epsilon = 6300 \text{ M}^{-1} \text{ cm}^{-1}$), which is consistent with the formation of a dihydroneopterin chromophore (Figure 36) [60, 104] The calculated specific activities for the formation of the dihydroneopterin compound were 4-6 fold lower than that measured in parallel for *E. coli* FoLE.

Fluorescence Based Assay for GCYH-I Activity

A highly sensitive fluorescence assay was also employed to monitor enzyme activity with the *B. subtilis*, *T. maritima* and *N. gonorrhoeae* COG1469 proteins and *E. coli* FoLE. The analysis entailed the dephosphorylation with alkaline phosphatase of the presumed reaction product, dihydroneopterin triphosphate, followed by oxidation to neopterin with an acidic iodine solution (Figure 37) [52]. Prior to oxidation none of the assay solutions exhibited any fluorescence, but upon oxidation all of the COG1469 catalyzed reaction products exhibited a fluorescence profile identical to that of the *E. coli* FoLE reaction and authentic neopterin (Figure 38).

HPLC Based Assay for GCYH-I Activity

To further aid with identification of the COG1469 reaction product, the dephosphorylated reaction products from *B. subtilis* COG1469 and *E. coli* FolE were analyzed by HPLC according to methods of Nar [52]. The HPLC chromatogram of the *B. subtilis* COG1469 reaction was identical to that of *E. coli* FolE (Figure 39A), with a new peak at ~ 9 min that co-eluted with authentic neopterin and which possessed an identical UV-visible spectrum to that of neopterin (Figure 39B).

When the reaction products from *E. coli* FolE, *N. gonorrhoeae* and *B. subtilis* COG1469 were directly analyzed by HPLC without alkaline phosphatase or acid treatment a new peak appeared at ~4 min that had a UV-vis spectrum that was identical to that of dihydroneopterin (Figure 40). Upon the addition of alkaline phosphatase, the peak eluting at ~ 4 min disappeared and a new peak emerging at ~ 9 min, which co-eluted with and had an identical UV-vis spectrum to that of authentic neopterin, as seen in Figure 40C. Under the work-up and HPLC conditions employed the reaction products were oxidized to neopterin.

LC-MS Analysis of COG1469 Reaction Products

E. coli FolE and *N. gonorrhoeae* COG1469 reaction products were isolated according to Yim utilizing activated charcoal which binds both GTP and dihydroneopterin triphosphate [105]. The reaction mixtures containing charcoal were filtered through a type HA Millipore filter (0.45 μ m) that was subsequently washed with water. GTP

and neopterin triphosphate were eluted from the charcoal with the successive addition of solutions of 5% ethanol and 50% ethanol solution containing 3.1% NH_4OH , respectively. It has been documented by Yim that dihydroneopterin triphosphate is oxidized to neopterin triphosphate under these conditions. MS analysis confirmed that the *E. coli* F01E and *N. gonorrhoeae* COG1469 reactions generated the same products with ions corresponding to unreacted GTP (m/z 522 M-H^- ; m/z 544, $\text{M-2H}^- + \text{Na}^+$; m/z 566, $\text{M-3H}^- + 2\text{Na}^+$), and neopterin triphosphate (m/z 492, M-H^- ; dihydroneopterin is oxidized to neopterin under these conditions). The reactions also contained neopterin cyclic monophosphate (m/z 314, M-H^-), but it has been previously documented that under the alkaline conditions used during the work up neopterin triphosphate is converted to the cyclic monophosphate [112-114].

Temperature and pH Optima

The optimal temperature for *N. gonorrhoeae*, *B. subtilis* and *T. maritima* COG1469 proteins were determined at pH 7.5 in a 100 mM phosphate buffer. *T. maritima* COG1469 protein was active over a broad range of temperatures (68-83 °C), with a maximal activity observed at 78 °C (Figure 41 A). These results are consistent with the organism's optimum growth temperature of 80 °C. *N. gonorrhoeae* and *B. subtilis* COG1469 proteins were active over a broad range of temperatures (30-50 °C) with maximal activity observed at 37 °C (Figure 41 B and C). Subsequent studies were performed at 37 °C for *B. subtilis* and *N. gonorrhoeae* COG1469, and 78 °C for *T. maritima* COG1469. Although the natural habitat of *B. subtilis*, a non-pathogenic soil

bacterium, varies considerably with respect to nutrient, temperature, pH and oxygen content, the temperature profile for *N. gonorrhoeae* COG1469 is consistent with the organism's optimum growth temperature. *N. gonorrhoeae* is a pathogenic bacterium that resides in the mucous membranes of the genital-urinary system of humans.

The effect of pH on *N. gonorrhoeae* and *B. subtilis* COG1469 activity was conducted at a constant ionic strength using a 3 component buffer system comprised of Tris-MES-acetic acid over a pH range of 7-9. The pH profile for both *B. subtilis* and *N. gonorrhoeae* COG1469 proteins displayed a bell shaped curve with activity observed over a pH range of 7.8 to 8.6 (Figure 42), with both proteins displaying maximal activity at a pH of 8.0. Based on these findings all subsequent studies were performed at a pH of 8.0.

Effects of Buffers upon COG1469 Activity

To determine the optimal buffer for activity assays, *B. subtilis* and *N. gonorrhoeae* COG1469 were assayed in various buffers (Figure 43). Maximum activity was observed in HEPES for both proteins. Approximately 15-25% relative activity was observed for both proteins in the presence of MOPS or Tricine.

The effect of HEPES concentration at pH 8.0 upon *B. subtilis* and *N. gonorrhoeae* COG1469 activity are summarized in Figure 44. Maximum activity was observed at a buffer concentration of 100 mM for both proteins. Less than 5% relative activity was

observed at concentrations below 50 mM. Subsequent studies were performed in 100 mM HEPES (pH 8.0).

Metal Analysis

To investigate the importance of metals upon COG1469 activity, the purified proteins were depleted of all metals by treatment with 5 mM EDTA for 1 h at room temperature followed by extensive dialysis against a metal free buffer containing 5 mM EDTA and Chelex-100. The protein samples were dialyzed further against an EDTA free buffer and then passed over Chelex-100 column prior to analysis. When the resulting apoenzymes were analyzed for enzyme activity by fluorescence, no activity was observed, suggesting that the enzymes are metal dependent.

The effect of various metals upon *N. gonorrhoeae* and *B. subtilis* COG1469 activity are summarized in Table 2 and Table 3, respectively. The enzymes were assayed for activity over a range of metal concentrations, and the concentrations supporting maximal activity is listed in Table 2. To circumvent any potential time dependence of metal binding, the apoenzymes were incubated for 10 min in the presence of the metal ions before the assays were initiated with the addition of GTP. *B. subtilis* and *N. gonorrhoeae* COG1469 activity was observed in the presence of Mn^{2+} , Fe^{2+} , Zn^{2+} , Mg^{2+} , Ni^{2+} and Co^{2+} , whereas no activity was observed in the presence of Ca^{2+} , Cd^{2+} , Cu^{2+} , Co^{3+} and Fe^{3+} . Both enzymes were maximally activated in the presence of Mn^{2+} at a concentration of 0.5 mM. The further addition of Mn^{2+} beyond 0.5 mM resulted

in a gradual decrease in enzyme activity (Figure 45). When assayed in the presence of Fe^{2+} under anaerobic conditions, *B. subtilis* and *N. gonorrhoeae* exhibited 75% and 50% relative activity, respectively, to that observed in the presence of 0.5 mM Mn^{2+} . Interestingly, the activity of *B. subtilis* and *N. gonorrhoeae* COG1469 in the presence of an optimal concentration of Zn^{2+} was only ~15% to that observed with Mn^{2+} . COG1469 activity decreased at Zn^{2+} concentrations above 50 μM , and no activity was observed at concentration above 0.5 mM (Figure 45). When the apoenzymes were assayed in the presence of 0.6 mM Mn^{2+} and varying Zn^{2+} concentration, an inhibitory affect was observed (Figure 46).

Various reconstitution procedures were explored with the *N. gonorrhoeae* and *B. subtilis* apoenzymes. The demetallated proteins were incubated in the presence of varying concentrations of Mn^{2+} or Zn^{2+} (2, 4 or 7 molar equivalents) at various temperatures (4, 25 and 37 °C) and times (1-2 h). Aliquots (10 μl) were taken into the appropriate reaction conditions lacking additional metals. The final protein concentration was 0.5 μM , and the final metal concentrations upon dilution were 1, 2 or 3.5 μM . No activity was detected except for control samples that included 0.5 mM MnCl_2 or 50 μM ZnCl_2 (Table 4). When 30 μl aliquots of the reconstitution protein samples were taken into the appropriate reaction conditions lacking metals, activity was observed in those samples in which the final metal concentration upon dilution was 10.5 μM (Table 4). These findings suggest that the metal may not be tightly bound within the active site. Removal of excess metal ion (not bound) was achieved

by passing the protein solution over a Sephadex G-25 or Chelex column, or by extensive dialysis against a metal free buffer, or by buffer exchange with a metal free buffer using an Amicon Ultra centrifugal device. No activity was detected after the removal of excess metal, regardless of method used.

ICP-MS

The metal content of as-isolated (not treated with EDTA) and apoenzyme *N. gonorrhoeae* and *B. subtilis* COG1469 proteins were analyzed by ICP-MS. All protein samples, including the as-isolated were prepared in metal free solutions and acidified with the addition of high purity nitric acid to release the metal into solution. The digested samples were analyzed for the presence of Mn^{2+} , Co^{2+} , Ni^{2+} , Cu^{2+} , Zn^{2+} and Cd^{2+} . Due to argon gas interference the Fe^{2+} content was not examined.

However, iron was not detected in the apoforms of *N. gonorrhoeae* and *B. subtilis* COG1469 proteins when analyzed by the ferrozine assay. Analysis revealed the presence of substoichiometric amounts of Mn^{2+} , Ni^{2+} and Zn^{2+} in all protein samples, including apoenzyme samples, with Zn^{2+} being the predominant metal. The results, summarized in Table 5A, represent the ratio of metal-to-protein (monomeric subunit). Treatment with EDTA resulted in a 3-9 fold decrease in the metal content of the proteins (Table 5A) compared with the protein as isolated, but did not completely remove metal ions from the protein. The presence of Ni^{2+} is likely due to leaching from the nickel metal affinity resin utilized in the purification of the proteins. Based on these results, the demetallation protocol failed to completely demetallate the

proteins, so a follow up analysis incorporated longer incubation and dialysis times in the presence of a higher concentration of EDTA.

In the follow-up analysis of *N. gonorrhoeae* and *B. subtilis* COG1469 proteins, the as isolated, apo-form and the reconstituted Mn^{2+} or Zn^{2+} forms were analyzed by ICP-MS. Again, substoichiometric amounts of metals were detected, with Zn^{2+} being the predominant species. The results, summarized in Table 5B, again represent the ratio of metal-to-protein (monomeric subunit). Demetallation resulted in a 5.5 fold decrease in the Zn^{2+} content and complete removal of Mn^{2+} . After reconstituting *N. gonorrhoeae* COG1469 with Mn^{2+} and removing excess metal, approximately $1.45 \times 10^{-3} \pm 5 \times 10^{-5}$ mol of manganese per mol of protein was detected, $1.71 \times 10^{-2} \pm 2 \times 10^{-4}$ mol of zinc per mol of protein. After reconstituting the apo-COG1469 from *N. gonorrhoeae* with zinc approximately $1.34 \times 10^{-2} \pm 8 \times 10^{-4}$ mol of Zn^{2+} was detected per mol of protein, 9 and 1.7 fold lower than that of the as-isolated and apoenzyme, respectively. Manganese was not detected in samples reconstituted with zinc.

Molecular Mass Determination

The native molecular mass of the wild-type *B. subtilis* and *N. gonorrhoeae* COG1469 proteins were estimated by size-exclusion chromatography on a BioSep-SEC-S4000 column. The column was calibrated using the following standards: Ferritin (443 kDa), pyruvate kinase (237 kDa), alcohol dehydrogenase (150 kDa), BSA (65.4 kDa), ovalbumin (48.9 kDa) and carbonic anhydrase (30 kDa) (Figure 47). *B. subtilis* and *N.*

gonorrhoeae COG1469 proteins eluted with an apparent molecular mass of 102250 ± 2577 and 91872 ± 1982 Da, respectively (Figure 47 and 48). These findings indicate that both enzymes are homotrimers. Incubating the proteins in the presence of GTP (0, 1, 2 mM) and 0.5 mM MnCl_2 at various temperatures and time and using an elution solvent containing 0.5 mM GTP, 0.5 mM MnCl_2 and varying concentration of phosphate buffer did not alter the apparent native molecular mass of either protein.

DTT analysis

The effect of a thiol reductant, DTT, upon *N. gonorrhoeae* and *B. subtilis* COG1469 activity was examined by UV-vis spectroscopy and fluorescence based assays. When analyzed by UV-vis spectroscopy, enzyme activity increased with increasing DTT concentration with maximal activity observed at 2 mM (Table 6). Higher concentrations of DTT up to 12 mM did not result in further stimulation of *B. subtilis* COG1469 activity, however, a gradual decrease in activity was observed for *N. gonorrhoeae* COG1469, with only 78% relative activity observed at 12 mM. When analyzed by fluorescence, fluorescent intensity increased with increasing DTT concentration with maximal fluorescence observed at 1 mM (Table 6). However, greater sensitivity is obtained when analyzing enzyme activity by fluorescence, therefore all subsequent analysis were conducted in the presence of 1 mM DTT and analyzed by fluorescence.

Substrate Analysis

The effects of various nucleosides were explored as potential substrates for the *N. gonorrhoeae* COG1469 enzyme. When GTP was replaced with GDP, GMP, 2'dGTP or guanosine, only GDP was observed by fluorescence, to function as a substrate. The compounds 8-oxoGTP, 7-deazaGTP and ATP were also investigated as alternate substrates, and their behavior was probed by HPLC, in each case only a single peak corresponding to the starting nucleotide was observed in assays with each of these compounds, indicating that they were not turned over by the enzyme.

Steady State Kinetic Analysis of *N. gonorrhoeae* and *B. subtilis* COG1469 Proteins

N. gonorrhoeae and *B. subtilis* COG1469 activity were both time (Figure 49A) and enzyme concentration (Figure 49B) dependent. Steady-state kinetic parameters, summarized in Table 7, were obtained for *N. gonorrhoeae* and *B. subtilis* COG1469 proteins under initial velocity conditions with varying substrate concentrations. Both proteins exhibited classical hyperbolic Michaelis-Menten behavior in all cases (Figure 50 and 51).

Inhibition Analysis of *N. gonorrhoeae* COG1469 Protein

The effects of substrate analogs as potential inhibitors of *N. gonorrhoeae* COG1469 protein are summarized in Table 8. 8-oxo-GTP, 7-deaza-GTP and 2'-deoxyGTP gave competitive inhibition patterns with respect to GTP with a calculated K_i 's of $0.149 \pm 5 \mu\text{M}$, $46 \pm 1.5 \mu\text{M}$, and $164 \pm 3 \mu\text{M}$, respectively (Figure 52).

Mutagenesis of *N. gonorrhoeae* COG1469 H245

The H245K, H245N, H245Q, H245D mutants of *N. gonorrhoeae* COG169 were generated to investigate the catalytic role of His 245. Each of the mutant proteins were successfully overproduced in *E. coli* BL21(DE) cells as soluble N-terminal His₆-tag fusion proteins and were purified to homogeneity in a single step by nickel metal affinity chromatography. Purified mutant proteins showed a major band on a coomassie stained SDS-PAGE gel with an apparent molecular weight of 33.6 kDa which was consistent with the molecular mass calculated by the amino acid sequence plus the mass of the His-tag (Figure 53). Typical yield of the purified proteins ranged from 40-80 mg protein per 10 g of cells. The His₆-tag was cleaved by incubating the fusion protein in the presence of Factor Xa followed by nickel metal affinity chromatography. Purified proteins lacking a His-tag showed a major band on a coomassie stained SDS-PAGE gel with an apparent molecular mass of 28.7 consistent with the molecular mass calculated from the amino acid sequence (Figure 53).

Radiochemical assays utilizing [8-¹⁴C]GTP for each of the *N. gonorrhoeae* COG1469 mutants with wild-type *N. gonorrhoeae* COG1469 and *E. coli* RibA as positive controls demonstrated that all of the mutants were capable of catalyzing the elimination of [¹⁴C]-formate. The calculated specific activities for each of the proteins are summarized in Table 9. Replacing the His residue located at position 245 with either an Asp or a Gln resulted in only a modest 1.5 fold decrease in activity compared

to wild-type, while replacing the His residue with either an Asn or a Lys resulted in an approximate 4 and 19 fold decrease in activity, respectively.

When the reactions catalyzed by the H245D and H245Q mutants were analyzed spectrophotometrically, there was a time dependent decrease in the GTP absorbance at 252 nm and a concomitant increase of a new broad peak centered at 330 nm ($\epsilon = 6300 \text{ M}^{-1} \text{ cm}^{-1}$), consistent with the formation of a dihydroneopterin chromophore (Figure 54A and B) [60, 104]. The specific activities for the formation of dihydroneopterin triphosphate were 4.3 and 3.4 $\text{nmol min}^{-1} \mu\text{mol}^{-1}$ for H245D and H245Q, respectively, which are 33 to 41 fold lower than that of the wild type (Table 10). Spectroscopic assays of the H245N and H245K did not result in the formation of dihydroneopterin as indicated by the lack of absorbance at 330 nm (Figure 54C and D).

In a type I GTP cyclohydrolase fluorescent assay, the H245D and H245Q mutants catalyzed reactions resulted in a product that displays a fluorescent spectra identical to that of wild-type, consistent with the formation of dihydroneopterin (Figure 55). H245N and H245K mutants did not generate products capable of fluorescence in this assay, indicating that dihydroneopterin was not generated. When analyzed as a function of substrate concentration, H245D and H245Q activity increased with increasing GTP up to 500 μM , whereas wild-type activity decreased at GTP concentrations above 200 μM (Table 11). The relative activities of H245D and

H245Q, as determined by fluorescence, were 19 and 48 fold lower than that of the wild-type.

In a type II and III GTP cyclohydrolase activity assay, the reaction assays were boiled in HCl, neutralized with NaOH and incubated with butanedione (Figure 56) [59]. The reaction was then analyzed by fluorescence with an excitation of 365 nm and an emission of 460 nm. Fluorescence was observed in all cases except for reactions catalyzed by H245K (Figure 57). Replacing the His residue with either an Asp or a Gln resulted in a 12 fold decrease in the relative activity compared to that of wild-type whereas replacing with an Asn resulted in a 33 fold decrease in activity.

Discussion

QueA Analysis

QueA catalyzes the penultimate step in the biosynthesis of queuosine; the unprecedented transfer and isomerization of the ribosyl moiety from AdoMet to preQ₁-tRNA to give epoxyqueuosine modified tRNA (oQ-tRNA) as illustrated in Figure 3. The reaction is accompanied by the rearrangement of the ribosyl moiety to form an epoxy-carbocycle and the elimination of methionine and adenine from AdoMet [32, 33]. A chemical mechanism has been proposed for QueA and is consistent with the kinetic mechanism and biochemical studies carried out to date (Figure 5) [44]. The first step of the QueA catalyzed reaction is proposed to be the deprotonation of AdoMet at C-5' to give the sulfonium ylide I.

To investigate the timing of proton abstraction of C-5', the sulfur atom of AdoMet was replaced with a selenium atom. SeAdoMet is both isosteric and isoelectric with AdoMet, but the replacement of sulfur with selenium increases the apparent pK_a of the C-5' hydrogen from 11.5 to 14.1 [94, 115]. It has been calculated that a pK_a difference of 2.6 units would result in a ~400 fold decrease in the deprotonation rate constant [94, 115]. If deprotonation is at least partially rate limiting SeAdoMet will react slower than AdoMet.

An alternative to the proposed mechanism involves the direct S_N2 attack by the preQ₁-tRNA aminomethyl at the 4' carbon of AdoMet followed by deprotonation to give the

sulfonium ylide **III** (Figure 58). Although the S_N2 route is mechanistically simpler than the proposed mechanism, it is not favorable at a 2° carbon, and nucleophilic substitution reactions in biology are dominated by elimination and addition mechanistically and not S_N2 [116]. Nevertheless, none of the results from previous mechanistic studies explicitly ruled out this mechanism, and thus remains a viable alternate to the existing proposal.

If the S_N2 mechanism is occurring then SeAdoMet should not act significantly different than AdoMet with respect to radioactive quantification because the ribosyl moiety would be attached to the tRNA that is precipitated upon the addition of TCA and quantified (Figure 59B).

QueA exhibited very low activity with [U-*ribosyl*]-SeAdoMet even when present at high concentrations. Replacing AdoMet with SeAdoMet had little effect upon substrate binding but exhibited 30-fold reduction in k_{cat} . When analyzed as a potential inhibitor, a K_i of $99.2 \pm 0.9 \mu\text{M}$ for SeAdoMet was obtained, which is comparable to the K_m of AdoMet. These results demonstrate that SeAdoMet binds to QueA with an affinity comparable to that of AdoMet and that the replacement of the sulfur atom with selenium decreased the rate of the catalytic steps, presumably deprotonation, following substrate binding. These results are most consistent with a mechanism in which deprotonation at C-5' precedes nucleophilic attack at C-4'.

While the substitution of selenium for sulfur in AdoMet decreases the reactivity of the 5'-hydrogen to deprotonation the electrophilicity of the 5' carbon of SeAdoMet is roughly ten times greater than in AdoMet [94]; this creates the potential for nucleophilic attack instead of deprotonation exist leading to the formation of a covalent adduct (Figure 59C).

However, we observe no time dependent inhibition of QueA when incubated with SeAdoMet, nor did we observe the transfer of ^{14}C from [U-ribosyl- ^{14}C]-SeAdoMet to enzyme, demonstrating that a covalent adduct between QueA and SeAdoMet did not occur. These results demonstrate the transfer of the ribosyl moiety from SeAdoMet to the modified tRNA, and not with the formation of a covalent adduct between protein and substrate.

QueA catalysis entails the transfer of the ribosyl moiety from AdoMet onto tRNA with the elimination of adenine and methionine. When the radiolabel is located in the ribosyl moiety of AdoMet, QueA activity can be assessed by measuring the amount of radioactivity incorporated into tRNA via TCA precipitation. When the isotopic label is located in methionine or adenine moiety of AdoMet, QueA activity can not be monitored by TCA precipitation because neither of the groups are transferred to the tRNA during catalysis. The development of an assay that allowed for the direct measurement of either methionine or adenine was crucial for the analysis of methionine and adenine labeled AdoMet analogs. Utilizing Dowex as a means to

quantify QueA activity proved successful with greater accuracy and resolution than other cation exchange methods involving P-11, P-81, and activated charcoal.

Furthermore, using Dowex gave flexibility in terms of quantifying methionine, adenine and/or AdoMet and was therefore used to evaluate [1-methionine-¹⁴C]-7-deazaAdoMet, [1-methionine-¹⁴C]-2'dAdoMet, and [1-methionine-¹⁴C]-3'dAdoMet as potential substrates for QueA.

The second step of the proposed chemical mechanism involves the opening of the ribose ring with concomitant elimination of adenine (Figure 5). The cleavage of the N-glycosidic bond of AdoMet and the subsequent release of adenine must occur in concert with the protonation of adenine to activate it for elimination. In principle this can occur at N-7, N-3 and/or N-1. Nucleoside hydrolases, which play an important role in the purine salvage pathways, are example of enzymes involved in the hydrolysis of the N-glycosidic bond of ribonucleosides to give free base and ribose. The catalytic mechanism of nucleoside hydrolase entails leaving group activation via protonation at the N-7 atom of the purine ring, a process that is also observed in many other N-glycosidic bond cleaving enzymes [117]. Replacing the natural substrate of nucleoside hydrolase or S-adenosylhomocysteine hydrolase (AdoHcy hydrolase) with a 7-deaza analog, in which the nitrogen at position 7 is replaced with a carbon atom, prevents the activation and elimination of the leaving group [90, 118-121].

7-deazaAdoMet failed to function as a substrate for QueA which is consistent with leaving group activation via protonation at N-7 is essential for QueA activity. The 7-deaza analog of AdoMet exhibited a K_i that was only slightly higher than the K_m for AdoMet, indicating that N-7 is critical for catalysis and not substrate binding.

Although not directly involved in catalysis or outlined in the proposed mechanism, the presence of the two ribose hydroxyl groups on the ribosyl moiety may collectively add to the binding energy by means of hydrogen bond formation. Disruption of the hydrogen bonding opportunities between nucleoside hydrolase and substrate by replacing the 2' or the 3' hydroxyl groups with a hydrogen atom resulted in little or no activity [117, 120]. Furthermore, deoxynucleoside analogs of nucleoside hydrolase functioned as poor inhibitors, thus demonstrating the necessity of the hydroxyls in substrate recognition and catalysis [120]. Neither the 2' nor 3' deoxyanalog functioned as a substrate for QueA, but unlike the results observed with nucleoside hydrolase the binding was only moderately compromised, with both compounds exhibiting K_i values only 2 fold above the K_m of AdoMet.

The results obtained from these studies are consistent with the proposed mechanism as outlined for QueA, where the first step involves the enzyme catalyzed deprotonation of AdoMet at C-5', and the cleavage of the C-N bond and the release of adenine occurs in concert with the protonation of adenine at N-7. Although not shown, the presence of the ribosyl hydroxyl groups is needed for catalysis.

COG1469 Analysis

Early biosynthesis studies had shown that GTP was the metabolic precursor to queuosine, in a transformation involving the loss of C-8 from guanine, suggesting GTP cyclohydrolase like chemistry [122]. Comparative genomics analysis was conducted to determine if the participation of GCYH-I in the biosynthesis of queuosine was a viable hypothesis. Analysis of all sequenced bacterial genomes revealed that *folE*, the gene encoding GCYH-I, clustered with known queuosine biosynthesis genes in a number of organisms. These findings support the potential involvement of GCYH-I in queuosine biosynthesis. However, *folE* was absent in a large number of bacterial genomes that contain queuosine biosynthetic genes, and more importantly other folate biosynthesis genes. It was therefore presumed that another unidentified protein family was responsible for conversion of GTP to H₂NTP in those organisms lacking *folE*. Utilization of the newly developed SEED database resulted in the identification of a protein family, COG1469, which was of unknown function and clustered with folate and/or queuosine biosynthesis genes in a number of organisms.

To test the hypothesis that members of COG1469 are type I GTP cyclohydrolases, an *E. coli* Δ *folE*::Kan^R mutant strain was constructed and utilized in complementation studies. The mutant proved to be lethal but partially rescued when grown in a rich medium supplemented with thymidine (LB/dT) (Figure 60) [123]. However, when transformed with COG1469 gene from *B. subtilis* (*yciA*), *T. maritima* (*tm0039*) or

Acinetobacter baylyi, complementation was observed even in the absence of thymidine. These observations are consistent with the COG1469 proteins exhibiting GCYH-I activity and, was therefore proposed to catalyze the conversion of GTP to H₂NTP.

Potential GTP cyclohydrolase activity was investigated by four different methods; radiochemical based release of [¹⁴C]-formate [103], UV-vis spectroscopy [104, 124], fluorescence [52, 58], and HPLC analysis. All assays were run in parallel with GTP cyclohydrolase I (FolE) from *E. coli* as a positive control, under standard GCYH-I conditions. Although [8-¹⁴C]GTP was commercially available, it was more economical to synthesize it enzymatically according to methods similar to those utilized in the synthesis of ribosyl-labeled ATP. In a radiochemical analysis, each of the proteins along with *E. coli* FolE catalyzed the elimination of [¹⁴C]-formate when incubated in the presence of [8-¹⁴C]GTP, consistent with the hydrolytic ring-opening and deformylation of GTP at C-8. When analyzed by UV-vis spectroscopy and fluorescence the catalytic formation of a dihydroneopterin compound was observed in all cases. To confirm that fluorescence was due to the formation of dihydroneopterin triphosphate, the dephosphorylated and oxidized reaction products from *B. subtilis* COG1469 and *E. coli* FolE catalyzed reactions were analyzed by HPLC. Each of the reactions contained a new peak that had the same retention time and UV-vis spectrum to that of neopterin. Furthermore, this new peak co-eluted with authentic neopterin, suggesting the formation of dihydroneopterin.

GCYH-I is known to convert GTP to H₂NTP and formate, however, recent studies conducted on COG1469 homolog from *M. jannaschii* had demonstrated the catalytic formation of 7,8-dihydro-D-neopterin 2,3-cyclic phosphate and formate from GTP (Figure 61) [125]. The cyclic monophosphorylated form of dihydroneopterin is not susceptible to dephosphorylation by alkaline phosphatase unless it is first subjected to acid hydrolysis [126]. When *N. gonorrhoeae* and *B. subtilis* COG1469 catalyzed reactions, along with *E. coli* FolE as a positive control, were analyzed by HPLC, each of the reaction products were dephosphorylated in the presence of alkaline phosphatase. These findings demonstrate the formation of a phosphorylated dihydroneopterin compound that is not cyclic in nature.

Finally, through MS analysis it was shown that like *E. coli* FolE, the *N. gonorrhoeae* COG1469 reaction produced a product whose molecular weight was identical to that of neopterin triphosphate. Notably, both reactions also contained neopterin cyclic monophosphate, but it has been previously documented that under the alkaline conditions used during the work up neopterin triphosphate is converted to the cyclic monophosphate [112-114].

These studies provided direct biochemical evidence that COG1469 catalyzes the conversion of GTP to dihydroneopterin triphosphate and formate. Collectively, the results obtained from biochemical and genomic analysis clearly demonstrate that COG1469 exhibit type I GTP cyclohydrolase activity, and therefore the gene and

proteins were renamed *folE-2* and GCYH-IB, respectively, and the canonical GCYH-I and the corresponding gene were renamed GCYH-IA and *folE1*, respectively. For the remainder of the discussion COG1469 proteins will be referred as GCYH-IB.

Primary sequence alignment of GCYH-IB (denoted as COG1469) and GCYH-IA proteins (Figure 62), demonstrates the apparent lack of homology between the two protein families. Notably, conserved residues involved in catalysis in GCYH-IA (His113, Glu152, and His179, numbering based on *E. coli* FolE) and metal binding (Cys110, His112 and Cys181; numbering based on *E. coli* FolE) are absent in GCYH-IB proteins [61]. GCYH-IB proteins also do not exhibit sequence homology to any other known protein family. However, when the primary and the predicted tertiary structure of the C-terminal region of GCYH-IB was aligned with GCYH-IA enzymes, a ~16% sequence similarity was observed (Figure 63) [123].

Based on the predicted 3D structure, GCYH-IB proteins are members of the tunnel-fold (T-fold) structural family [123], a superfamily of enzymes that include urate oxidase (UOX), 6-pyruvyl tetrahydropterin synthase (PTPS), dihydroneopterin aldolase (DHNA), GTP cyclohydrolase I (GCYH-I) and QueF. Despite the low sequence identity (~10%), observed among family members, there is high tertiary structural homology among T-fold proteins. All members have identical topologies containing a T-fold domain which is composed of four antiparallel β -sheet and two antiparallel α -helices between the second and third strand, forming a $\beta_2\alpha_n$ barrel

(Figure 64) [127]. All are large multimeric structures composed of smaller monomeric subunits of ~130 residues. The oligomerization of the functional enzymes entails the association of two multimeric barrels in a “head-to-head” fashion resulting in the formation of a tunnel-like center running through the multimer (Figure 65). Although members differ with respect to function and catalytic mechanism they all bind to planar substrates such as purine or pterin like compounds at the interface between monomers in which a conserved glutamate or a glutamine residue anchors the substrate at the bottom of the active site (Figure 66) [127]. Importantly, the conserved Glu residue (Glu 152 of *E. coli* FolE numbering) involved in substrate binding in GCYH-I enzymes was conserved in a comparable position in GCYH-IB proteins.

GCYH-IA enzymes can be categorized into two structural subfamilies; homodecameric enzymes consisting of unimodular 26 kDa T-fold domains as observed in the bacterial and mammalian GTPCH-IA, and bimodular 50 kDa proteins consisting of two tandem T-fold domains as observed in plant GCYH-IA [58, 112, 128]. The predicted tertiary structure of the N-terminal region of COG1469 proteins is most similar to 7,8-dihydroneopterin triphosphate epimerase, whereas the predicted tertiary structure of the C-terminal region is most similar to 7,8-dihydroneopterin aldolase (DHNA) (Figure 67). Based on the size of the GCYH-IB proteins (~250-300 residues) and the presence of two predicted T-fold domains suggest the GCYH-IB proteins are members of the bi-modular subfamily of the T-fold superfamily (Figure

67). In addition to plant GCYH-IA, other bi-modular T-fold proteins include urate oxidase [127] and the type II QueF proteins exemplified by the *E. coli* homolog [129].

By size-exclusion chromatography both the *B. subtilis* and the *N. gonorrhoeae* GCYH-IB were determined to be homotrimers. *E. coli* FolE is reported to be a 247 kDa decamer that consists of a tightly associated dimer of pentamers that dissociates into smaller molecular weight subunits under high salt conditions [52, 58, 130]. However, in the presence of GTP the ionic dissociation of FolE is prevented. This phenomenon was not observed with GCYH-IB from *B. subtilis* or *N. gonorrhoeae*; the trimeric nature of the proteins was not altered under high ionic strength or in the presence of GTP and $MnCl_2$ suggesting that the monomeric units are tightly associated. In contrast to the gel filtration analysis, the crystal structure revealed that the GCYH-IB from *N. gonorrhoeae* was a homotetramer. The results obtained from X-ray crystallography are consistent with the oligomerization pattern of T-fold proteins and therefore may be a more accurate representation of the oligomeric nature of *N. gonorrhoeae* GCYH-IB.

GCYH-IA contains an essential zinc metal ion that has been shown to function as a Lewis acid in the activation of the water molecule that subsequently undergoes a nucleophilic attack at C-8 of GTP (Figure 9). The zinc ion has also been proposed to assist in the nucleophilic attack of a second water molecule by polarizing the resulting amide carbonyl. In *E. coli* FolE the zinc atom is coordinated by Cys-110,

His-113 and Cys-181. These residues are strictly conserved in all GCYH-IA [58, 61]. Furthermore, the zinc coordinating residues are located in two conserved motifs, CEHH and HXC, which are separated by ~70 residues. In GCYH-IB enzymes, these two conserved motifs are missing and replaced with CP-C/H/S-A/S and ESXHXH, that are separated by ~100 residues [123]. Also, the zinc coordinating residues His-113 and Cys-181 found in GCYH-IA are replaced with Ser/Ala and His residues, respectively (Figure 63), suggesting that metal binding may be substantially different.

The *N. gonorrhoeae* and *B. subtilis* GCYH-IB were treated with metal chelating reagents, EDTA and Chelex-100, to remove all metals from the proteins. As a result the proteins were rendered inactive. Although, it has been reported that *E. coli* F0I E is not dependent upon any coenzymes or metals besides zinc for activity, GCYH-IB proteins were maximally activated in the presence of Mn^{2+} , whereas only 15% activity was restored by the addition of Zn^{2+} . GCYH-IB homolog from *M. jannaschii* was shown to be maximally activated in the presence of Fe^{2+} [125]. However, for the bacterial enzymes, Fe^{2+} restored 50-75% activity compared to that of Mn^{2+} .

By ICP-MS analysis only substoichiometric amounts of Mn^{2+} and Zn^{2+} were detected in all protein samples, even after reconstitution. These findings suggest that manganese is not tightly associated to the proteins and readily dissociate from the protein upon purification and dilution, consistent with the intrinsic properties of manganese.

Manganese is a characteristically labile metal that readily dissociates from proteins upon purification. The lability of manganese is reflected in the thermodynamic instability of its complexes with the side chains of amino acids and its affinity for water [131, 132]. Furthermore, the manganese ions found in manganese dependent enzymes are in dynamic equilibrium with the metal ions of the surrounding environment, and binding is dependent upon the environmental concentrations and the protein affinity towards Mn^{2+} [132]. Restoration of manganese dependent enzyme activity can be achieved upon the addition of manganese to the assay mixture.

The detection of Mn^{2+} and Zn^{2+} by ICP-MS and knowing that GCYH-IA is a zinc dependent enzyme, lead us to examine the effects of both metals on activity. An antagonistic effect was observed, where Mn^{2+} stimulated activity decreased with increasing zinc concentration. These findings are consistent with loosely associated manganese that is readily replaced with a zinc ion.

Although Zn^{2+} (0.74 Å) and Mn^{2+} (0.75 Å) are almost the same size, the metals differ with respect to ligand preference [133]. Manganese has been characterized as a hard metal ion that favors oxygen over nitrogen or sulfur donating ligands. Some common oxygen donating ligands are; H_2O , OH^- , OR^- , Glu, Asp, Tyr, Ser, and Thr [134]. Zinc has been described as borderline in hardness which favors nitrogen, oxygen and sulfur donating ligands such as His, Glu and Cys residues [134]. Although GCYH-IB proteins from *B. subtilis* and *N. gonorrhoeae* are less active in the presence of zinc, the

proposed metal binding site made up of Cys, Ser (or an Ala) and a His, may favor the binding of zinc and not manganese, however a detailed examination is needed to confirm the binding affinity of each metal in GCYH-IB proteins. However, these results clearly demonstrate that GCHY-IB homologs found in *N. gonorrhoeae* and *B. subtilis* are manganese dependent enzymes. Since divalent manganese can also function as a Lewis acid with properties comparable to that of zinc, it is believed that manganese maybe functioning analogous to that of zinc found in GCYH-IA by activating a nucleophilic water molecule needed in the deformylation of GTP [134, 135].

Although the K_m values for GTP were not substantially affected, the addition of DTT resulted in a 7 and 3 fold increase in k_{cat} for *N. gonorrhoeae* and *B. subtilis* GCYH-IB, respectively. Though the effects of DTT upon *B. subtilis* GCYH-IB activity were not as substantial as those observed for GCYH-IB from *N. gonorrhoeae*, this could be rationalized by the use of freshly purified *B. subtilis* protein that had been extensively dialyzed against a buffer containing DTT. The effects of DTT upon catalytic efficiency occur at the chemical steps following substrate binding, as reflected in the increase in k_{cat} . Thiol reagents, such as DTT, are known to prevent the oxidation of thiol containing residues and the formation of disulfide bonds. Although there are 3 cysteine residues, only two are conserved (Cys-146 and Cys-148, numbering based on *N. gonorrhoeae* enzyme) in GCYH-IB proteins. The two conserved Cys residues are

in close proximity to one another and are believed participate in catalysis by coordinating the metal ion, consistent with the mechanism proposed for GCYH-IA.

Although GTP was the preferred substrate, it was demonstrated that GDP also reacted with GCYH-IB. GDP exhibited a 20-25 fold increase in K_m and a 1.5-3 fold decrease in k_{cat} . These findings indicate that the removal of the γ phosphate group has little effect upon the catalytic steps occurring after substrate binding. Although GDP functions as an inhibitor of *E. coli* FolE with a K_i of 1.5 μ M, the kinetic constants obtained for GDP were comparable to those reported for *T. thermophilus* GCYH-I [105, 136]. When GMP and guanosine were analyzed as substrates no activity was observed. These results clearly demonstrate that the phosphate groups are necessary for substrate binding and therefore catalytic efficiency.

In addition to substrate analysis, inhibition studies using 8-oxoGTP, 7-deazaGTP and 2'-dGTP were also conducted with GCYH-IB from *N. gonorrhoeae* in hopes of gaining insight into the catalytic mechanism. While all three functioned as competitive inhibitors with respect to GTP only 8-oxo-GTP functioned as a potent inhibitor of GCYH-IB with a K_i/K_m of 0.022, which is 300 and 1000 fold lower than the K_i/K_m for 7-deazaGTP and 2'-dGTP, respectively.

The higher affinity to the enzyme exhibited by 8-oxoGTP and its structural resemblance to the putative reaction intermediate, suggest that 8-oxoGTP maybe

functioning as a transition state inhibitor of GCYH-IB, consistent with what has been reported for GCYH-IA from *T. thermophilis* [136]. Although 8-oxoGTP can undergo keto-enol tautomerization, it has been reported that at neutral pH the keto form predominates (Figure 68) [137]. When 8-oxoGTP was analyzed as a potential substrate, no activity was detected. These results are consistent with the proposed GCYH-IA chemical mechanism in which replacing GTP with 8-oxoGTP, where N-7 is protonated and C-8 is oxidized to the carbonyl state (keto form), would prevent the hydrolysis and deformylation of GTP (Figure 9).

The 7-deazaGTP analog exhibited a K_i value that was 7 fold lower than the K_m of GTP, suggesting that binding was moderately affected. However, 7-deazaGTP did not function as a substrate for GCYH-IB. These results are consistent with the proposed chemical mechanism of GCYH-IA, in which replacing the nitrogen at position 7 with a carbon, would prevent the hydrolysis and deformylation of GTP (Figure 9).

Hydrogen bond formation is an integral part of substrate binding and catalysis.

Studies with crystal structure of GCYH-IA from *T. thermophilis* had reported the formation of 4 hydrogen bonds between the enzyme and the ribosyl moiety of GTP and replacing the hydroxyl group would result in the loss of 3 hydrogen bonds [136].

The 2'-deoxy analog of GTP exhibited a K_i value that was 24 fold higher than the K_m of GTP, suggesting binding was compromised with the removal of the 2'-hydroxyl group. When GTP was replaced with 2'dGTP, the formation of dihydroneopterin

triphosphate was not observed, as determined by fluorescence. Although these results indicate that the 2'-hydroxyl group is needed in the formation of dihydroneopterin triphosphate, consistent with the proposed mechanism of GCYH-IA (Figure 9), they fail to determine if 2'dGTP undergoes the initial deformylation when assayed with GCYH-IB proteins. Utilizing [8-¹⁴C]-2'dGTP or employing a type III GTP cyclohydrolase fluorescence based assay will determine if GCYH-IB catalyzes the deformylation of 2'dGTP.

Despite the structural differences between the type IA and IB cyclohydrolase families, we believe that the chemical mechanism of GCYH-IB is similar to that of GCYH-IA, which catalyzes the conversion of GTP to dihydroneopterin triphosphate and formate through a mechanistically complex ring expansion reaction (Figure 9). A chemical mechanism has been proposed for GCYH-IA and is consistent with crystallography and biochemical studies, including mutagenesis, NMR analysis and transient state kinetics [52, 58-61]. The reaction is initiated with the reversible hydrolysis of GTP at C8-N9 via a nucleophilic attack of a zinc activated water molecule to form an N-formyl intermediate, which subsequently undergoes a 2nd hydrolysis reaction resulting in the elimination of C-8 as formate. The ribosyl moiety undergoes ring opening and an Amadori rearrangement followed by cyclization and dehydration to give the pterin ring.

In the primary and predicted tertiary alignment, His 245 of *N. gonorrhoeae* GCYH-IB was conserved in a comparable position to His 179 of *E. coli* FolE (Figure 63). Based on these findings it was believed that H245 may function analogously to H179 by facilitating the elimination of C-8 as formate either by donating a proton to N-7 of GTP directly [59] or by coordinating a second water molecule needed for hydrolysis (Figure 9) [136]. To test the necessity of H245 in the elimination of formate the His residue at position 245 was mutated to Asp, Gln, Lys and Asn and the resulting mutants were analyzed for activity. Upon analysis utilizing [8-¹⁴C]GTP, each of the mutants demonstrated the release of [¹⁴C]-formate which is consistent with the hydrolytic ring opening and deformylation of GTP at C-8. Furthermore, these results are not consistent with those of H179 of *E. coli* FolE, therefore H245 may have a different role in catalysis other than in the deformylation of GTP.

When analyzed by UV-vis and fluorescence, dihydroneopterin triphosphate formation was observed for H245D and H245Q mutants. In contrast, the H245N and H245K mutants failed to generate dihydroneopterin triphosphate. It has been reported that the replacement H179 of *E. coli* GCYH-IA results in the accumulation of the N-formyl reaction intermediate, which can be analyzed in a type III GTP cyclohydrolase fluorescence based assay. The assay entails the derivatization of the reaction product to 6,7-dimethylpterin. However the same assay can be used to analyze type II GTP cyclohydrolase activity which catalyzes the formation of the deformylated reaction product. Fluorescence was observed in those reactions catalyzed by H245D, H245Q,

and H245N mutants, and not for H245K mutant. By radiochemical analysis, we were able to demonstrate that each of the mutants catalyzes the release of formate, therefore the formation of 6,7-dimethylpterin could be due to the catalytic generation of the deformylated product.

The results obtained from the biochemical analysis are consistent with H245 functioning different to that of H179 of *E. coli* GCYH-IA. Insight into the probable role of H245 came with the realignment of GCYH-IB and GCYH-IA primary structures based on the X-ray crystal structure of *N. gonorrhoeae* GCYH-IB. Due to a pending patent the new alignment and the recently solved crystal structure of *N. gonorrhoeae* GCYH-IB will not be presented nor discussed in detail. The realignment revealed that H245 was not located in a comparable position to that of H179 of *E. coli* FolE, and instead it is involved in the coordination of a second metal ion. Though the rates of deformylation were lower to that of the wild-type, mutating His 245 could have disrupted the second metal site that is needed in the steps following the elimination of C-8.

COG1469 proteins represent a new prokaryotic type I GTP cyclohydrolase that requires a Mn^{2+} ion for maximal activity. We are currently conducting further biochemical analysis that will help elucidate the chemical mechanism of this new family of enzymes. Further analysis will entail, but not limited to site directed mutagenesis of the conserved residues believed to be involved in metal ion

coordination and acid/base chemistry; transient state kinetics which allows for a detail characterization of the events taking place during catalysis and in the identification of stable reaction intermediates, and the examination of the metal binding affinity.

Future work will also entail the development of a high throughput assay allowing for the screening of potential inhibitors of GCYH-IB which is present in a number of pathogenetic bacteria such as; *N. gonorrhoeae* and *S. aureus*. Knowledge of the crystal structure will aid in the structure base design of potential inhibitors that are selective towards this new family of enzymes.

The phylogenetic distribution of *folE-1* and *folE-2* genes among sequenced organisms revealed *folE2* is present in most archaea and ~20% of bacteria (Table 13). However, homologs of *folE2* are absent in eukaryotes including humans [123]. The distribution of *folE* and *folE2* varies among bacteria and can be divided into 4 groups. In group one which includes *E. coli*, only one *folE* homolog was observed whereas the second group that includes *S. aureus* and *N. gonorrhoeae*, contain only the *folE2* homolog. A third group which includes *B. subtilis* and *A. baylyi*, contains a *folE* and a *folE2* homolog whereas the fourth group that includes *P. aeruginosa* contains multiple copies of each genes. It is unclear as to why both or multiple copies of each gene are present in a number of organisms, but it may be attributed to the affects of environmental conditions upon organism growth and/or the potential involvement of these genes in other pathways besides folate biosynthesis. Comparative genomic analysis revealed that *folE-2* genes clustered with genes encoding putative metal

chaperones, suggesting that *folE-2* genes may be up-regulated under zinc starved conditions, which is consistent with the differences in metal specificity to that of GCYH-IA and observed inhibitory effects of zinc upon manganese stimulate GCYH-IB activity. We are currently examining the putative function and role of these metal chaperones upon GCYH-IB activity. The necessity of *folE-1* and *folE-2* in the biosynthesis of queuosine has been examined in gene knockout studies. The $\Delta folE$ and $\Delta folE-2$ mutations resulted in the absence of queuosine modified tRNA suggesting that both *folE-1* and *folE-2* are essential in the biosynthesis of queuosine (de Crécy-Lagard, unpublished work).

Table 1. Michaelis and inhibition constants for QueA

Substrate/ Inhibitor	K_m (μM) ^d	k_{cat} (min^{-1}) ^d	k_{cat}/K_m ($\mu\text{M}^{-1}\text{min}^{-1}$)	Inhibition Pattern ^b	K_i (μM) ^{c/d}	K_i/K_m
AdoMet ^a	104.4 ± 8.6	2.3 ± 0.1	45.4			
SeAdoMet	111.5 ± 3.2	0.0838 ± 0.003	7.50x10 ⁻⁰⁴	C	99.2 ± 2.9 138.4 ±	0.95
7-deazaAdoMet				C	3.5 217.1 ±	1.32
2'-dAdoMet				C	7.3 224.4 ±	2.07
3'-dAdoMet				C	5.1	2.15

^a Kinetic parameters for AdoMet were obtained from Van Lanen, et. al. [78].

^b C = competitive inhibition.

^c Values for the inhibition constants were obtained from data fitted to equation 1 for competitive inhibition against adomet.

^d Values are also expressed with respect to their standard deviation

Table 2. Effect of metal ions upon *N. gonorrhoeae* apoenzyme COG1469 Activity

Metal	[Metal]^a (μM)	Relative Activity (%)
As-isolated ^b	0	0.3
No Metal ^c	0	0
Mn(II) ^c	500	100
Fe(II) ^{c,d}	2000	51
Mg(II) ^c	100	29
Co(II) ^c	50	27
Zn(II) ^c	50	15
Ni(II) ^c	50	5
Ca(II) ^c	NA ^e	0
Cd(II) ^c	NA ^e	0
Cu(II) ^c	NA ^e	0
Co(III) ^c	NA ^e	0
Fe(III) ^c	NA ^e	0

^a The metal concentration for optimal activity. Each metal was surveyed over a concentration range of 0-2 mM.

^b As-isolated refers to protein that had not been treated to EDTA and Chelex prior to analysis.

^c All proteins utilized in the metal analysis were treated with EDTA and Chelex prior to analysis.

^d Assays were conducted under anaerobic conditions in the presence of 100 mM HEPES (pH 8.0), 100 mM KCl, 0.1 mM GTP, 2 μ M protein, and varying concentrations of Fe(SO₄)₂.

^e NA refers to no activity detected regardless of metal concentration

Table 3. Effect of metal ions upon *B. subtilis* apoenzyme COG1469 Activity

Metal	[Metal]^a (μM)	Relative Activity (%)
As-isolated ^b	0	1.7
No Metal ^c	0	0
Mn(II) ^c	500	100
Fe(II) ^{c,d}	1000	75
Mg(II) ^c	100	43
Co(II) ^c	100	24
Zn(II) ^c	50	14
Ni(II) ^c	100	9.8
Ca(II) ^c	NA ^e	0
Cd(II) ^c	NA ^e	0
Cu(II) ^c	NA ^e	0
Co(III) ^c	NA ^e	0
Fe(III) ^c	NA ^e	0

^a The metal concentration for optimal activity. Each metal was surveyed over a concentration range of 0-2 mM.

^bAs-isolated refers to protein that had not been treated to EDTA and Chelex prior to analysis.

^cAll proteins utilized in the metal analysis were treated with EDTA and Chelex prior to analysis.

^d Assays were conducted under anaerobic conditions in the presence of 100 mM HEPES (pH 8.0), 100 mM KCl, 0.1 mM GTP, 2 μ M protein, and varying concentrations of Fe(SO₄)₂.

^eNA refers to no activity detected regardless of metal concentration

Table 4. COG1469 activity prior to excess metal removal

Metal Concentration ^a	Specific Activities (μmol/min/μmol)	
	<i>N. gonorrhoeae</i> ^b	<i>B. subtilis</i> ^b
0.5 mM Mn ²⁺ Control	0.28	0.068
1 μM Mn ²⁺	ND	ND
2 μM Mn ²⁺	ND	ND
3.5 μM Mn ²⁺	ND	ND
3 μM Mn ²⁺	ND	ND
6 μM Mn ²⁺	ND	ND
10.5 μM Mn ²⁺	9.1x10 ⁻⁰⁵	1.8x10 ⁻⁰⁵
50 μM Zn ²⁺ Control	0.022	0.011
1 μM Zn ²⁺	ND	ND
2 μM Zn ²⁺	ND	ND
3.5 μM Zn ²⁺	ND	ND
3 μM Zn ²⁺	ND	ND
6 μM Zn ²⁺	ND	ND
10.5 μM Zn ²⁺	4.5x10 ⁻⁰⁵	2.8x10 ⁻⁰⁵

^a Final metal concentration when an aliquot of the reconstitution mixture is taken into standard reaction conditions containing 100 mM HEPES (pH 8.0), 100 mM KCl, 1 mM DTT and 0.1 mM GTP.

^b ND denotes no activity detected

Table 5A. Initial ICP-MS analysis of GCYH-IB metal ion content

Metal / Protein Ratio (mol/mol)	Mn(II)	Ni(II)	Zn(II)
<i>N. gonorrhoeae</i> as-isolated	1.60x10 ⁻⁴	2.80x10 ⁻³	3.47 x10 ⁻¹
<i>N. gonorrhoeae</i> apoenzyme	3.10x10 ⁻⁵	8.20x10 ⁻⁴	3.70 x10 ⁻²
<i>B. subtilis</i> as-isolated	4.20x10 ⁻⁴	3.48x10 ⁻³	2.56 x10 ⁻¹
<i>B. subtilis</i> apoenzyme	5.00x10 ⁻⁵	4.74 x10 ⁻⁴	9.54 x10 ⁻²

Table 5B. Follow-up ICP-MS analysis of GCYH-IB metal ion content

Metal / Protein Ratio (mol/mol)	Mn(II)	Zn(II)
<i>N. gonorrhoeae</i> as-isolated	1.16 x10 ⁻² ± 4 x 10 ⁻⁴	1.20 x10 ⁻¹ ± 4 x 10 ⁻³
<i>N. gonorrhoeae</i> apoenzyme	ND ^a	2.24 x10 ⁻¹ ± 8 x 10 ⁻⁴
<i>N. gonorrhoeae</i> Mn ²⁺ Reconstituted	1.45 x10 ⁻³ ± 5 x 10 ⁻⁵	1.71 x10 ⁻² ± 2 x 10 ⁻⁴
<i>N. gonorrhoeae</i> Zn ²⁺ Reconstituted	ND ^a	1.34 x10 ⁻² ± 8 x 10 ⁻⁴
<i>B. subtilis</i> as-isolated	2.06 x10 ⁻³ ± 7 x 10 ⁻⁵	4.84 x10 ⁻² ± 3 x 10 ⁻³
<i>B. subtilis</i> apoenzyme	2.00 x10 ⁻⁶ ± 1 x 10 ⁻⁷	4.59 x10 ⁻² ± 5 x 10 ⁻⁴
<i>B. subtilis</i> Mn ²⁺ Reconstituted	1.53 x10 ⁻³ ± 6 x 10 ⁻⁵	4.34 x10 ⁻² ± 6 x 10 ⁻⁵
<i>B. subtilis</i> Zn ²⁺ Reconstituted	6.00 x10 ⁻⁵ ± 1 x 10 ⁻⁶	5.29 x10 ⁻² ± 4 x 10 ⁻⁴

^aNo activity detected

Table 6A. Effects of DTT upon *N. gonorrhoeae* COG1469 activity

[DTT] (mM)	UV-vis Relative Activity (%)	Fluorescence Relative Activity (%)
0	31	18
0.5	86	90
1	88	100
2	100	77
4	89	76
8	87	0
12	78	0

Table 6B. Effects of DTT upon *B. subtilis* COG1469 activity

[DTT] (mM)	UV-vis Relative Activity (%)	Fluorescence Relative Activity (%)
0	49	14
0.5	82	80
1	91	100
2	100	71
4	97	62
8	98	0
12	99	0

Table 7 A. Michaelis constants for *N. gonorrhoeae* COG1469

Substrate		K_m (μM) ^a	k_{cat} (min^{-1}) ^a	k_{cat}/K_m ($\mu\text{M}^{-1}\text{min}^{-1}$)
GTP	without DTT	9.15 ± 0.67	0.0159 ± 0.0013	0.0017
	with DTT	6.76 ± 0.62	0.1160 ± 0.0050	0.0171
GDP	without DTT	172.8 ± 10.1	0.00321 ± 0.00027	1.86 X 10 ⁻⁵
	with DTT	146.7 ± 6.8	0.0793 ± 0.0081	0.00054

^aValues are also presented with respect to their standard deviation.

Table 7 B. Michaelis constants for *B. subtilis* COG1469

Substrate		K_m (μM) ^a	k_{cat} (min^{-1}) ^a	k_{cat}/K_m ($\mu\text{M}^{-1}\text{min}^{-1}$)
GTP	without DTT	8.12 ± 0.48	0.0212 ± 0.0016	0.0026
	with DTT	9.87 ± 0.82	0.0655 ± 0.0014	0.0066
GDP	without DTT	248.2 ± 13.0	0.00627 ± 0.00029	2.42 X 10 ⁻⁵
	with DTT	238.3 ± 5.7	0.0224 ± 0.0016	9.42 X 10 ⁻⁵

^aValues are presented with respect to their standard deviation.

Table 8. Inhibition constants and patterns for *N. gonorrhoeae* COG1469 with substrate analogs

Inhibitor	Inhibition Pattern^a	K_i (μM)^b	K_i/K_m
7-deazaGTP	C	45.7 ± 1.5	6.8
2'-deoxyGTP	C	164.2 ± 3.1	24.3
8-oxoGTP	C	0.149 ± 0.0049	0.022

^aC denotes competitive inhibition pattern

^bValues are presented with respect to their standard deviation.

Table 9. Radiochemical analysis of *N. gonorrhoeae* His 245 mutants

Protein	Relative Activity (%)
Wild-type	100
<i>E. coli</i> RibA	80
H245D	72
H245Q	67
H245N	24
H245K	5

Table 10. UV-vis analysis of *N. gonorrhoeae* His 245 mutants

Protein	Relative Activity (%)
Wild-type	100
H245D	3.0
H245Q	2.4
H245K	0
H245N	0

Table 11. GCYH-I Fluorescence analysis of *N. gonorrhoeae* His 245 mutants

[GTP] (μM)	Relative Activity (%)				
	H245D	H245Q	H245K	H245N	Wild-type
24	0.0	0.6	0.0	0.0	68
50	0.0	1.2	0.0	0.0	81
200	0.4	0.8	0.0	0.0	100
500	3.0	2.1	0.0	0.0	93

Table 12. GCYH-II and III fluorescence analysis on *N. gonorrhoeae* His 245 mutants

	Relative Activity (%)
Wild-type	100
<i>E. coli</i> RibA	8.2
H245D	8.0
H245Q	8.1
H245N	3.0
H246K	0.0

Table 13. Distribution of FolE, FolE2 (denoted as COG1469), FolKP and YkvLKJ homologs in a subset of sequenced genomes.

Organism	Domain	FolE	COG1469	FolKP	YkvLKJ
<i>M. jannaschii</i>	A		+	+	+
<i>M. burtonii</i>	A		+	+	+
<i>P. abyssi</i>	A		+	+	+
<i>P. torridus</i>	A		+	+	+
<i>B. bronchiseptica</i>	B		+	+	+
<i>S. aureus</i>	B		+	+	+
<i>T. maritima</i>	B		+	+	+
<i>N. europaea</i>	B		+	+	+
<i>N. gonorrhoeae</i>	B		+	+	+
<i>N. meningitidis</i>	B		+	+	+
<i>B. subtilis</i>	B	+	+	+	+
<i>A. baylyi</i>	B	+	+	+	+
<i>M. capsulatus</i>	B	+	+	+	+
<i>X. fastidiosa</i>	B	+	+	+	+
<i>E. coli</i>	B	+		+	+
<i>C. jejuni</i>	B	+		+	+
<i>Y. pestis</i>	B	+		+	+
<i>Z. mobilis</i>	B	+		+	+

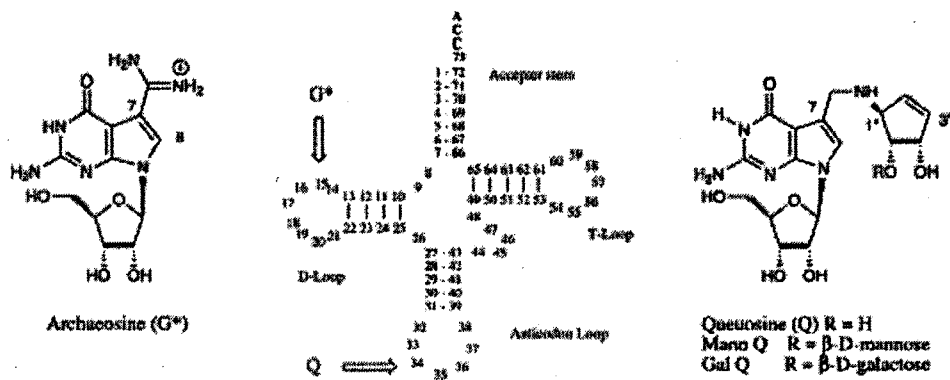


Figure 1. The chemical structure of archaeosine (G*) and queuosine (Q) and their location in tRNA. Image taken from published work of Iwata-Reuyl [138].

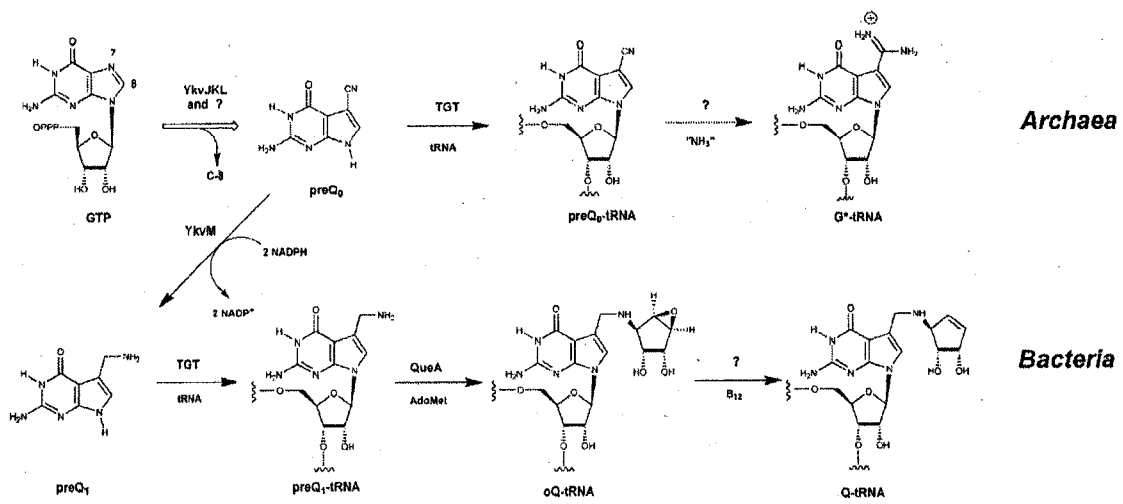


Figure 2. The biosynthetic pathway of archaeosine (G*) and queuosine (Q) in archaea and bacteria, respectively.

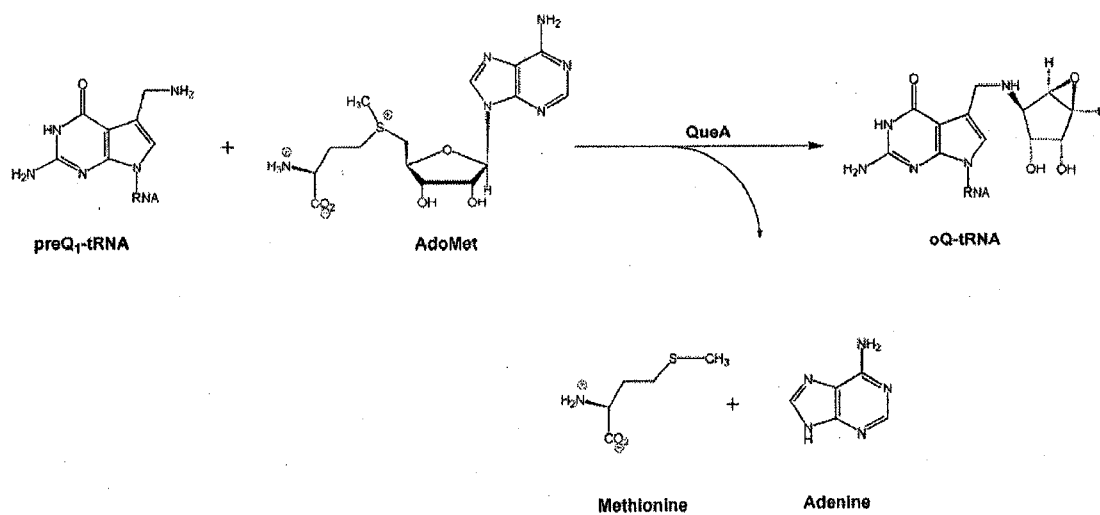


Figure 3. The reaction catalyzed by QueA.

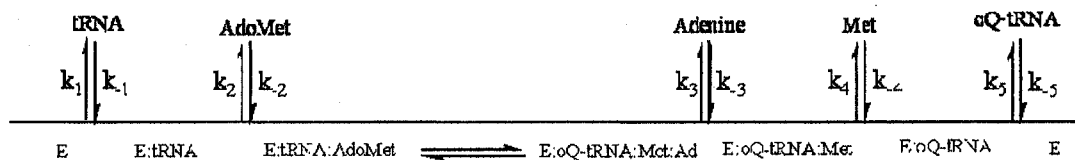


Figure 4. Proposed kinetic mechanism for the QueA catalyzed reaction. Image taken from published work of Van Lanen [43].

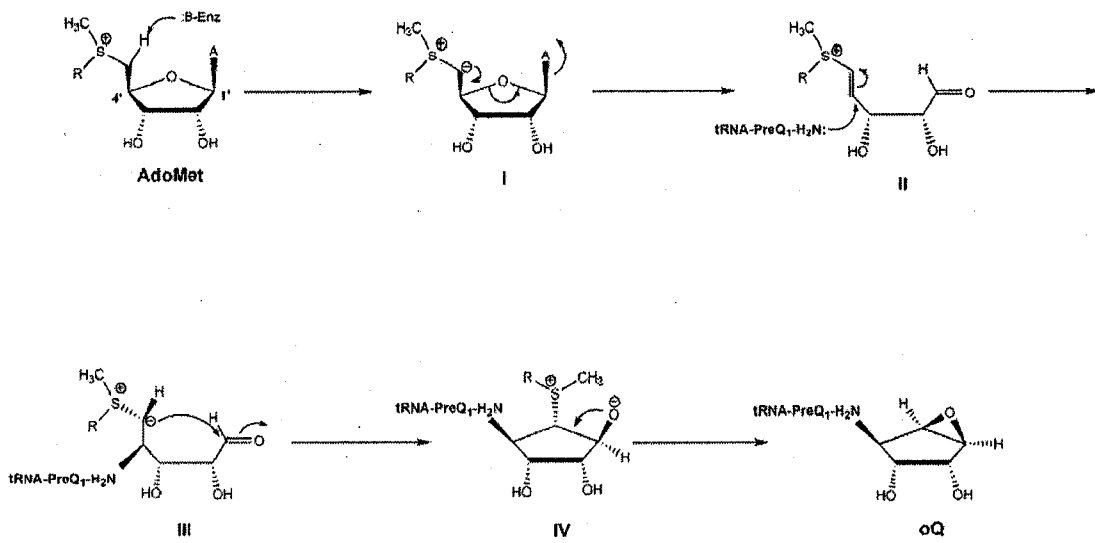


Figure 5. Proposed chemical mechanism for the QueA catalyzed reaction.

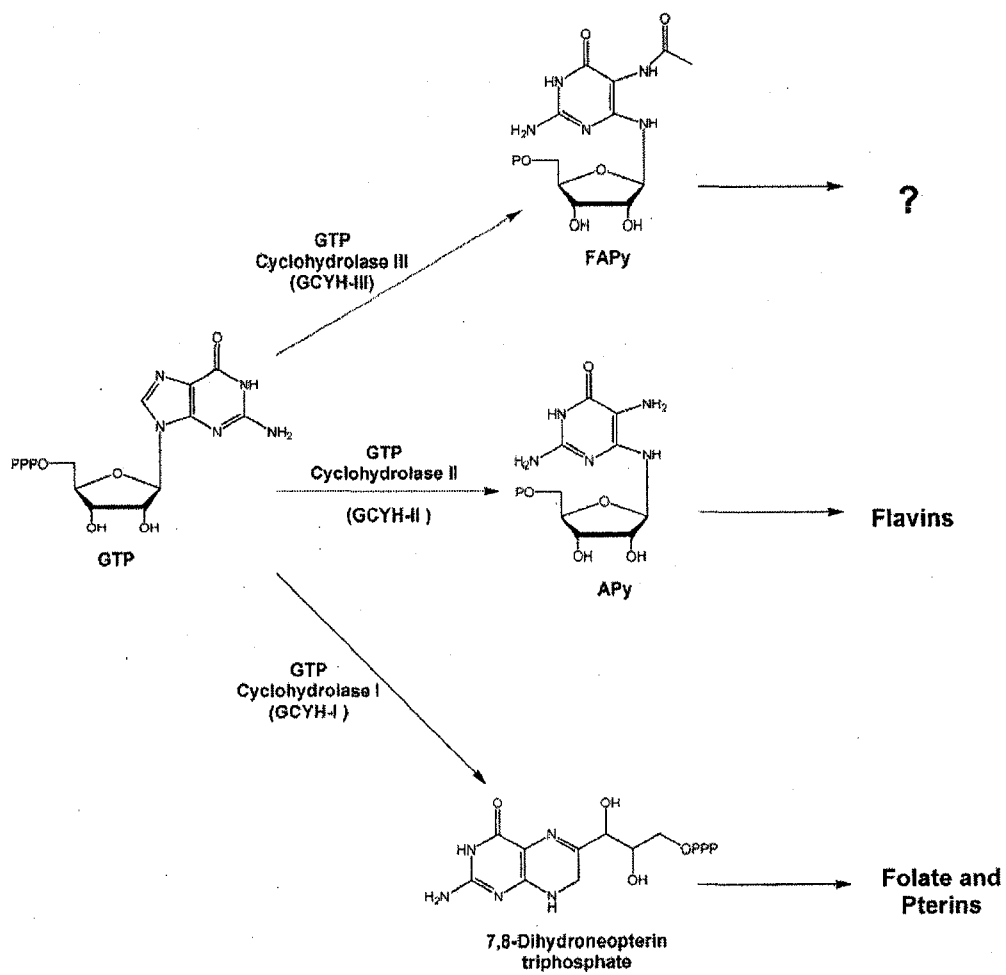


Figure 6. Reactions catalyzed by GCYH-III, GCYH-II and GCYH-I

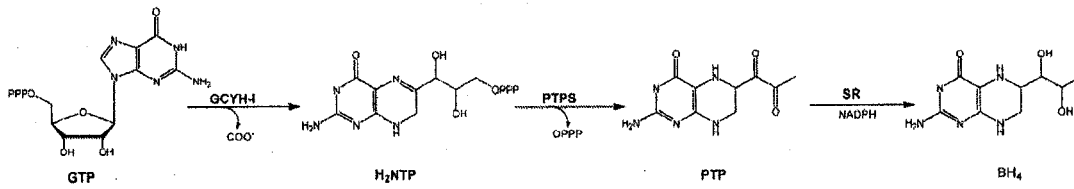


Figure 7. Biosynthetic pathway of BH₄ in higher eukaryotes.

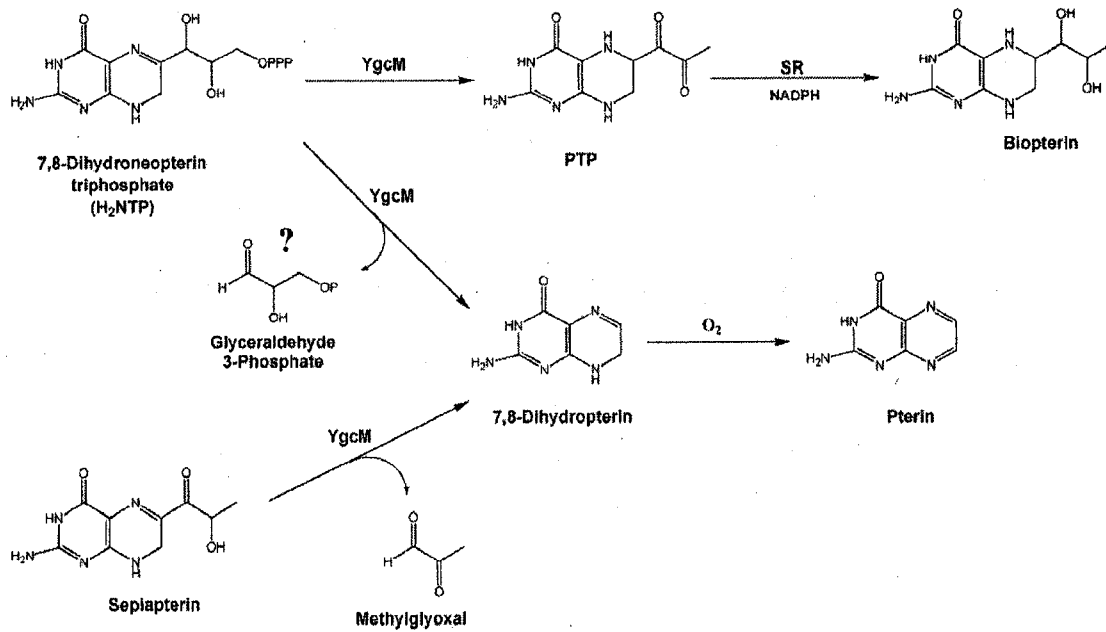


Figure 8. Reactions catalyzed by YgcM.

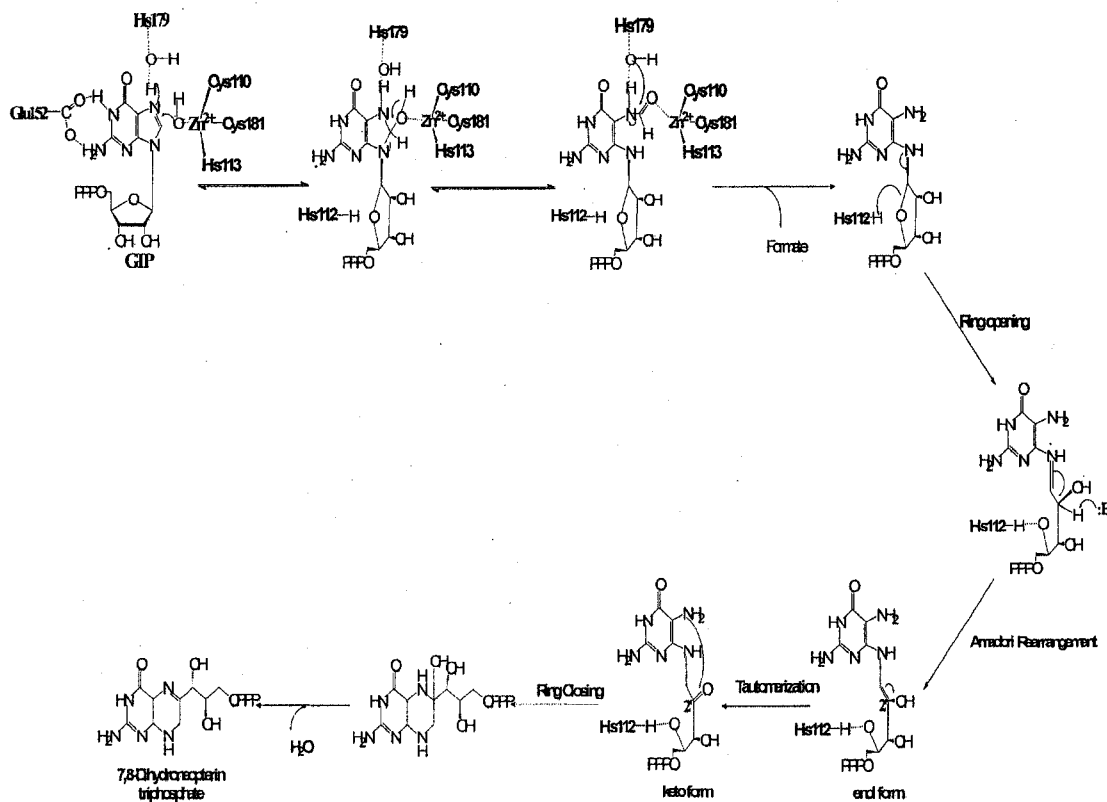


Figure 9. Proposed Chemical Mechanism of GCYH-I

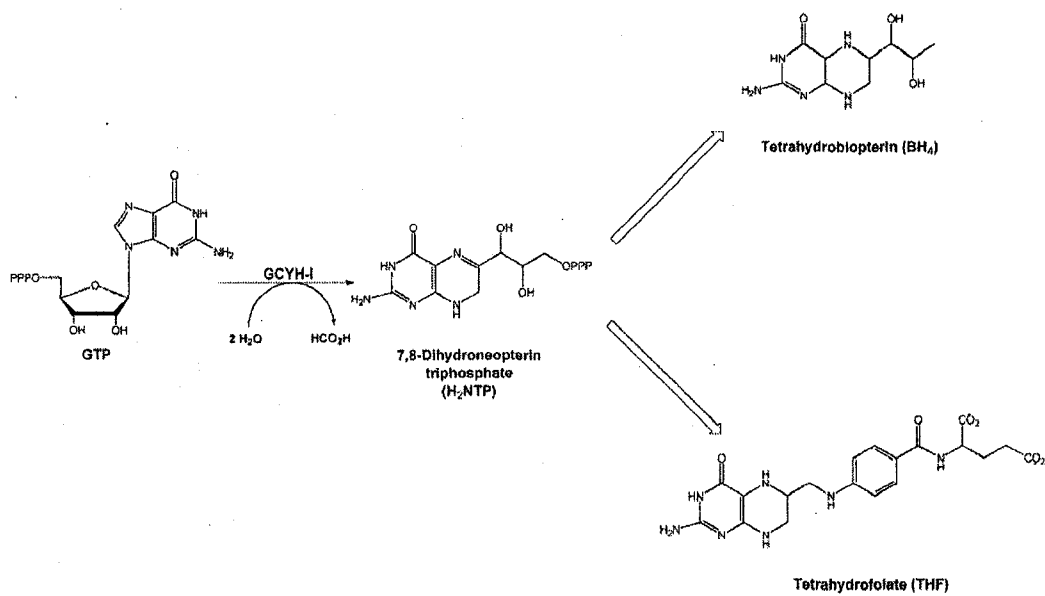


Figure 10. GCYH-I catalyzed reaction and the metabolic fate of dihydroneopterin triphosphate.

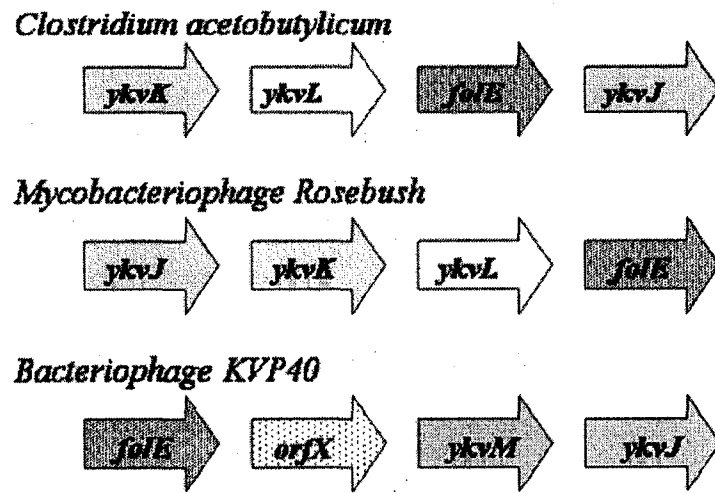


Figure 11. Examples of physical clustering of *folE* with queuosine biosynthetic genes.

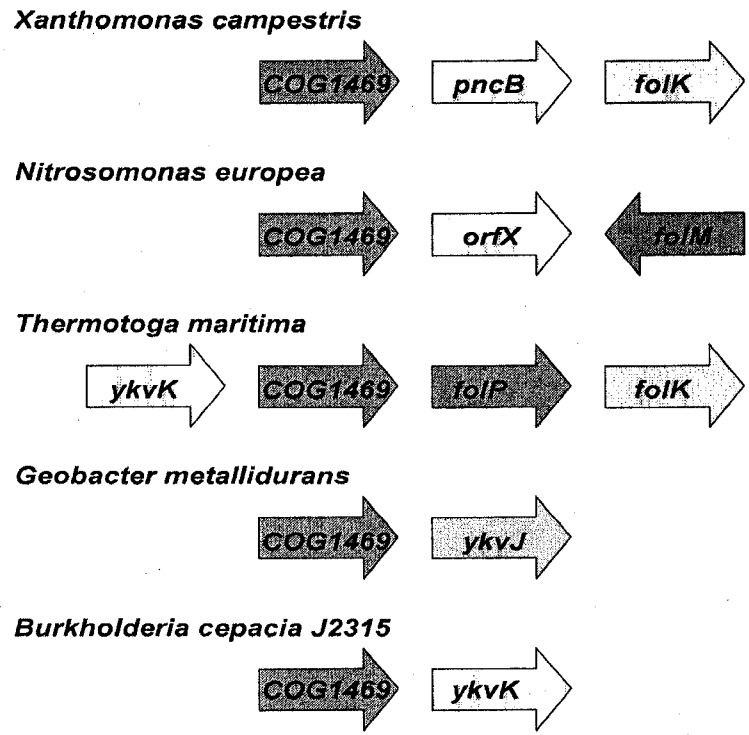


Figure 12. Examples of physical clustering of COG1469 encoding genes with folate (*folKMP*) and/or queuosine (*ykvJK*) biosynthetic genes.

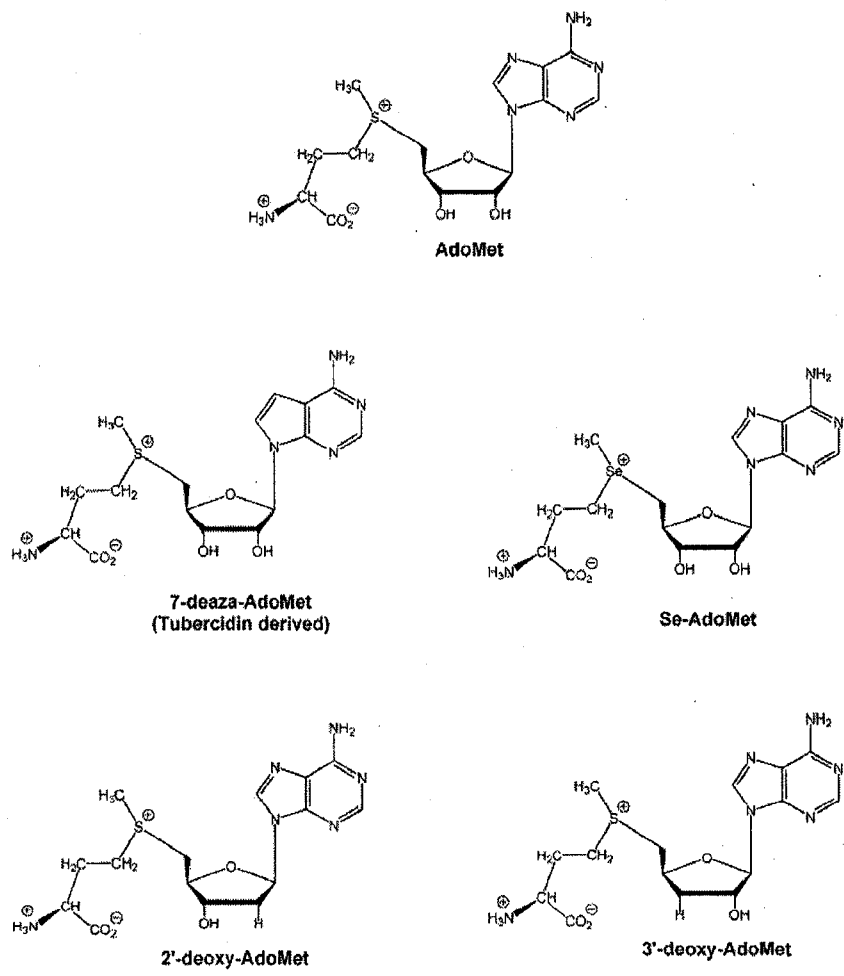


Figure 13. Chemical structures of AdoMet and AdoMet analogs.

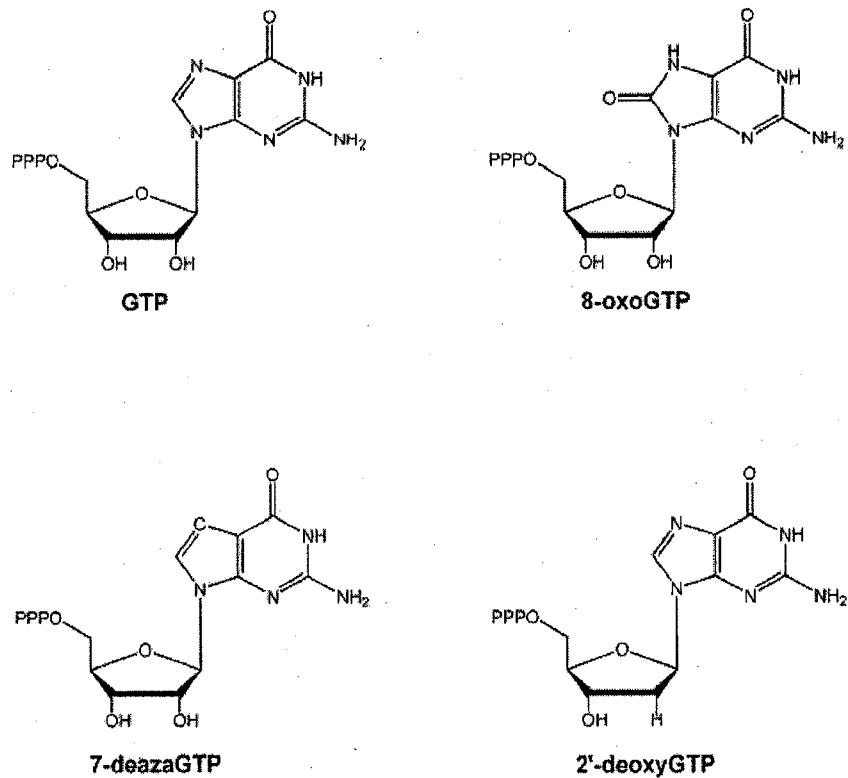


Figure 14. Structure of Substrate GTP and Analogs.

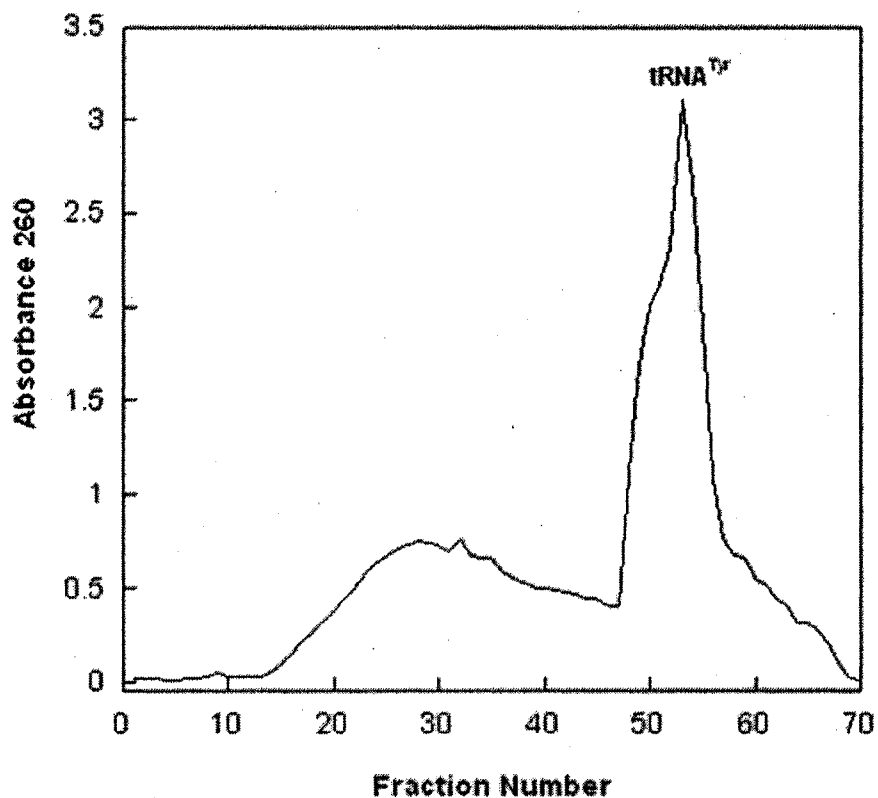


Figure 15. Purification of tRNA^{Tyr} on BND cellulose. Crude tRNA (20 mg) was loaded onto a 12 ml BND-cellulose column equilibrated in Buffer A (20 mM sodium acetate (pH 4.5), 10 mM MgCl₂ and 0.5 M NaCl). The column was washed with 20 ml of Buffer A at a flow rate of 0.5 ml/min followed by an 80 ml salt gradient (0.5M-1.0M NaCl) in Buffer A from 20-100 ml. After washing the column with 10 ml of Buffer B (Buffer A containing 1 M NaCl), tyrosine specific tRNA was eluted from the column with a 40 ml ethanol gradient (0-20% v/v) in Buffer B. Fractions (2 ml) were assayed for tyrosine-tRNA synthetase activity. Fractions 56 to 70 were pooled and the tRNA was precipitated from solution with the addition an equal volume of cold isopropanol.

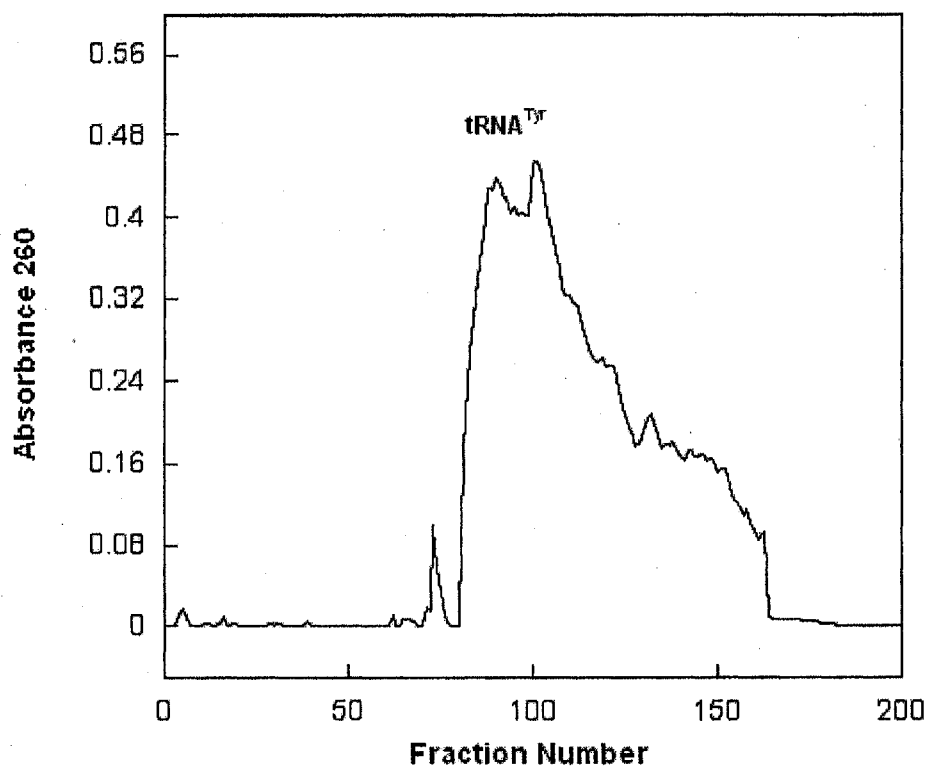


Figure 16. Purification of tRNA^{Tyr} on NACS. Enriched tRNA^{Tyr} (~15 mg) was loaded onto a column containing 10 ml NACSTM resin equilibrated in Buffer C (10 mM sodium acetate (pH 4.5), 10 mM MgCl₂ and 0.2 M NaCl). The column was washed with a 100 ml of Buffer C at a flow rate of 1 ml/min. The tyrosyl-tRNA was eluted with a 400 ml salt gradient (0.2 M - 1M) in Buffer C. Fractions (2.5 ml) were assayed for tRNA^{Tyr} content by tyrosine-tRNA synthetase assays, pooled and the tRNA was precipitated from solution with the addition of cold isopropanol.

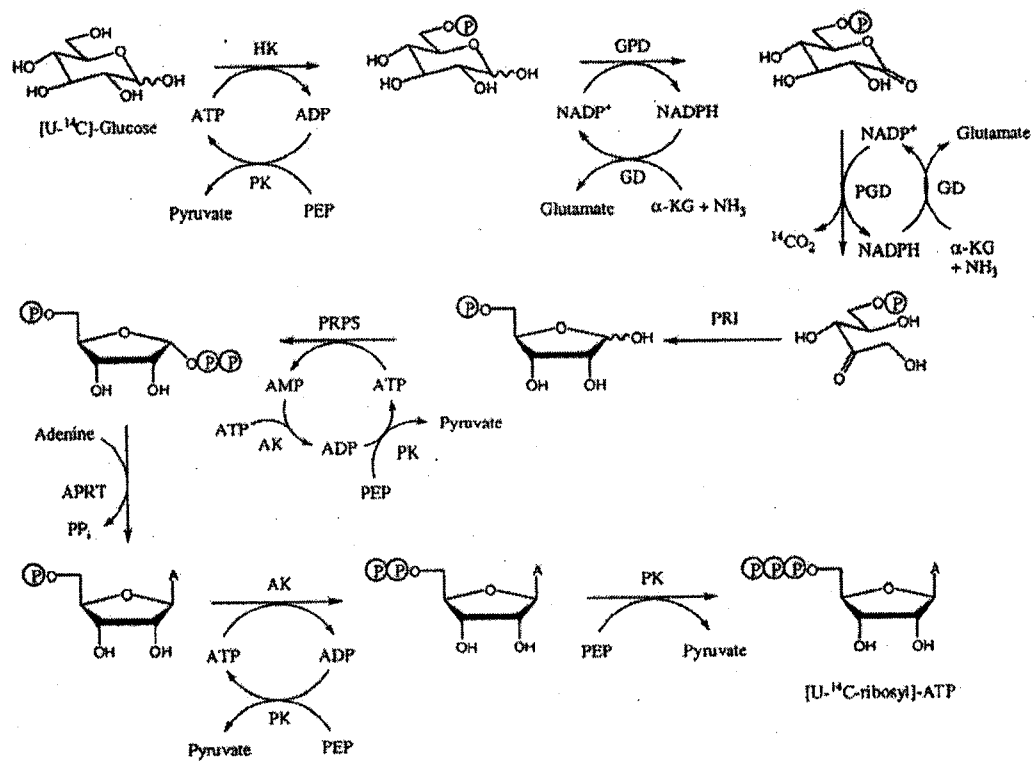


Figure 17. Enzymatic synthesis of [U-riboseyl-¹⁴C]ATP. In a multienzyme reaction, [U-riboseyl-¹⁴C]ATP was synthesized from [U-¹⁴C]glucose. Enzymes involved in the synthesis are as follows; hexokinase (HK), pyruvate kinase (PK), glucose-6-phosphate dehydrogenase (GPD), 6-phosphogluconate dehydrogenase (PGD), glutamate dehydrogenase (GD), phosphoriboisomerase (PRI), phosphoribosylpyrophosphate synthetase (PRPS), adenine phosphoribosyltransferase (APRT) and myokinase (AK).

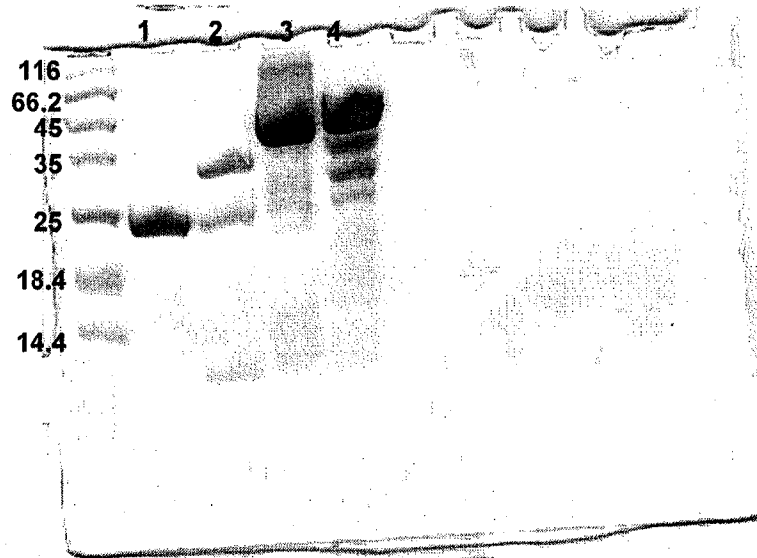


Figure 18. SDS-PAGE analysis of purified recombinant APRTase-His₆ (25 kDa), Lane 1; PRPP synthetase (34 kDa), Lane 2; EcMAT (42 kDa), Lane 3; MjMAT-His₆ (49 kDa), Lane 4.

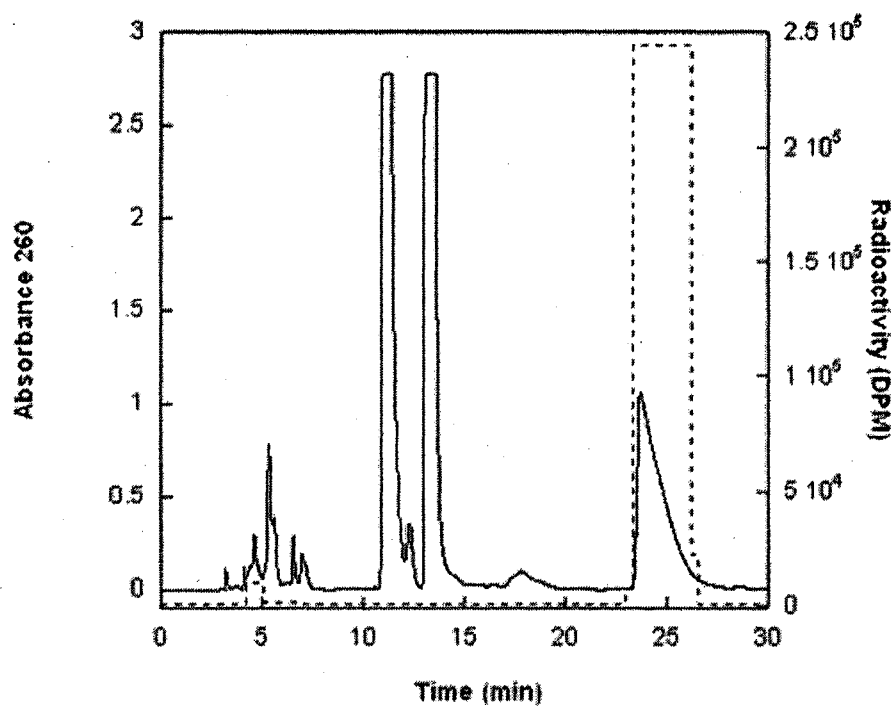


Figure 19. HPLC purification of [U-ribosyl-¹⁴C]ATP. Purification was carried out by reverse phase HPLC utilizing a semipreparative Luna C18 column. The radio-labeled ATP eluted from the column under isocratic conditions using 83.3 mM triethylammonium acetate (pH 6.0) and 6 % methanol at 4 ml/min. Under these conditions adenine eluted ~11 min, NADPH at 13 min and [U-ribosyl-¹⁴C]ATP at 23 min. Absorbance at 260 is represented by a solid line and radioactivity is represented by a dashed line.

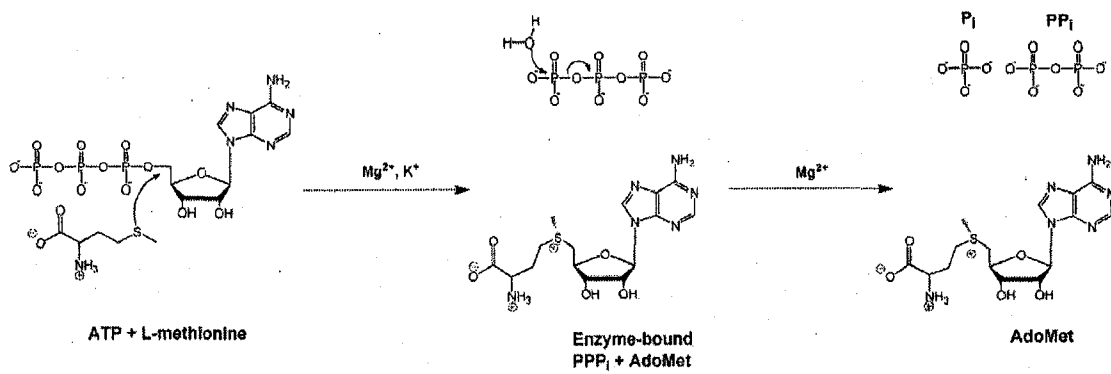


Figure 20. The reaction catalyzed by AdoMet synthase (MAT)

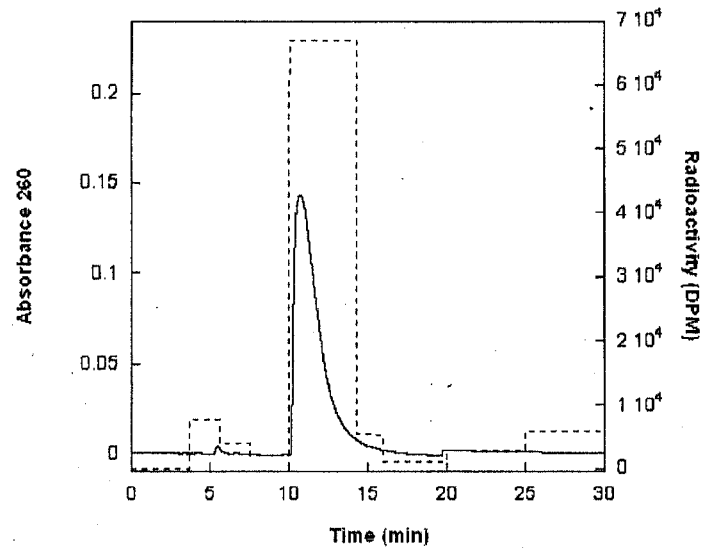
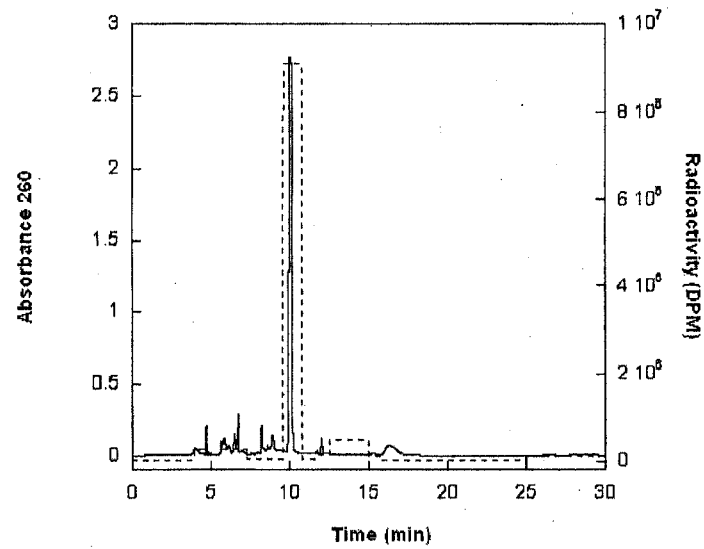
A**B**

Figure 21. [*U-ribosyl*- ^{14}C]AdoMet and [*U-ribosyl*- ^{14}C]SeAdoMet HPLC Purification. AdoMet and SeAdoMet were purified by reverse phase HPLC on a Luna C18 column with 20 mM ammonium acetate (pH 6.0) and 20% methanol mobile phase. ATP eluted ~6 min, AdoMet (A) at 10 min and SeAdoMet (B) at 10.5 min. Absorbance at 260 is represented by a solid line and total radioactivity is represented by a dashed line.

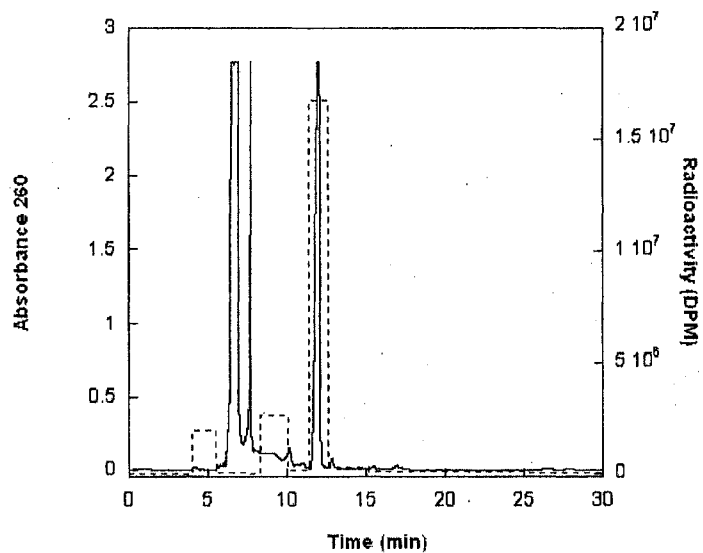
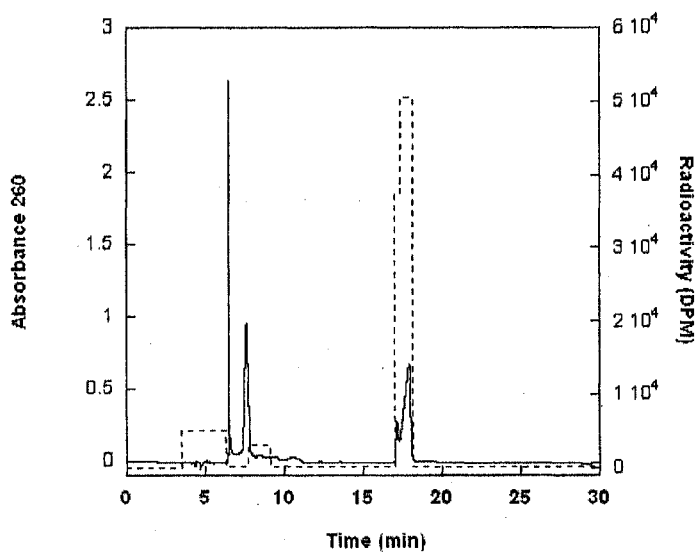
A**B**

Figure 22. 3'dAdoMet and 7-deazaAdoMet HPLC Purification. AdoMet analogs were purified by reverse phase HPLC on a Luna C18 column with 20 mM ammonium acetate (pH 6.0) and 20% methanol mobile phase. (A) 3'dATP eluted ~6 min and 3'dAdoMet eluted at 11.5 min. (B) 7-deazaATP eluted ~7 min and 7-deazaAdoMet eluted ~17 min. Absorbance at 260 is represented by a solid line and total radioactivity is represented by a dashed line.

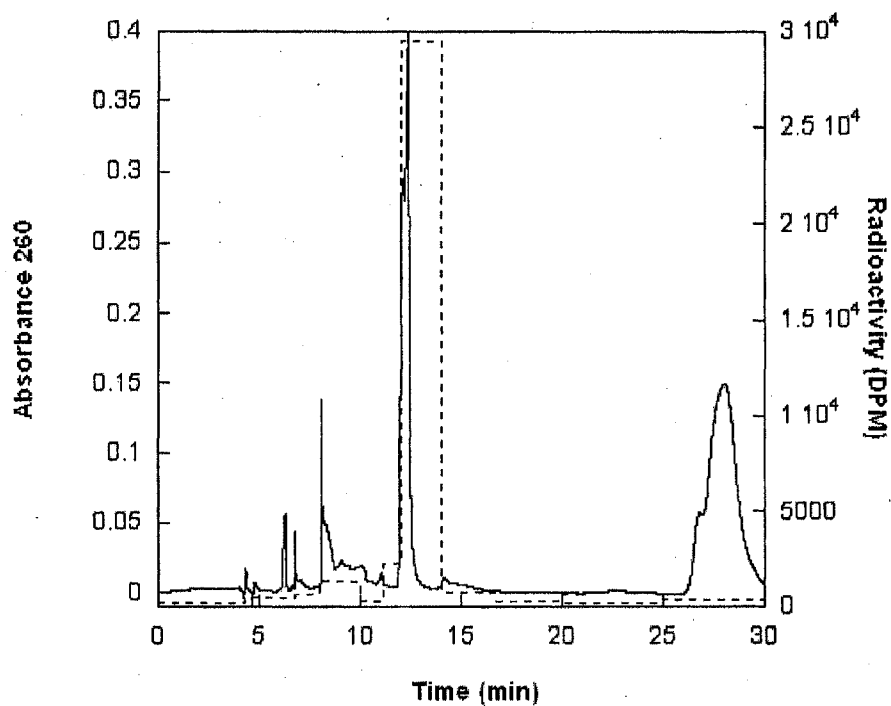


Figure 23. 2'dAdoMet HPLC Purification. [1C-methionine- 14 C]-2'dAdoMet was purified by reverse phase HPLC on a Luna C18 column with a mobile phase of 20 mM ammonium acetate (pH 6.0) and 20% methanol. 2'dATP eluted ~6 min, 2'dAdoMet eluted at 11.5 min and 2'dMTA eluted at 26 min. Absorbance at 260 is represented by a solid line and total radioactivity is represented by a dashed line.

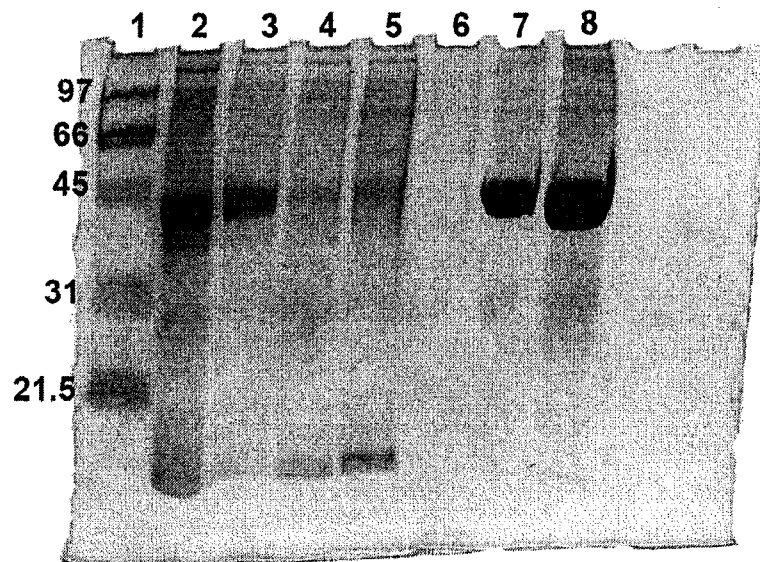


Figure 24. SDS-PAGE of purified QueA His₆-tag fusion protein (~44 kDa). Lane 1, MW markers; lane 2, crude lysate; lane 3, CFE; lane 4, Buffer 1 wash; lane 5, Buffer 2 wash ; lane 6, Buffer 3 wash; lane 7, nickel agarose purified protein; lane 8, concentrated protein.

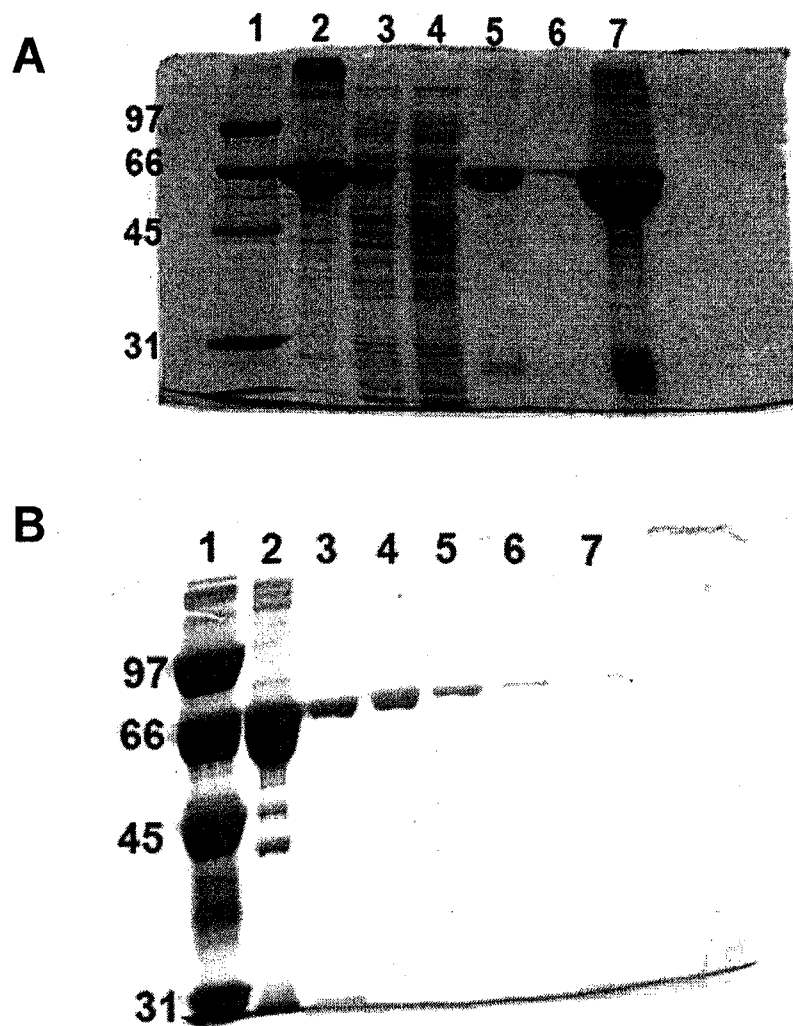
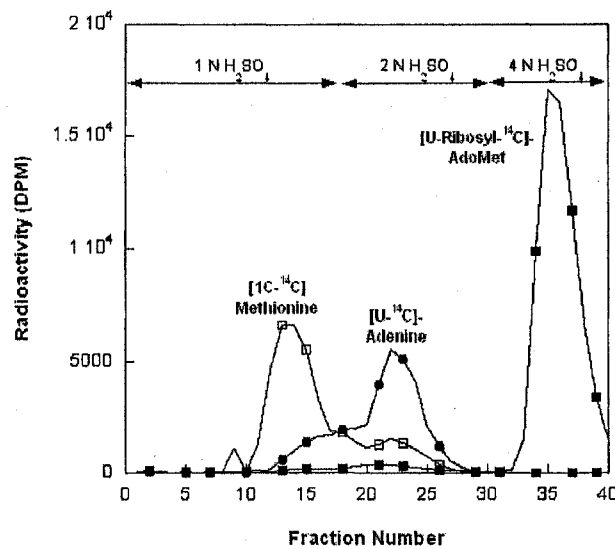


Figure 25: SDS-PAGE analysis of (A) Glutathione sepharose 4B affinity purification of QueA-GST (65 kDa). Lane 1 MW; lane 2 CFE; lane 3 Buffer L wash; lane 4 Buffer M wash; lane 5 Elution of protein with Buffer N, lane 6 filtrate from concentration; lane 7 concentrated QueA-GST. (B) SDS-PAGE analysis of HPLC purification of QueA-GST. Lane 1 MW; lane 2 Sepharose purified protein; lane 3-7 HPLC purified QueA-GST.

A



B

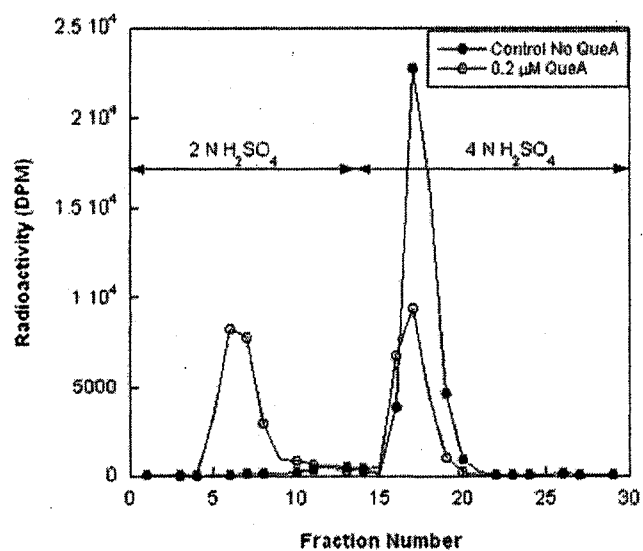


Figure 26. Dowex-50WX4 Analysis. (A) the elution profile of $[1C-^{14}C]$ -methionine, $[U-^{14}C]$ -adenine and $[U-ribosyl-^{14}C]$ -AdoMet on Dowex with increasing H_2SO_4 concentration. (B) Product formation in the presence of QueA was quantified by fractionation on Dowex. The arrows in the upper region of each plot indicate the concentration of H_2SO_4 utilized in the elution.

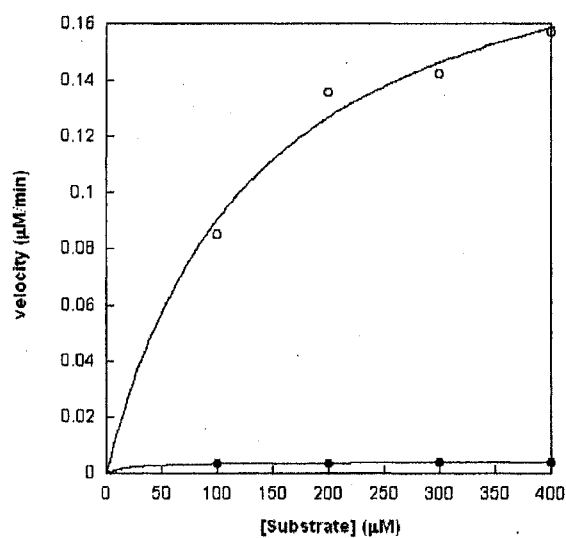
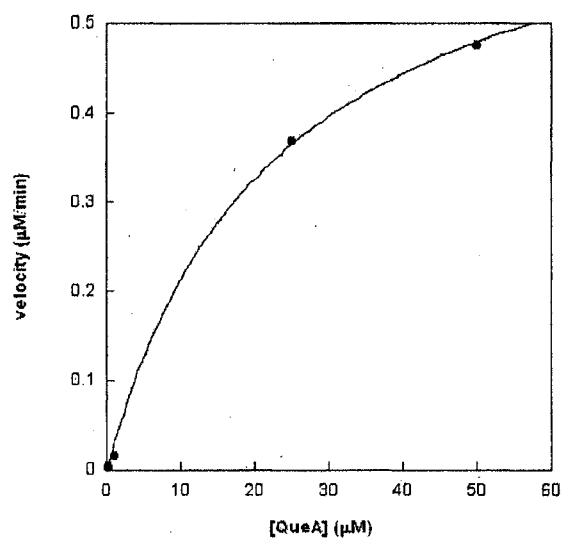
A**B**

Figure 27. (A) QueA (0.2 μM) activity as a function of substrate concentration (●) SeAdoMet and AdoMet (○). (B) Effect of QueA activity as a function of protein concentration in the presence of 100 μM SeAdoMet (●).

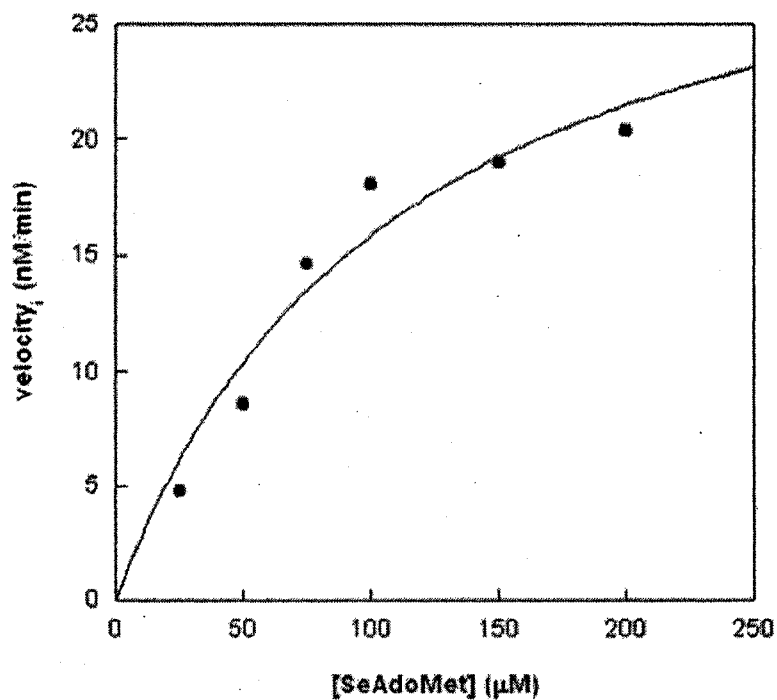


Figure 28. Substrate Kinetic Analysis of QueA with SeAdoMet. Reactions were carried out in 100 mM gly-gly (pH 8.7), 100 mM EDTA (pH 8.7), 100 mM KCl, 0.5 mM DTT and 0.4 μM QueA at 37°C under initial velocity conditions. The concentration of SeAdoMet varied from 25 to 200 μM SeAdoMet. Nonlinear regression analysis of the data was conducted using KaleidaGraph 4.0.

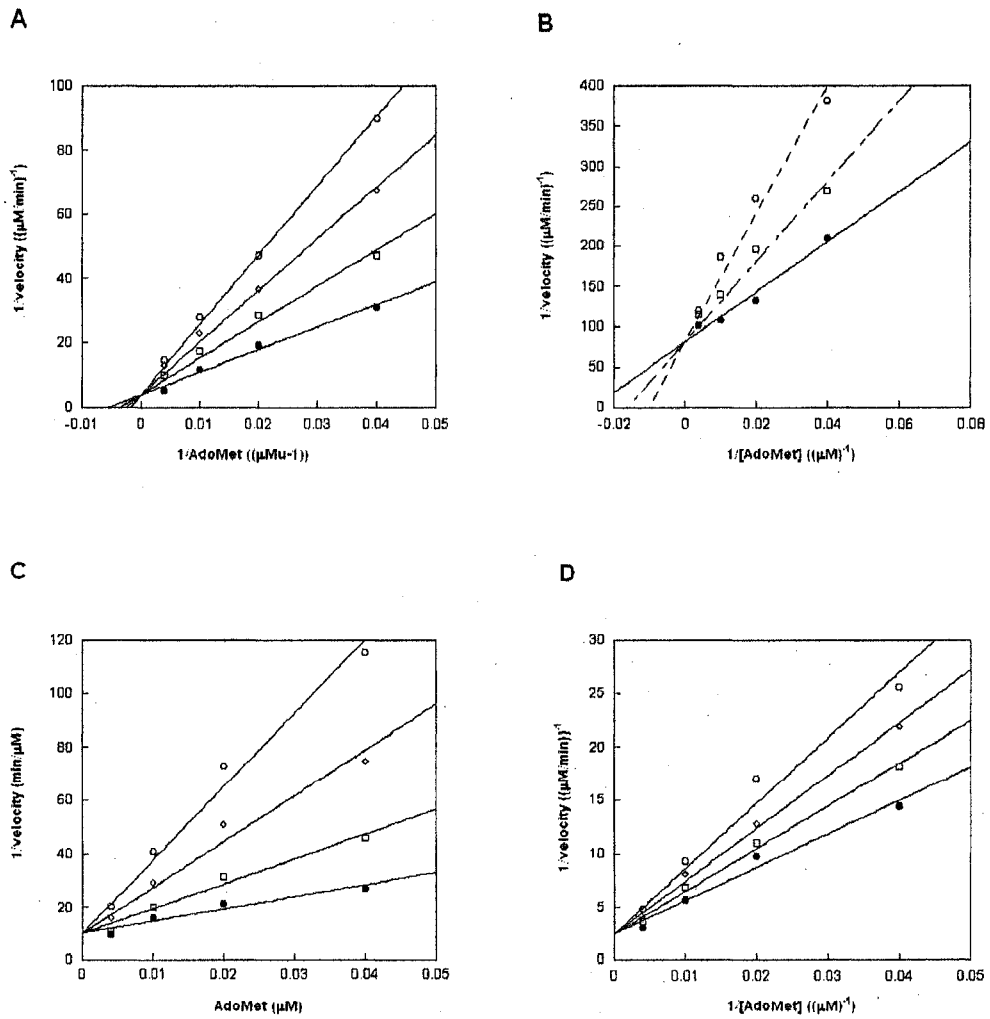


Figure 29. Competitive Inhibition with AdoMet Analogs. (A) SeAdoMet, (B) 2'dAdoMet, (C) 3'dAdoMet and (D) 7-deazaAdoMet.

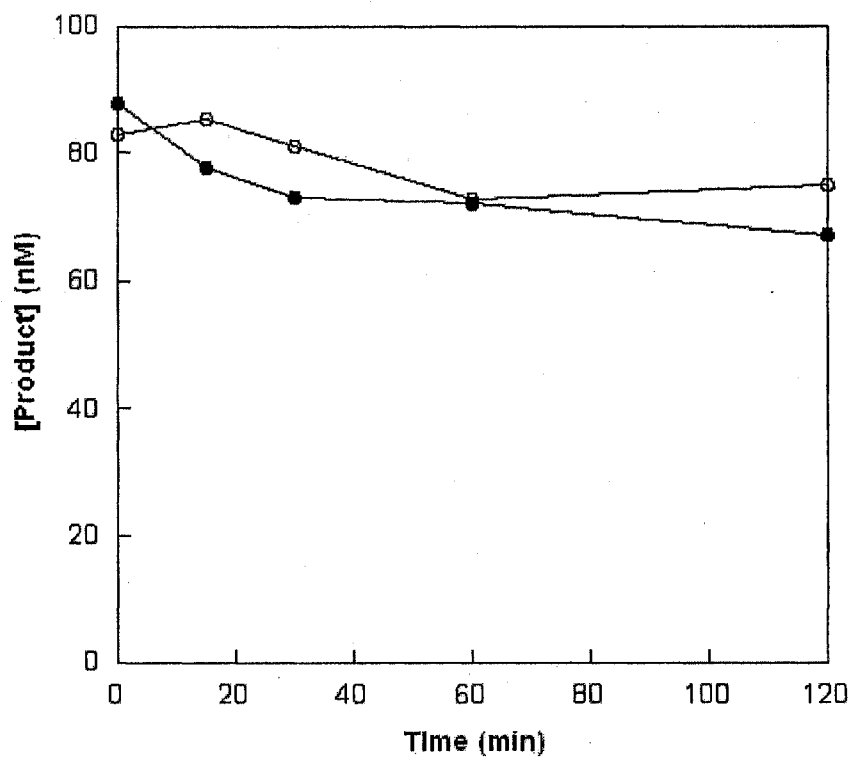


Figure 30. Time dependent inactivation studies were conducted in which QueA was preincubated in the presence (○) or absence (●) of SeAdoMet. Aliquots of the preincubation mixture were taken into standard QueA assay conditions containing AdoMet at various times.

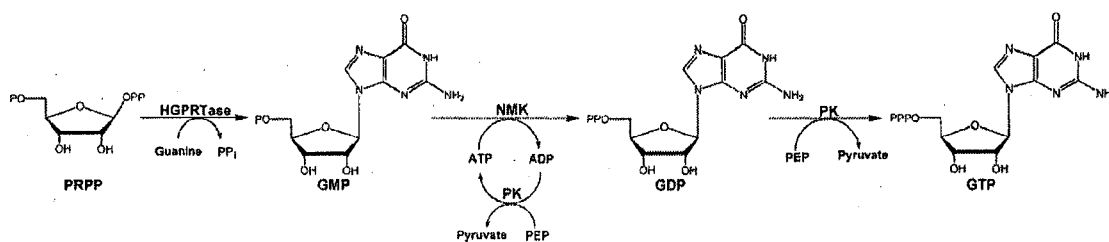


Figure 31. Enzymatic synthesis of [8C-¹⁴C]GTP. In a multienzyme reaction, [8C-¹⁴C]GTP was synthesized from phosphoribosyl pyrophosphate (PRPP) and [8C-¹⁴C]guanine. Enzymes involved in the synthesis are as follows; Hypoxanthine phosphoribosyltransferase (HGPRTase), nucleoside monophosphate kinase (NMK), and pyruvate kinase (PK).

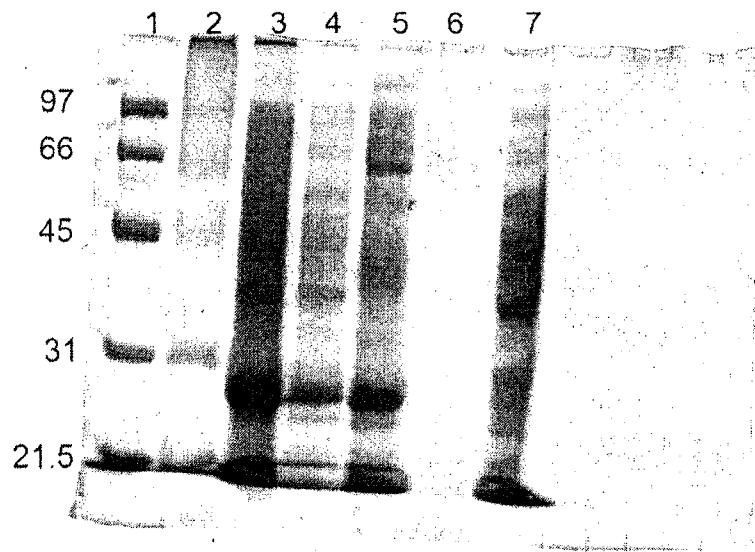


Figure 32. SDS-PAGE Analysis of HGPRTase (24 kDa) purification. Lane 1 and 2, MW markers; lane 3, supernatant after 40% ammonium sulfate fractionation; lane 4, resuspended pellet after 80% ammonium sulfate fractionation; lane 5, resuspended pellet from 40% ammonium sulfate fractionation; lane 6, empty; lane 7, supernatant after 80% fractionation.

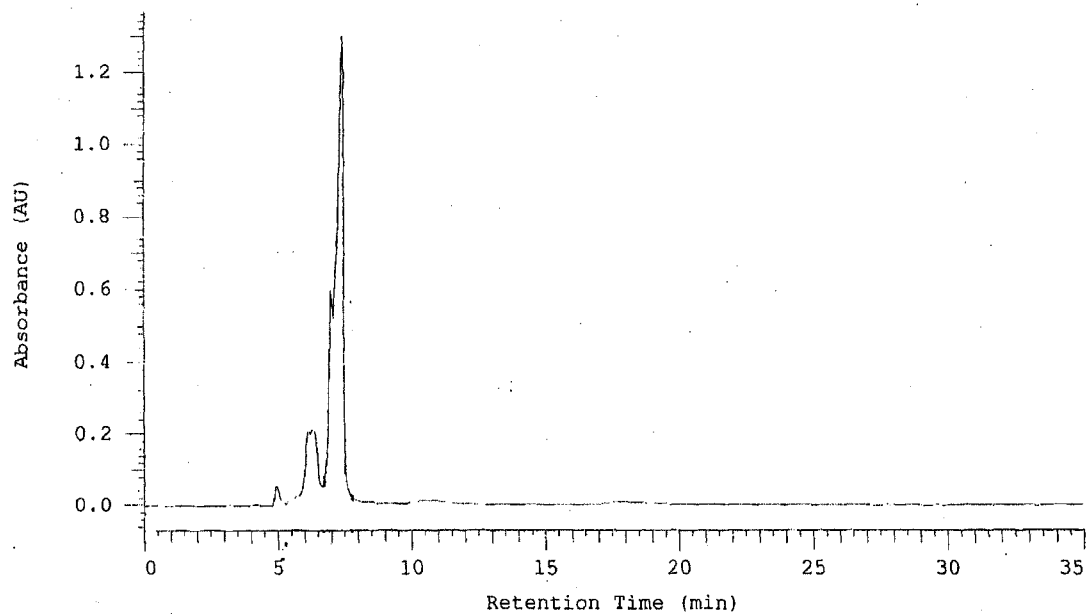


Figure 33. HPLC purification of [C8 -¹⁴C]GTP by reverse phase HPLC on a Luna C18 column using a mobile phase of 83.3 mM triethylammonium acetate (pH 6.0) and 5 % methanol at 4 ml/min. Radiolabeled GTP eluted ~7 min, whereas AdoMet eluted at 5.5 min.

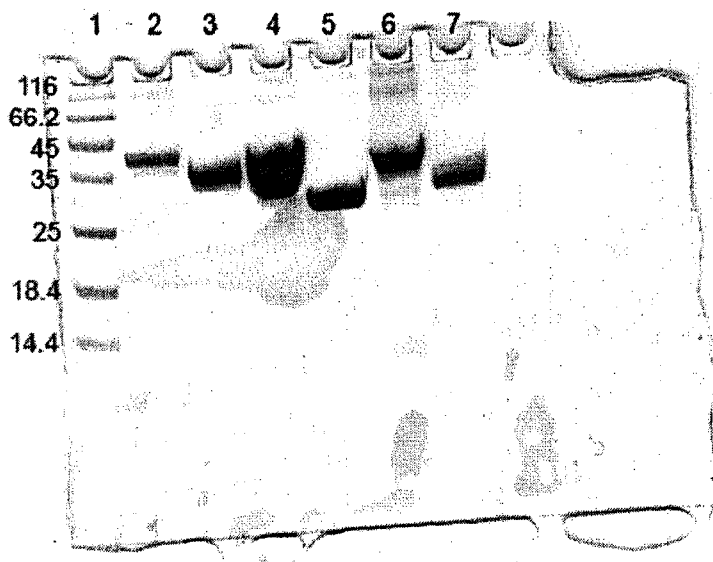


Figure 34. SDS-PAGE analysis of purified recombinant and wild-type COG1469 proteins . Lane 1, MW markers; lane 2, *B. subtilis* COG1469 His₆-tag (39.7 kDa); lane 3, *B. subtilis* COG1469 wild-type (34.7 kDa); lane 4, *N. gonorrhoeae* COG1469 His₆-tag (33.6 kDa); lane 5, *N. gonorrhoeae* COG1469 wild-type (28.7 kDa); lane 6, *T. maritima* COG1469 His₆-tag (35.2 kDa); lane 7, *T. maritima* COG1469 wild-type (30.3 kDa).

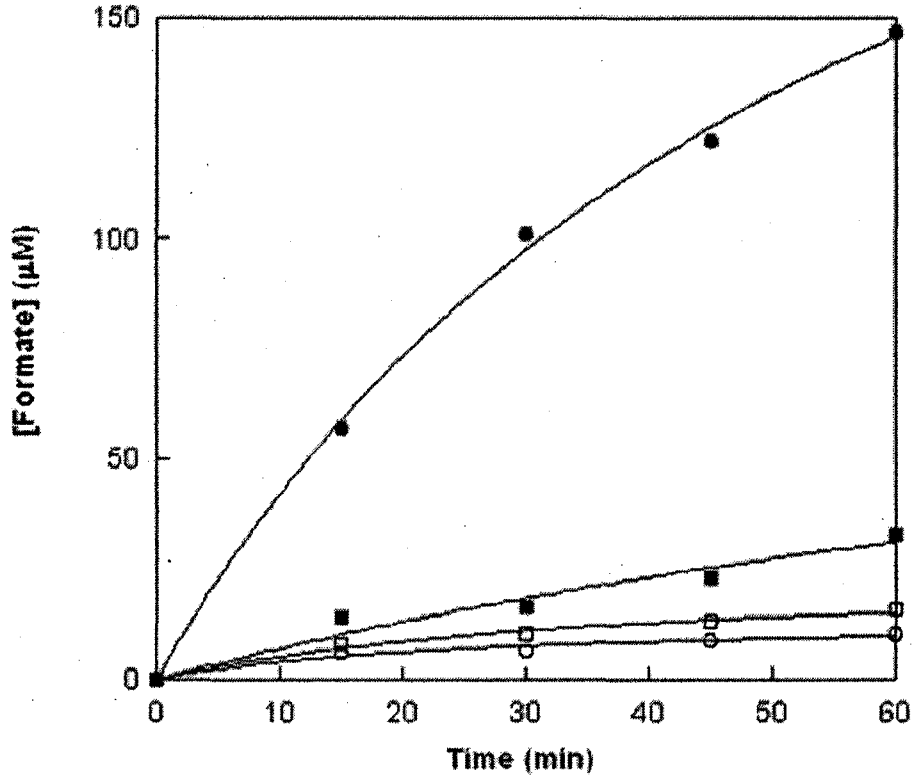


Figure 35. Radiochemical based assay for GCYH-I and GTPCH-II activity utilizing [8-¹⁴C]GTP. *T. maritima* COG1469 (□), *N. gonorrhoeae* COG1469 (■), *B. subtilis* COG1469 (○) and *E. coli* FOLE (●).

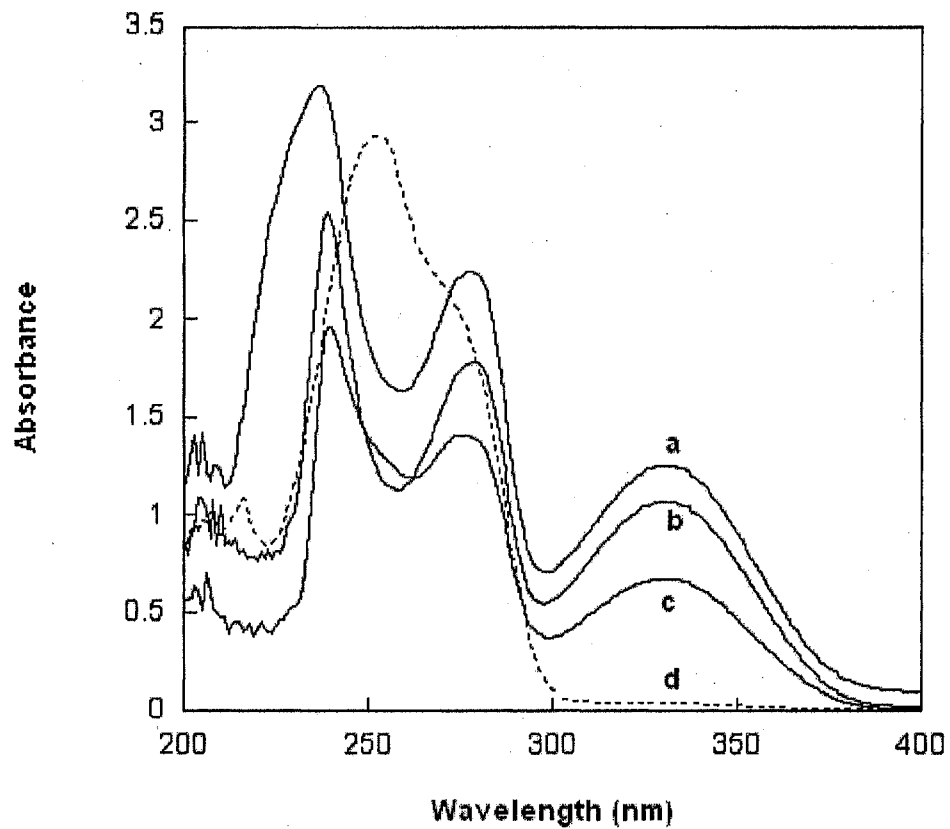


Figure 36. Spectrophotometric based assay for GCYH-I activity. Assays were performed in 100 mM Tris-HCl (pH 8.0), 100 mM KCl, 2 mM MgCl₂ and either 20 μ M *E. coli* FolE or 40 μ M COG1469 proteins in a total volume of 100 μ l. Reactions initiated upon the addition of GTP to a final concentration of 0.1 mM and incubated at 37 °C. Reactions were allowed to proceed for 60 min while monitoring the absorbance from 200-400 nm. (a) *E. coli* FolE; (b) *N. gonorrhoeae* COG1469; (c) *B. subtilis* COG1469; (d) no enzyme.

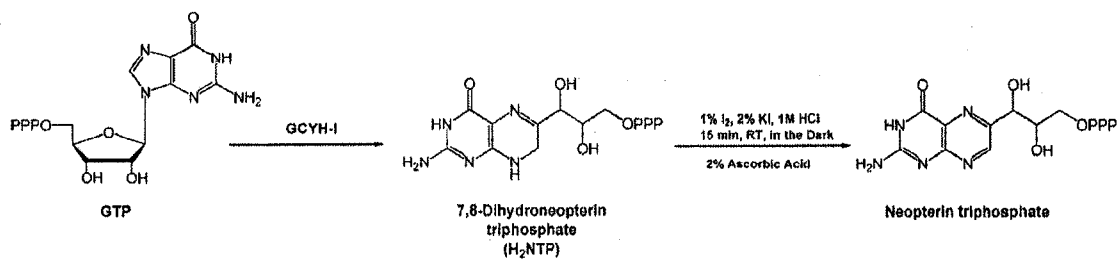


Figure 37. Schematic representation of the oxidation of the GCYH-I reaction product, 7,8-dihydroneopterin triphosphate, to neopterin triphosphate.

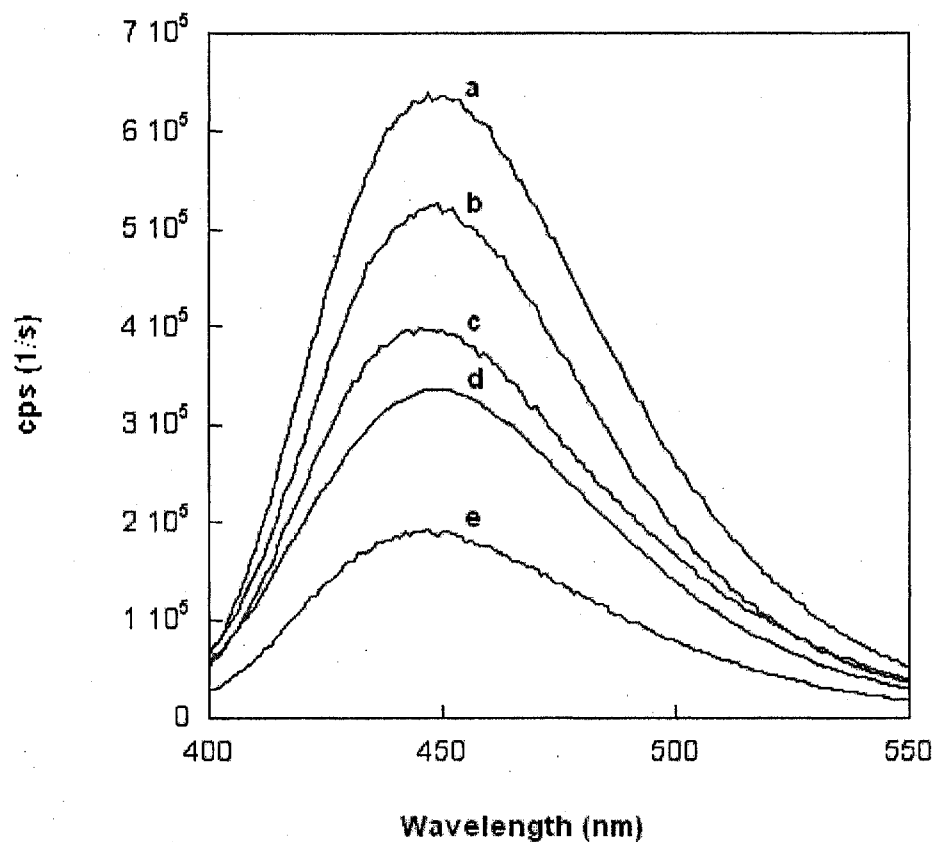


Figure 38. Fluorescence based assay for GCYH-I activity. Fluorescence was measured with excitation at 365 nm. (a) *T. maritima* COG1469; (b) *B. subtilis* COG1469; (c) *E. coli* FolE; (d) authentic neopterin; and (e) *N. gonorrhoeae* COG1469. Reactions were performed in 100 mM Tris-HCl (pH 8.0), 100 mM KCl, 2 mM MgCl₂, 1 mM GTP and either 10 μM *E. coli* FolE or 40 μM COG1469 proteins in a total volume of 100 μl at 37 °C (*E. coli* FolE and *B. subtilis* and *N. gonorrhoeae* COG1469) or 75 °C (*T. maritima* COG1469). Reaction products were dephosphorylated by alkaline phosphatase followed by oxidation upon the addition of an acidic iodine solution.

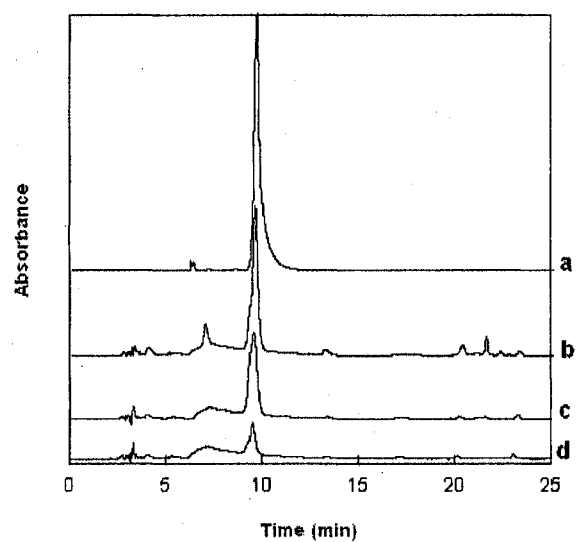
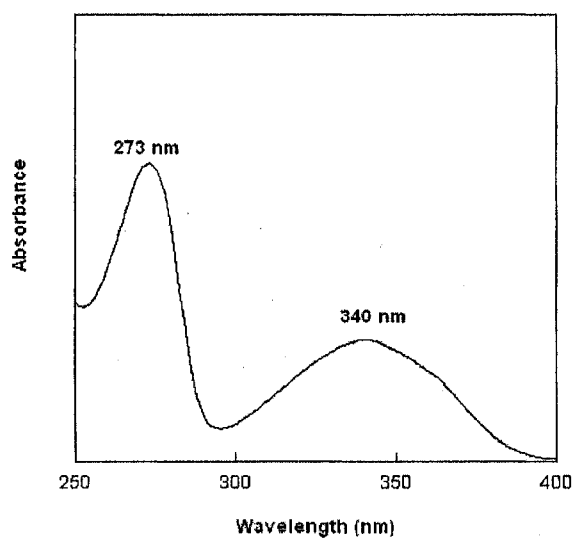
A**B**

Figure 39. HPLC Based Assay For GCYH-I Activity. (A) HPLC chromatograms of authentic neopterin (a), an *E. coli* FolE reaction (b), *B. subtilis* COG1469 reaction spiked with authentic neopterin (c), and *B. subtilis* COG1469 reaction without neopterin (d). Assays were subjected to postreaction dephosphorylation and oxidation. (B) The UV-vis spectrum of the peak eluting ~ 9 min from (d).

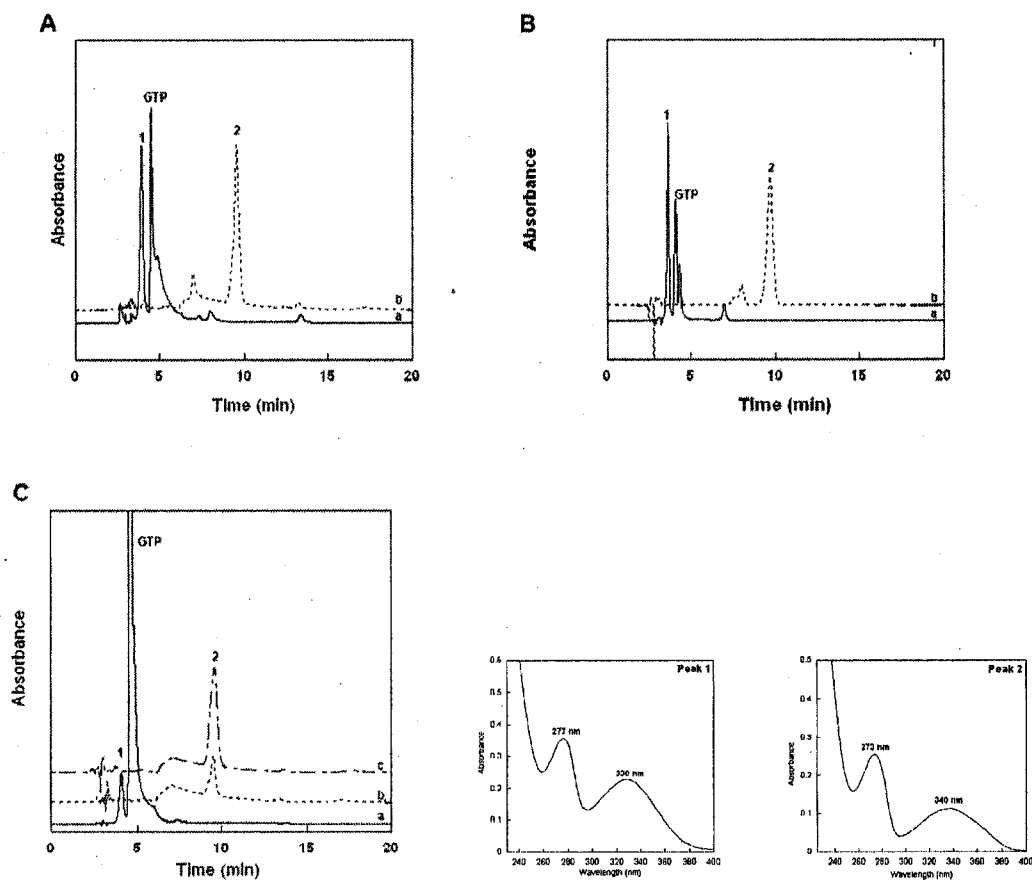


Figure 40. HPLC Analysis of reaction products from *E. coli* Fole and *N. gonorrhoeae* and *B. subtilis* COG1469 with and without alkaline phosphatase treatment. Upper case lettering represents reactions catalyzed by; (A) *E. coli* Fole, (B) *N. gonorrhoeae* COG1469, and (C) *B. subtilis* COG1469. Lower case lettering in figure represents; (a) direct analysis of reaction products, (b) analysis of reaction products after alkaline treatment, and (c) analysis of reaction products after alkaline spiked with authentic neopterin (*B. subtilis* COG1469 only). The UV-vis spectra for peaks 1 and 2 are characteristic of dihydroneopterin and neopterin, respectively [60, 104].

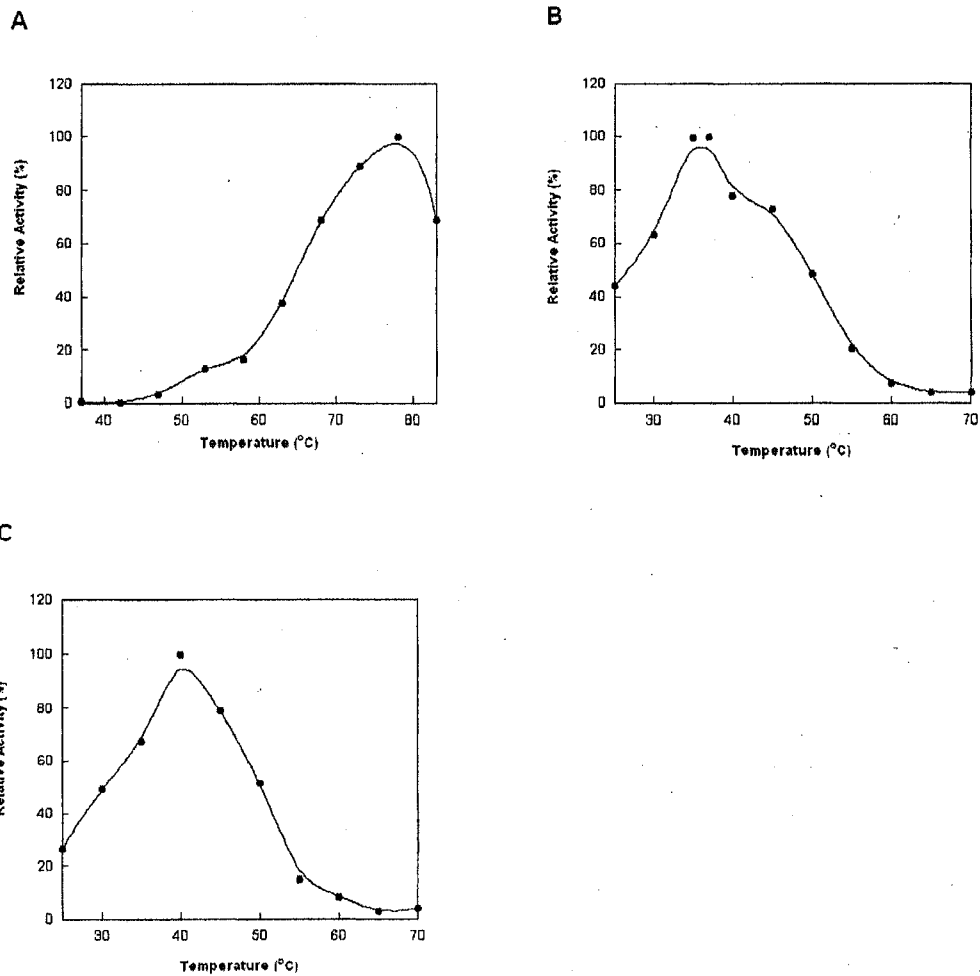


Figure 41. Effect of temperature on the relative activity of COG1469 proteins. (A) *T. maritima* COG1469, (B) *N. gonorrhoeae* COG1469 and (C) *B. subtilis* COG1469. Activity assays were performed in 100 mM phosphate (pH 7.5), 100 mM KCl, 0.5 mM MnCl₂, 0.5 mM GTP and 2 μM protein in a final volume of 100 μl. Reactions were incubated for 30 min and analyzed by fluorescence. Data points represent the average of 3 triplicates.

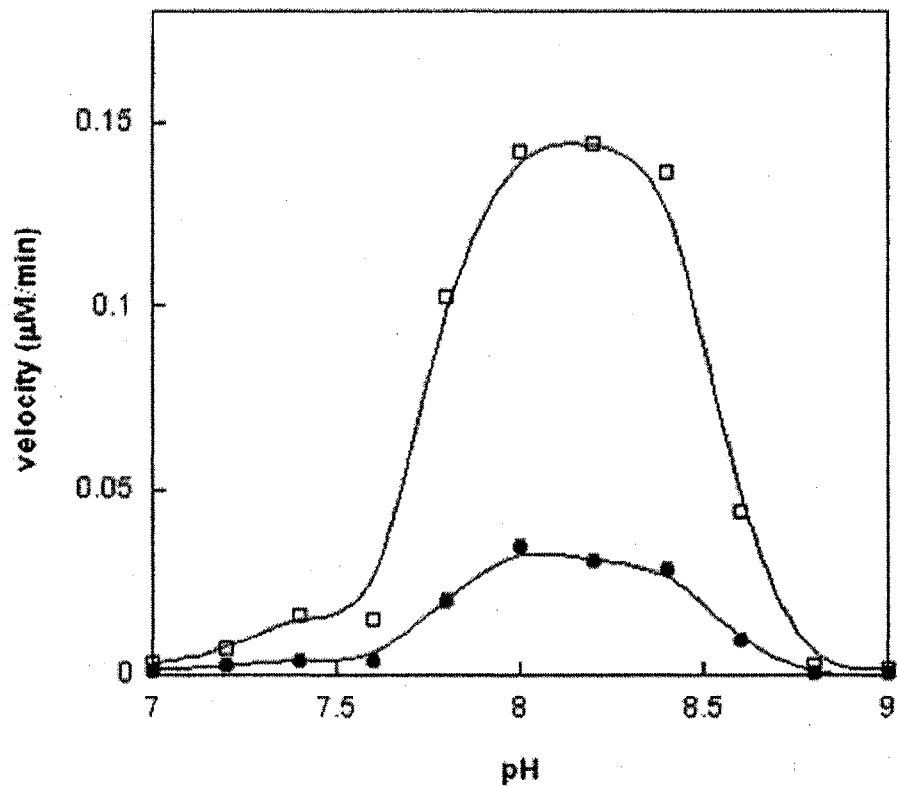


Figure 42 pH profile for *N. gonorrhoeae* COG1469 (□) and *B. subtilis* COG1469 (●) proteins. Activity assays were performed in 100 mM Tris, 50 mM MES, 50 mM acetic acid, 100 mM KCl, 0.5 mM MnCl₂, 2 mM DTT, 50 μM GTP and 1 μM protein under initial velocity conditions and analyzed by fluorescence. Data points represent the average of 3 triplicates.

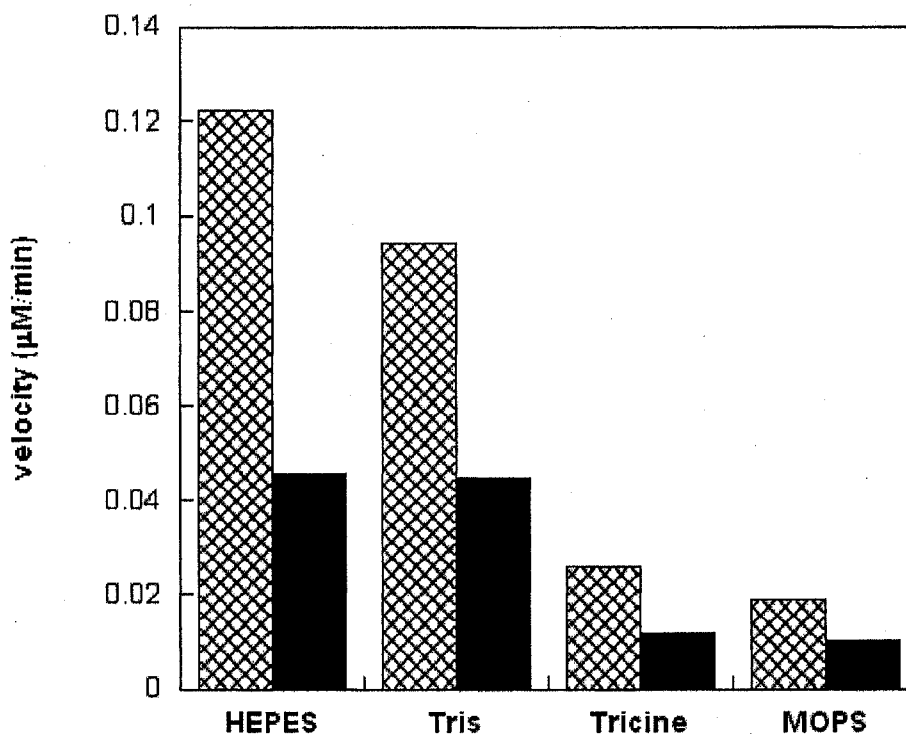


Figure 43. Effect of buffers on maximal activity. Enzyme activity from *N. gonorrhoeae* and *B. subtilis* COG1469 was measured with different buffers (pH 8.0, 100 mM). Reactions were carried out at 37 °C for 20 min 100 mM buffer (pH 8.0), 100 mM KCl, 0.5 mM MnCl₂, 1 mM DTT, 50 μM GTP and 0.5 μM protein. Enzyme assays were subjected to postreaction oxidation and analyzed by fluorescence. Hashed columns represents *N. gonorrhoeae* COG1469, and the solid columns represent *B. subtilis* COG1469.

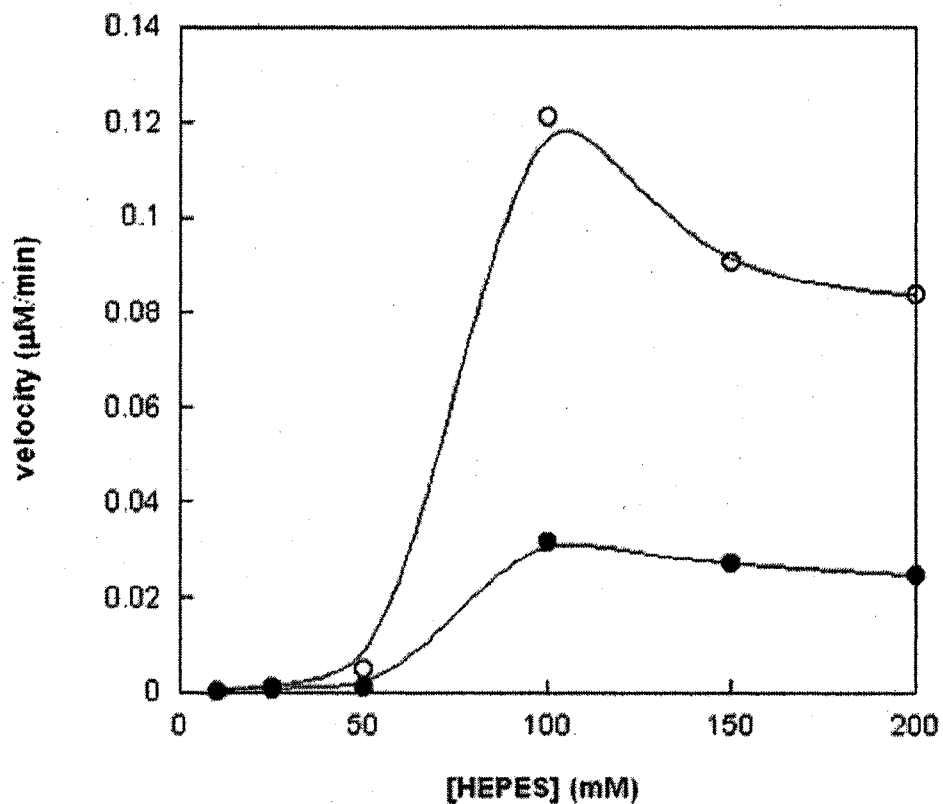


Figure 44. Effect of buffer strength on activity. Enzyme activity of *N. gonorrhoeae* (○) and *B. subtilis* (●) COG1469 with variable HEPES concentration. Reactions were carried out at 37 °C for 20 min in 0-200 mM HEPES (pH 8.0) 100 mM KCl, 0.5 mM MnCl_2 , 1 mM DTT, 50 μM GTP and 0.5 μM protein. Enzyme assays were subjected to post-reaction oxidation and analyzed by fluorescence.

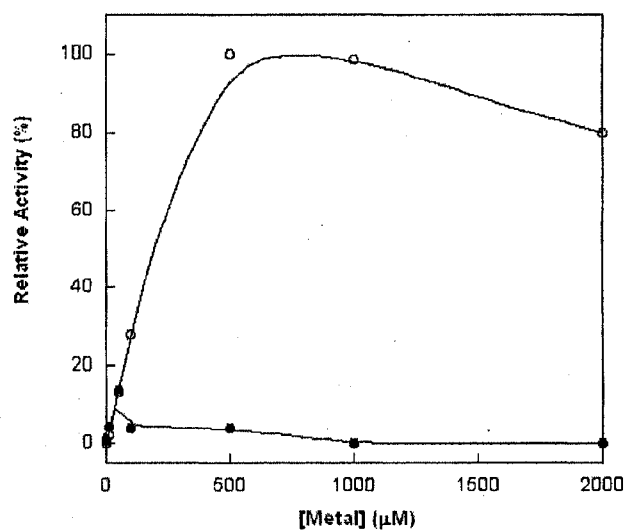
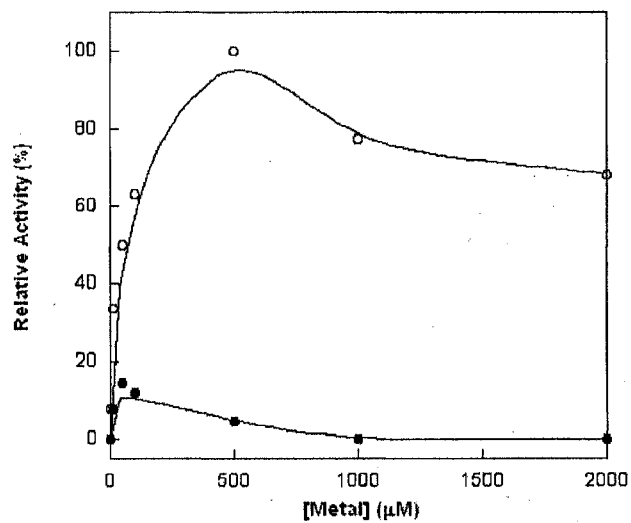
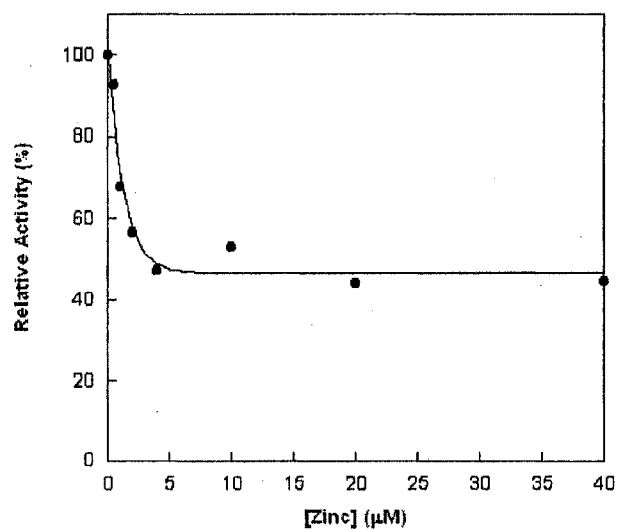
A**B**

Figure 45. COG1469 from *N. gonorrhoeae* (A) and *B. subtilis* (B) as a function of manganese (○) and zinc (●) concentration. Reactions were carried out in the presence of 100 mM HEPES (pH 8.0), 100 mM KCl, 0.1 mM GTP, 2 μM protein and varying concentration of metal ions.

A



B

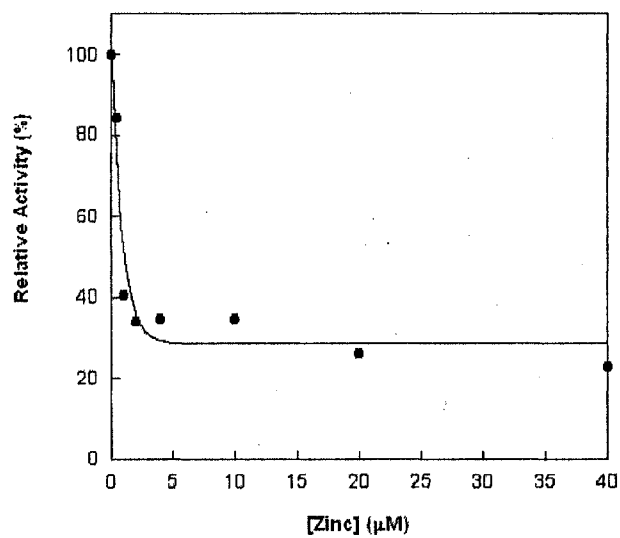


Figure 46. The inhibitory effect of zinc on manganese dependent enzyme activity of *N. gonorrhoeae* (A) and *B. subtilis* (B) COG1469. Each data point represents the average of 4 sets of triplicates.

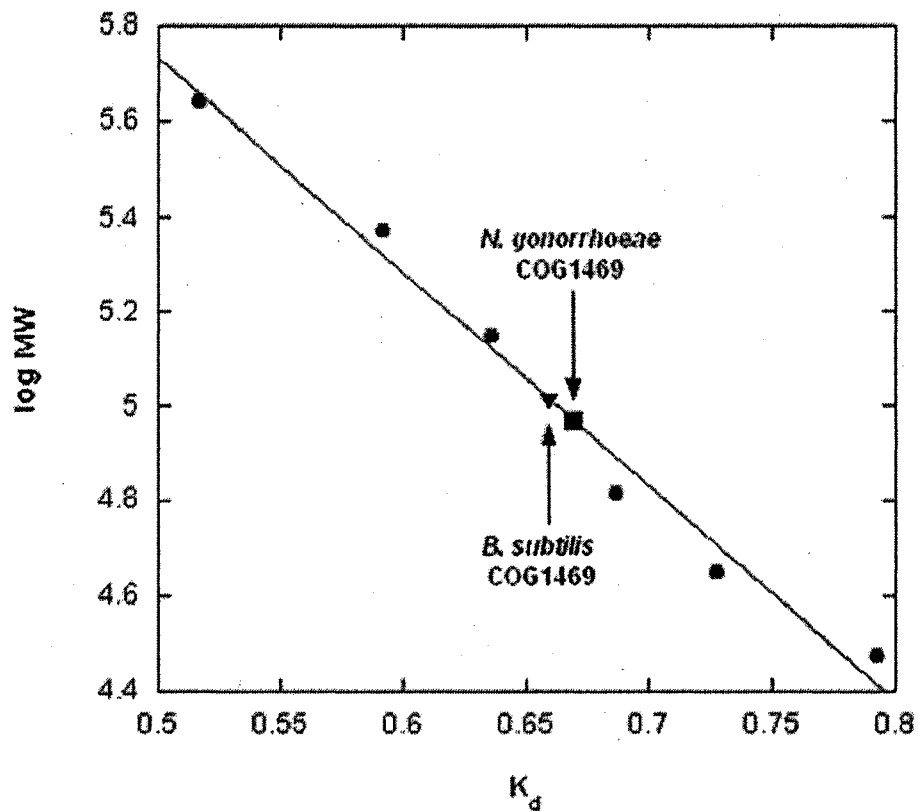


Figure 47. Molecular weight estimation for *B. subtilis* and *N. gonorrhoeae* COG169 proteins. The plot illustrates the elution position of wild-type *B. subtilis* (▼) and *N. gonorrhoeae* (■) COG1469 proteins relative to proteins of known molecular weight (Ferritin, 443 kDa; pyruvate kinase, 237 kDa; alcohol dehydrogenase, 150 kDa; bovine serum albumin, 65.4 kDa; ovalbumin, 48.9 kDa and carbonic anhydrase 30 kDa). The void and total volume were calculated from the elution volumes of blue dextran and DNP-aspartate (299 Da), respectively.

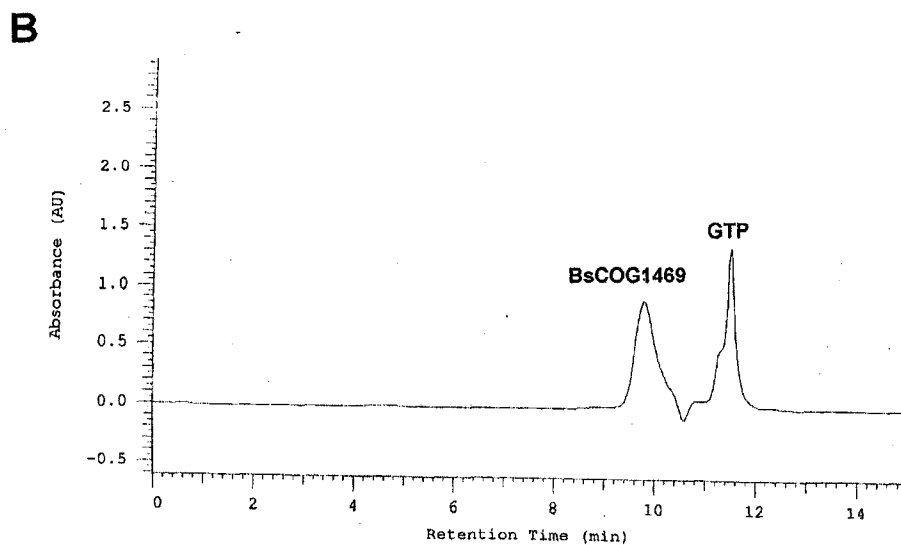
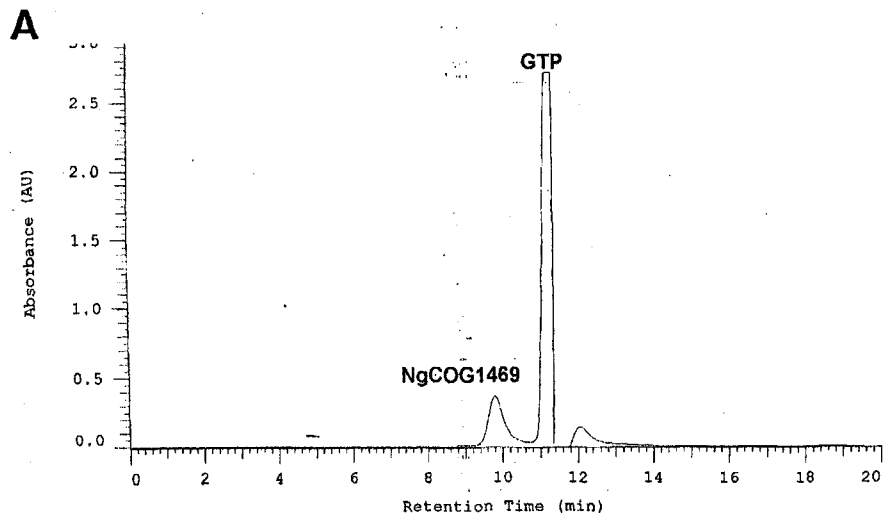


Figure 48. HPLC chromatograms of the elution profile of (A) *N. gonorrhoeae* COG1469, and (B) *B. subtilis* COG1469 on a BioSep-SEC-S4000 gel filtration column. Proteins were incubated in the presence of 0.5 mM GTP and 0.5 mM MnCl₂ prior to injection and eluted with 20 mM sodium phosphate (pH 7.2), 100 mM NaCl, 0.1 mM GTP and 0.5 mM MnCl₂.

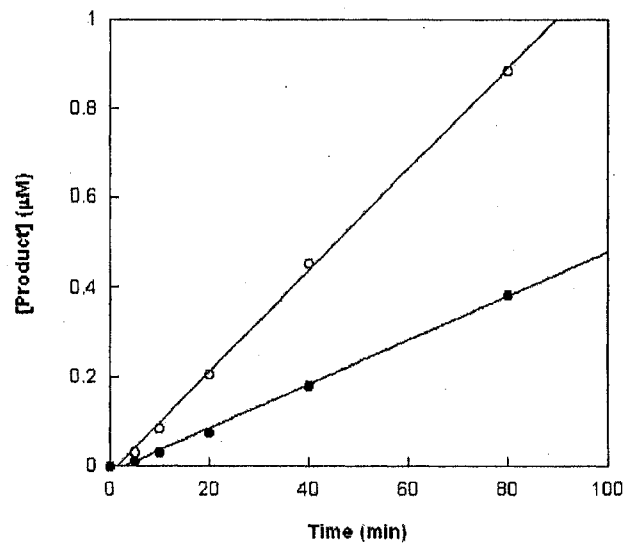
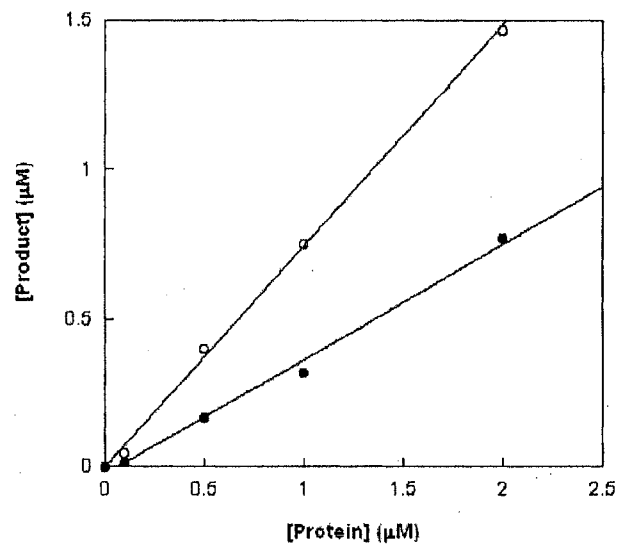
A**B**

Figure 49. *N. gonorrhoeae* (\circ) and *B. subtilis* (\bullet) COG1469 activity as a function of time (A) and enzyme concentration (B). Reactions were carried out in 100 mM HEPES (pH 8.0), 100 mM KCl, 1 mM DTT, 0.5 mM MnCl_2 , and 30 μM GTP. Time dependent analysis was conducted in the presence of 0.5 μM protein. Analysis of enzyme activity as a function of enzyme concentration were carried out for 30 min.

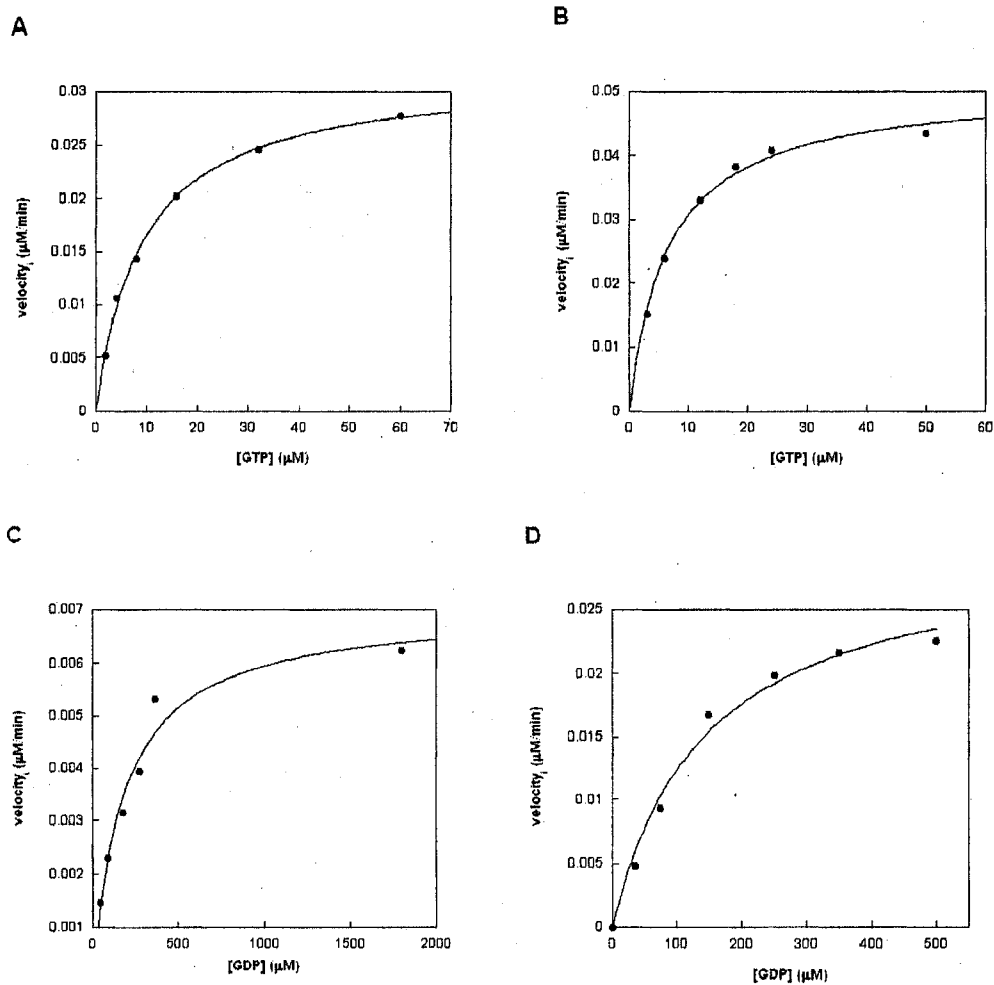


Figure 50. Substrate Kinetic Analysis of *N. gonorrhoeae* COG1469. Reactions were carried out in 100 mM HEPES (pH 8.0), 100 mM KCl, 0.5 mM MnCl₂ at 37°C. Assays performed in the presence of (A) varying concentrations of GTP and 2 μM protein; (B) varying concentrations of GTP, 1 mM DTT and 0.5 μM Protein; (C) varying concentrations of GDP and 2 μM protein; (D) varying concentrations of GDP, 1 mM DTT and 0.5 μM protein. Activity was measured every 10 min for a total of 30 min. Nonlinear regression analysis of the data (minimally 4 sets of triplicates) was conducted using KaleidaGraph 4.0.

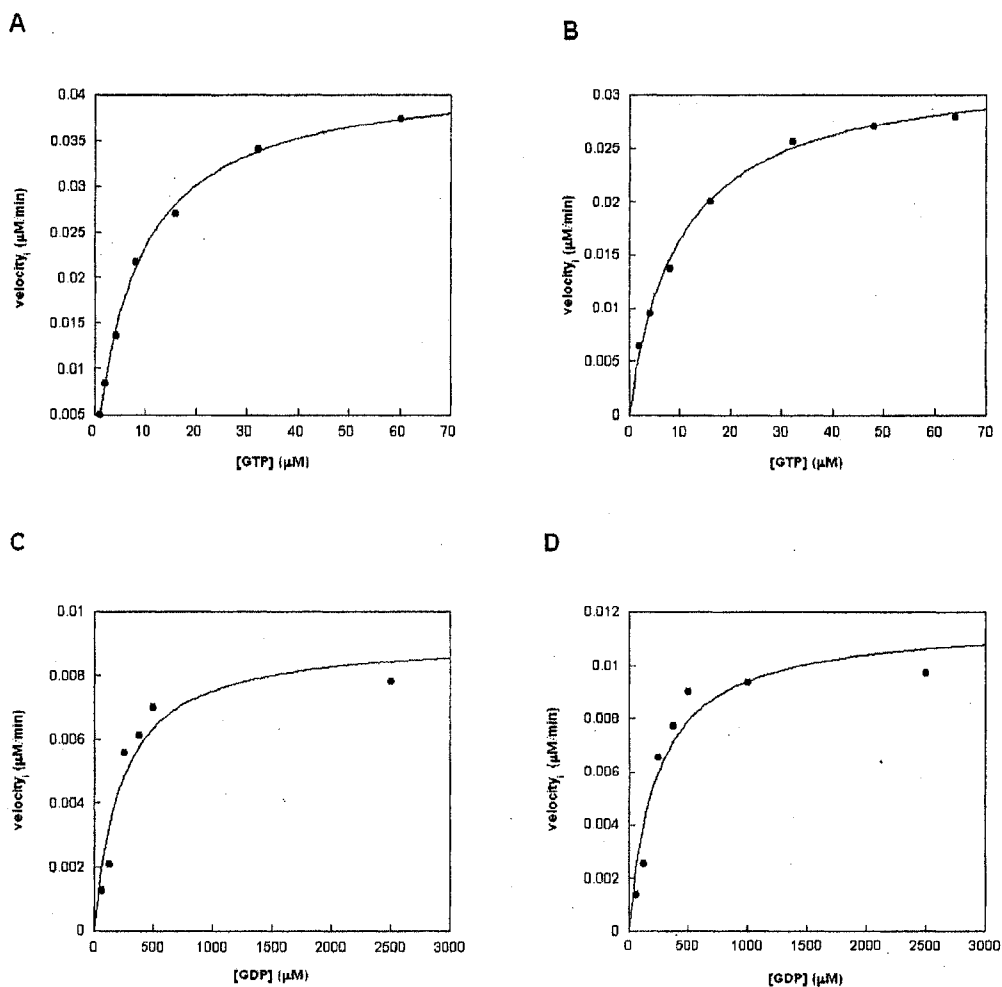


Figure 51. Substrate Kinetic Analysis of *B. subtilis* COG1469. Reactions were carried out in 100 mM HEPES (pH 8.0), 100 mM KCl, 0.5 mM MnCl₂ at 37°C. Assays performed in the presence of (A) varying concentrations of GTP and 2 μM protein; (B) varying concentrations of GTP, 1 mM DTT and 0.5 μM protein; (C) varying concentrations of GDP and 2 μM protein; (D) varying concentrations of GDP, 1 mM DTT and 0.5 μM protein. Activity was measured every 10 min for a total of 30 min. Nonlinear regression analysis of the data (minimally 4 sets of triplicates) was conducted using KaleidaGraph 4.0.

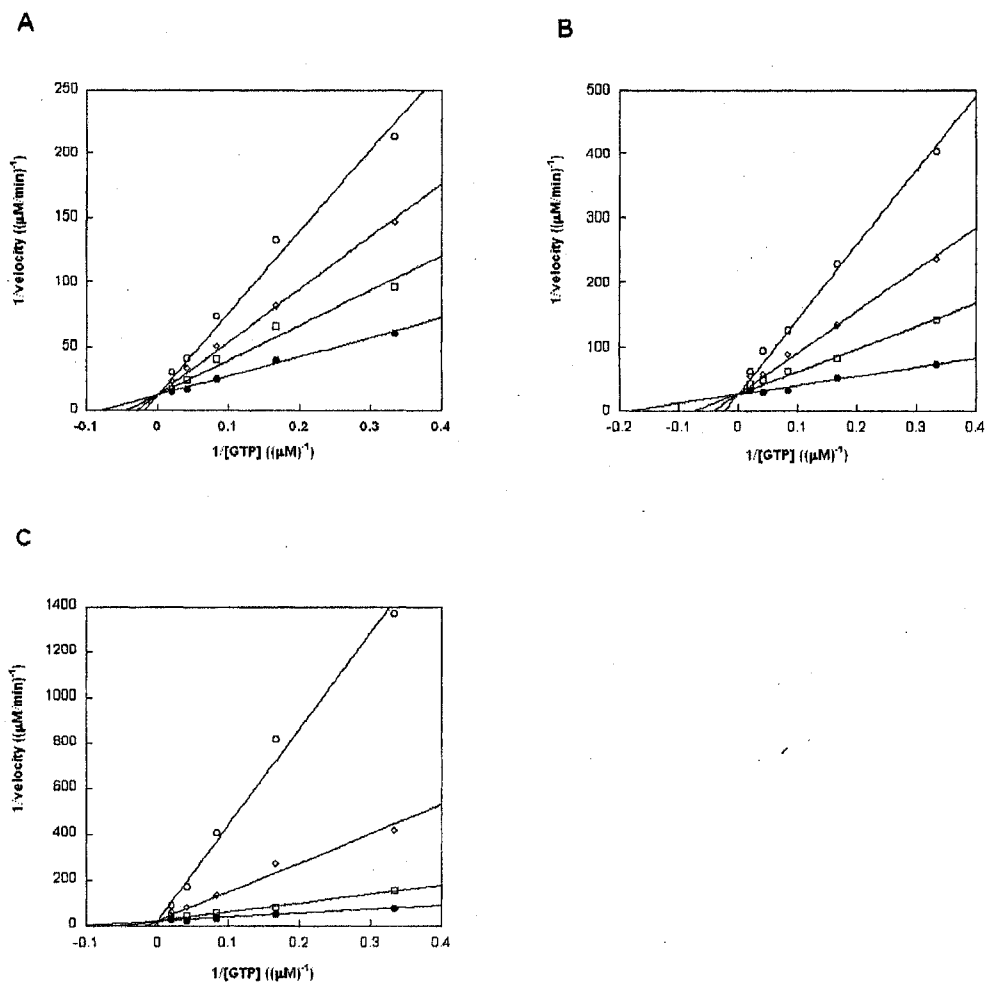


Figure 52. Inhibition analysis of *N. gonorrhoeae* COG1469. Reactions were performed with varied GTP concentration (3-50 μM) and various fixed concentrations of inhibitor. Activity was monitored by fluorescence. (A) 2'-deoxyGTP: (\bullet) 0, (\square) 50, (\diamond) 100, and (\circ) 200 μM ; (B) 7-deazaGTP: (\bullet) 0, (\square) 15, (\diamond) 30, and (\circ) 60 μM ; and (C) 8-oxoGTP: (\bullet) 0, (\square) 0.1, (\diamond) 0.25, and (\circ) 0.5 μM . Activity was measured every 10 min for a total of 30 min. Data (minimally 4 sets of triplicates) were fit to eq 1, competitive inhibition, using KaleidaGraph 4.0.

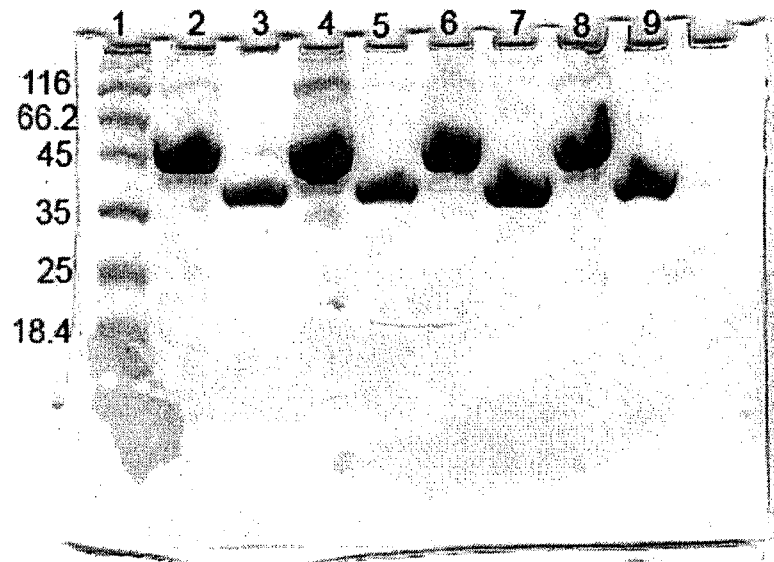


Figure 53. SDS-PAGE analysis of purified *N. gonorrhoeae* COG1469 H245 His₆-tag (33.6 kDa) and non-His₆-tag (28.7 kDa) mutants. Lane 1, MW markers; lane 2, H245K His₆-tag; lane 3, H245K; lane 4, H245N His₆-tag; lane 5, H245N; lane 6, H245D His₆-tag; lane 7, H245D; lane 8, H245Q His₆-tag; lane 9, H245Q.

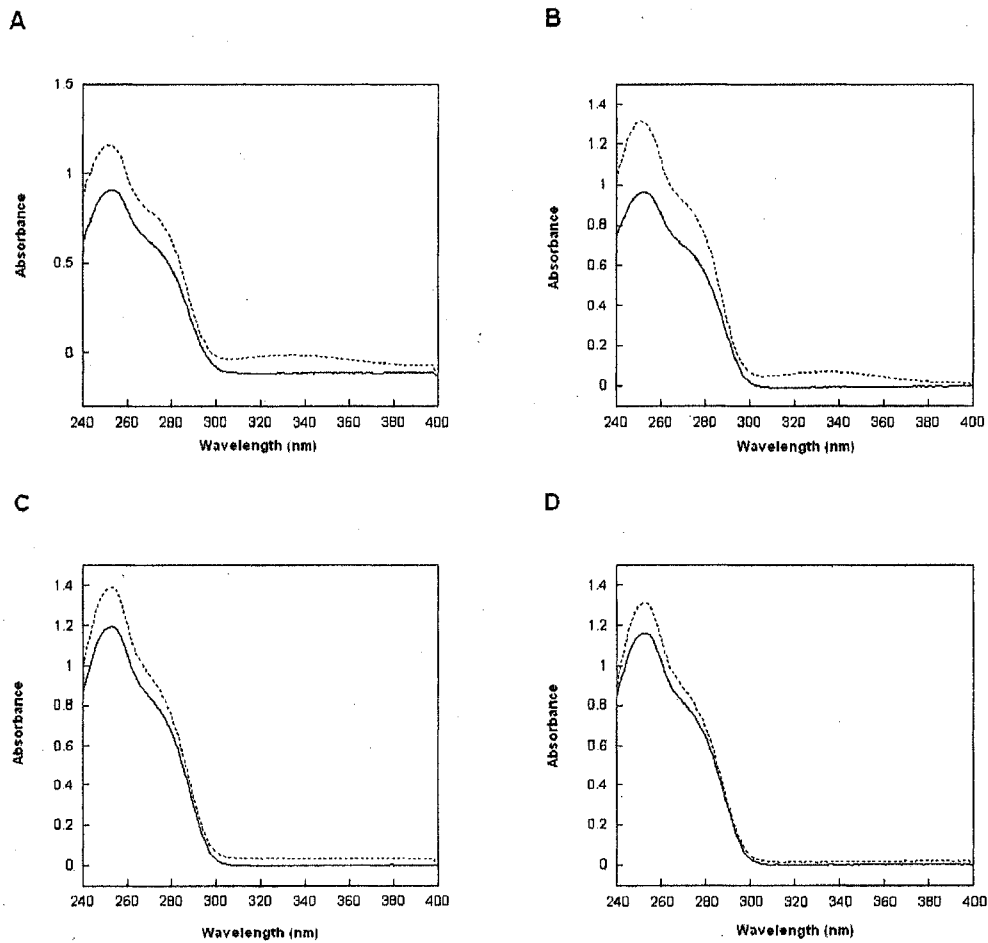


Figure 54. Spectrophotometric based assay for *N. gonorrhoeae* COG1469 H245 mutant activity. Assays were performed in 100 mM HEPES (pH 8.0), 100 mM KCl, 1 mM DTT, 0.5 mM MnCl₂, and 50 μ M mutant *N. gonorrhoeae* COG1469 protein in a total volume of 150 μ l. Reactions were initiated upon the addition of GTP to a final concentration of 0.1 mM and incubated at 37°C. The reactions were allowed to proceed for 2 h while monitoring the absorbance from 200-400 nm. (A) H245D, (B) H245Q, (C)H245N, (D) H245K.

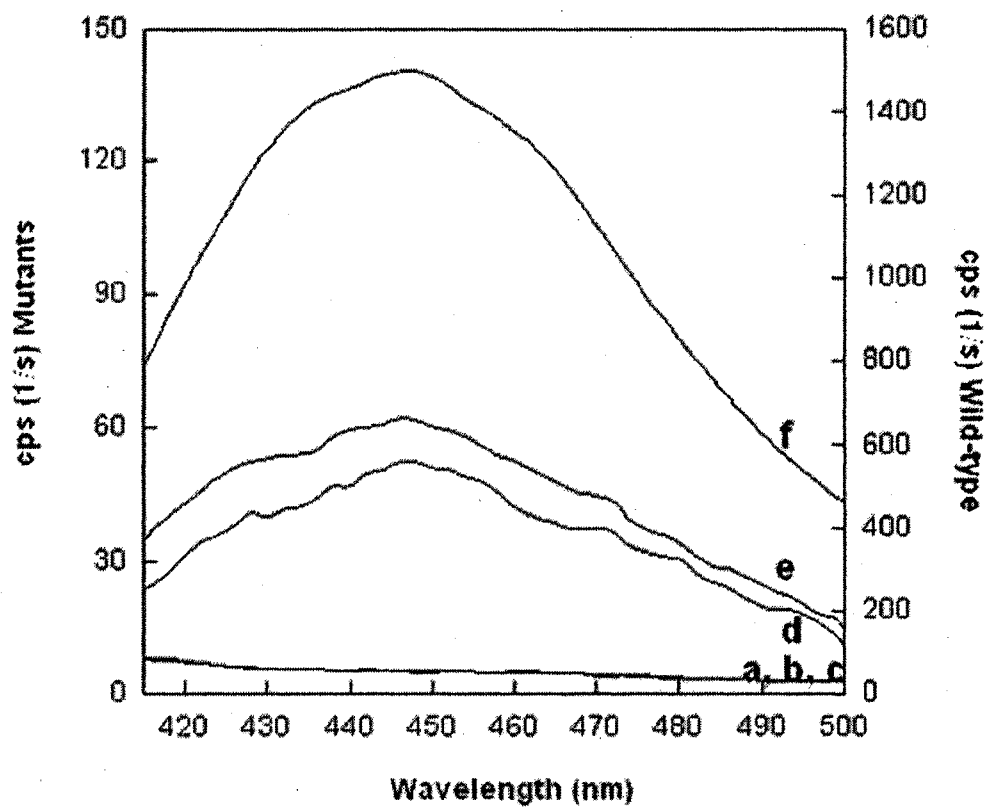


Figure 55. GYH-I fluorescence activity assay of H245 *N. gonorrhoeae* COG1469 mutants. Fluorescent spectra of (a) control, (b) H245N, (c) H245K; (d) H245Q; (e) H245D and (f) wild-type.

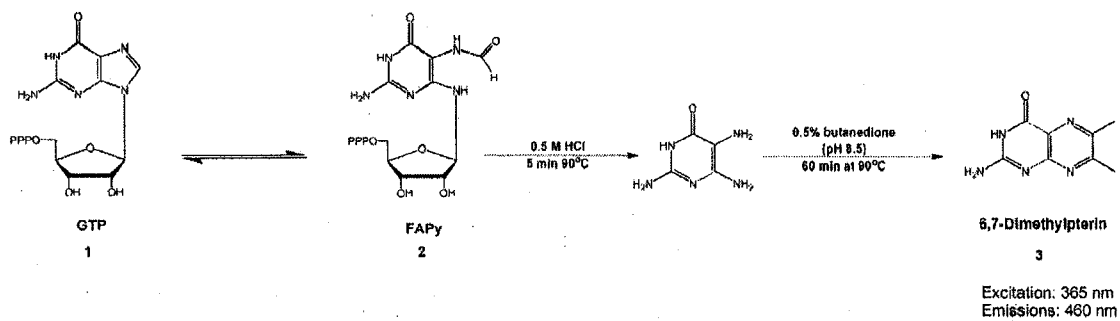


Figure 56. Derivatization of FAPy (or APy, structure not shown) for GCYH-II and III Fluorescence Analysis. The assay of H245 mutants of *N. gonorrhoeae* COG1469 were boiled in HCl for 5 min, followed by a pH adjustment to 8.5 with the addition of NaOH. After the addition of butanedione, the samples were incubated for 60 min at 90°C and the resulting formation of 6,7-dimethylpterin was analyzed by fluorescence (excitation 365 nm, emission 460 nm).

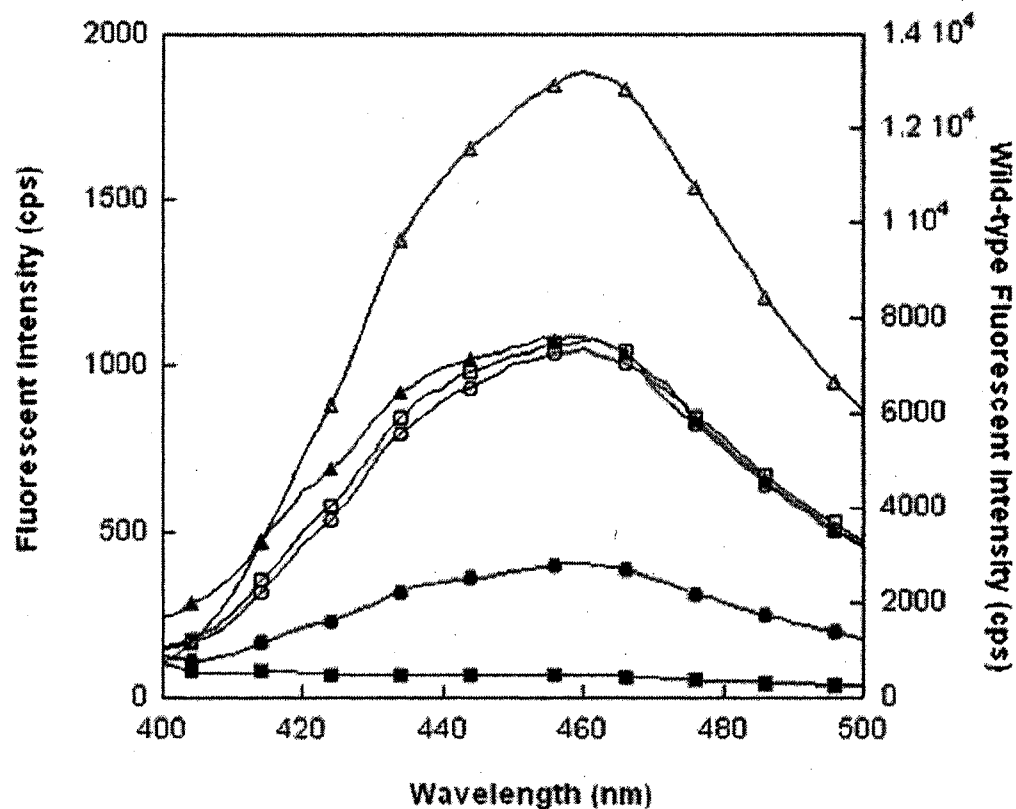


Figure 57. Fluorescence based assay for GCYH-III activity. GCYH-III activity of *N. gonorrhoeae* COG1469 H245 mutants was measured by fluorescence with excitation at 365 nm. H245K (■), H245N (●), H245D (○), H245Q (□), *E. coli* RibA (▲) and wild-type *N. gonorrhoeae* COG1469 (Δ). Reactions were carried out at 37°C for 1 h in 100 mM HEPES (pH 8.0), 100 mM KCl, 0.5 mM MnCl₂, 1 mM DTT 0.1 mM GTP and 2 μM enzyme. Enzyme assays were subjected to post-reaction steps.

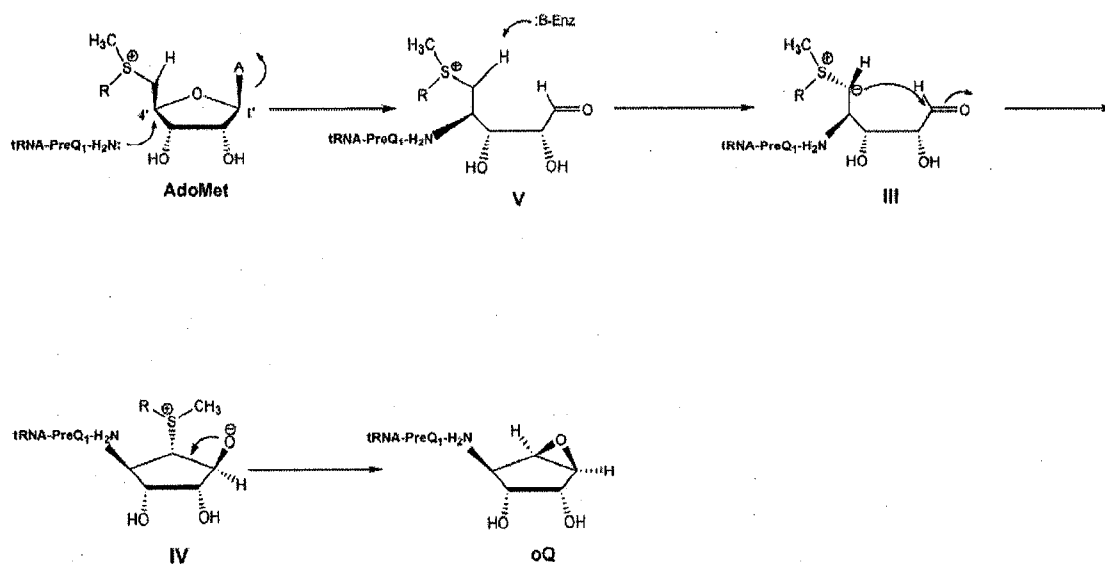


Figure 58. An alternative QueA chemical mechanism involving the direct S_N2 attack of the preQ1 methylamine group at C-4' followed by deprotonation to give sulfonium ylide III.

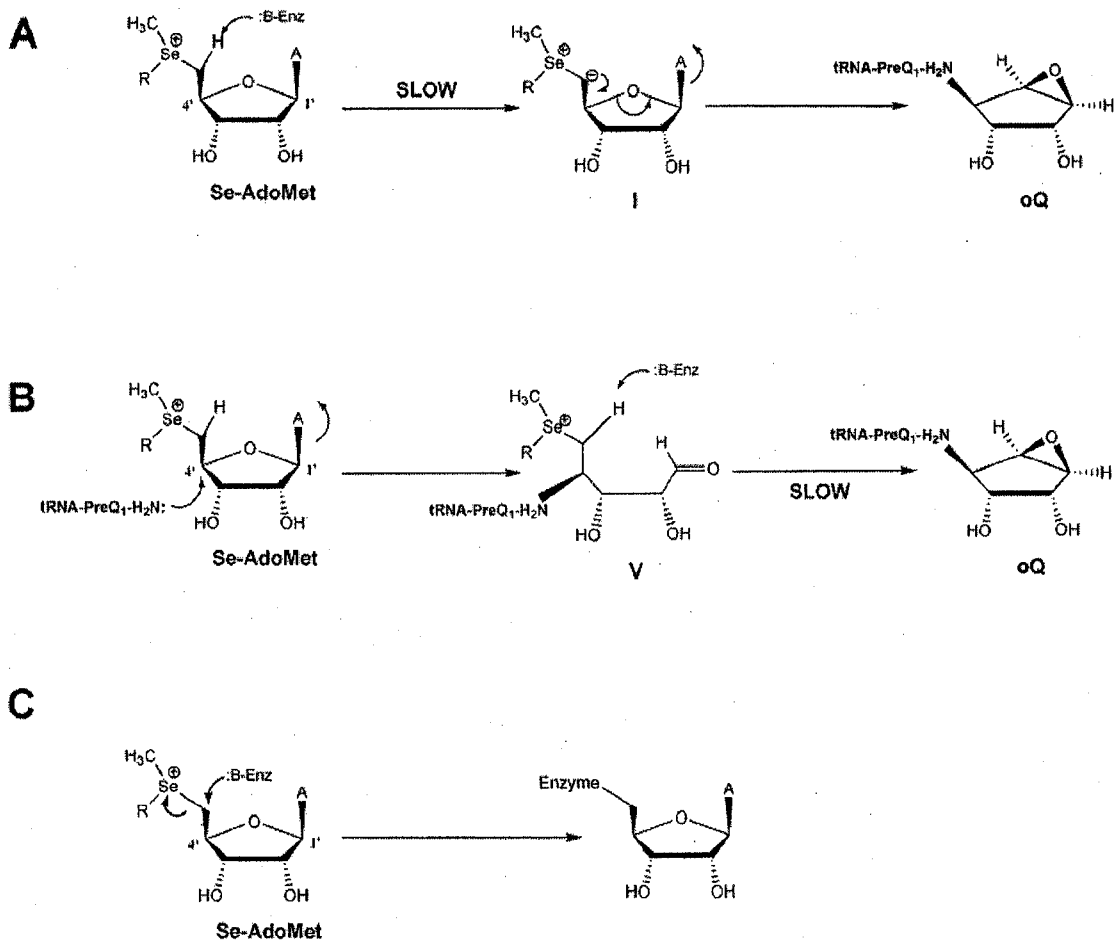


Figure 59. The potential consequences of substituting AdoMet with SeAdoMet in a QueA reaction. (A) Reaction initiated with the deprotonation of the C5' hydrogen as outlined in the proposed chemical mechanism. Rate of deprotonation would be much slower than that of AdoMet; (B) Direct S_N2 attack of the methylamine group of preQ₁ would not expect SeAdoMet to act significantly differently to that of AdoMet with respect to radioactive quantification; (C) Formation of a covalent adduct between QueA and SeAdoMet.

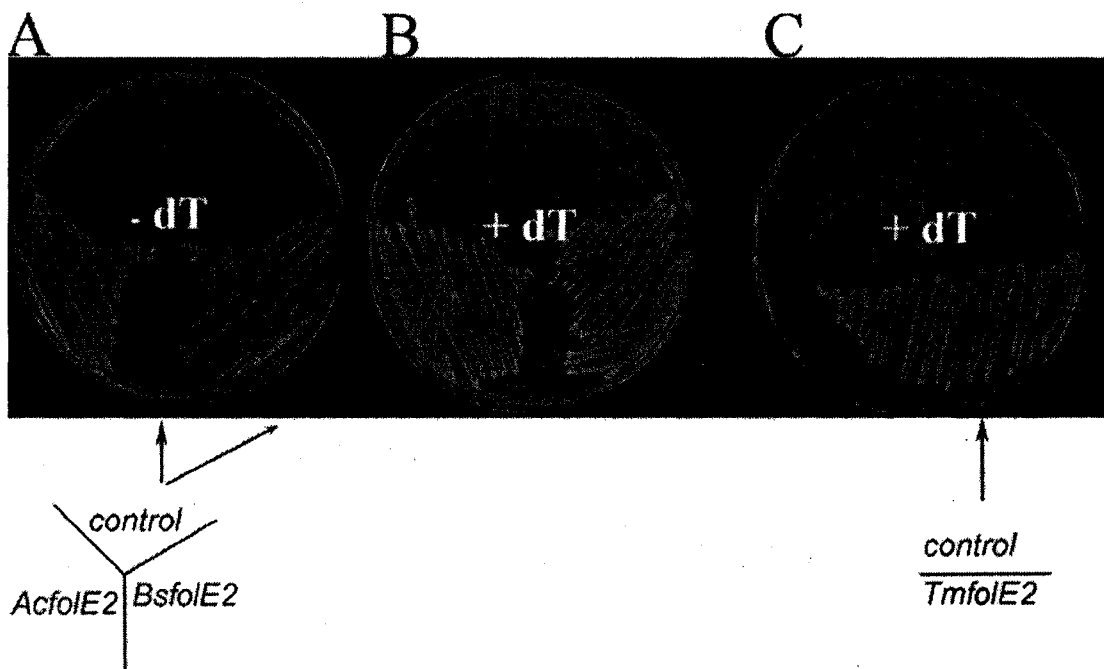
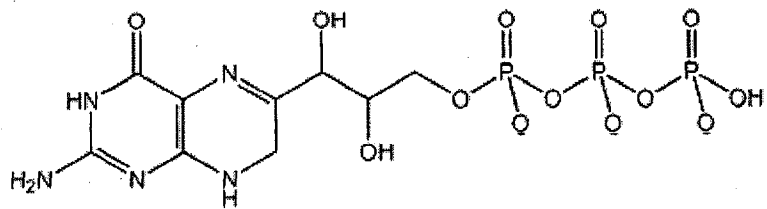
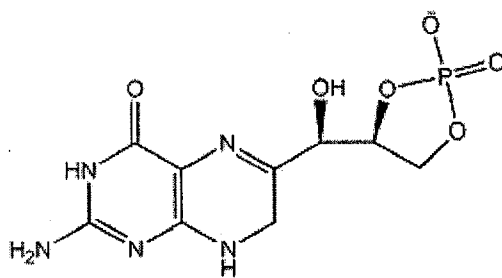


Figure 60. Complementation of the $\Delta folE::Kan^R$ by a plasmid expressing COG1469 gene from *B. subtilis* and *A. baylyi* on LB in absence of dT (A) and presence of dT (B). Complementation of the $\Delta folE::Kan^R$ by a plasmid expressing COG1469 gene from *T. maritima* on LB in the presence of dT (C). Image taken from publication by El Yacoubi, et. al. [123].



**7,8-Dihydroneopterin
triphosphate
(H₂NTP)**



**7,8-Dihydroneopterin
2',3'-cyclic phosphate**

Figure 61. The chemical structure of dihydroneopterin triphosphate and dihydroneopterin 2',3'-cyclic phosphate.

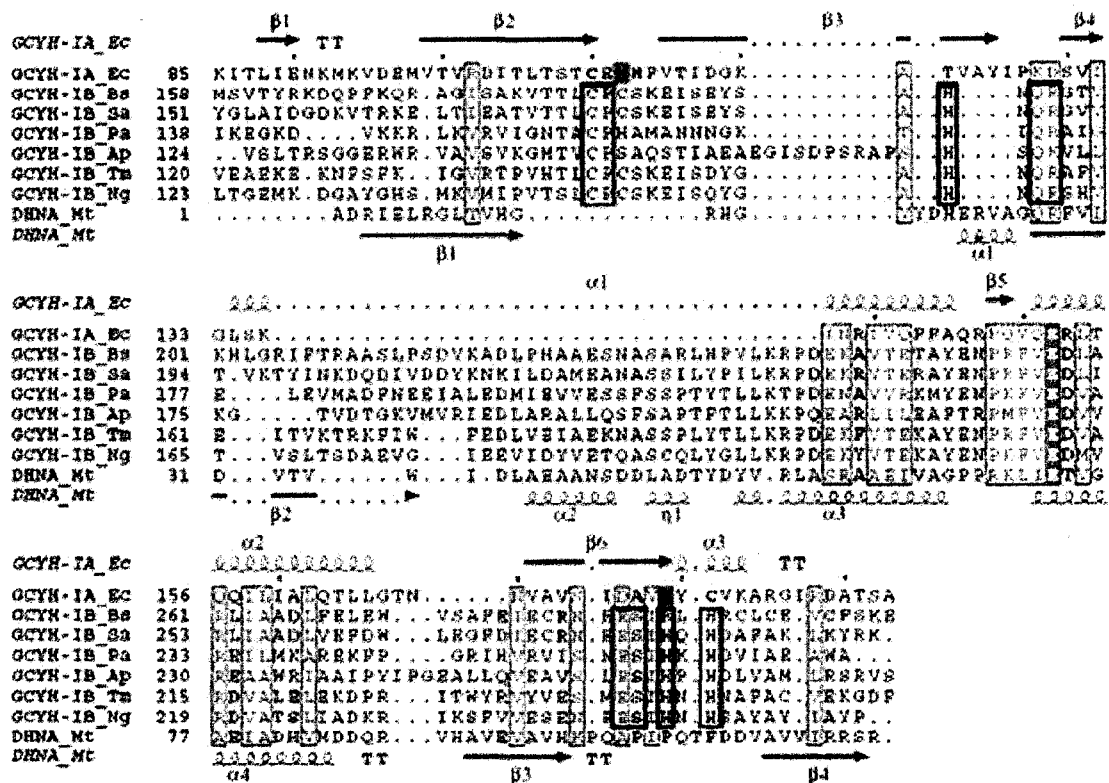


Figure 63. The primary and tertiary structure alignment of the C-terminal region of GCYH-IA, GCYH-IB and DHNA. The secondary structural elements from GCYH-IA and DHNA derived from their respective crystal structures are shown above whereas the primary sequences are shown below. Conserved residues in all three enzyme families are represented by red boxes. The invariant Glu residue is highlighted in red. Residues involved in zinc binding and catalysis in GCYH-IA are highlighted yellow and cyan, respectively. Predicted metal binding and catalytic residues, as determined on their predicted spatial homology to active site residues of GCYH-IA and DHNA, in GCYH-IB are indicated by the bold black boxes. *Ec*, *E. coli*; *Bs*, *B. subtilis*; *Sa*, *S. aureus*; *Pa*, *Pyrococcus abyssi*; *Ap*, *Aeropyrum pernix*; *Tm*, *T. maritima*; *Ng*, *N. gonorrhoeae*; *Mt*, *M. tuberculosis*. The image was taken from published work of El Yacoubi [123].

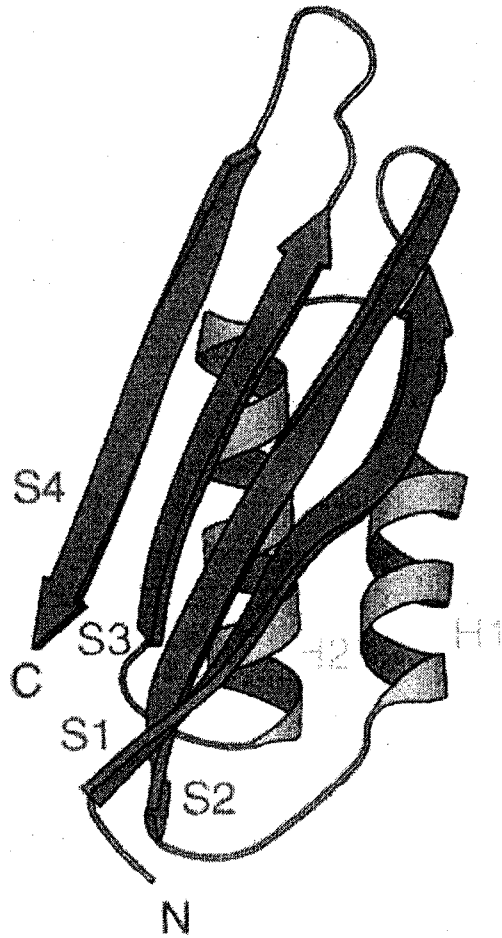


Figure 64. Structural Representation of the T-fold Domain. The T-fold domain is composed of 4 antiparallel β -sheets and two antiparallel α -helices that spanning between the second and third β -sheet. Image taken from published work of Colloc'h [139].

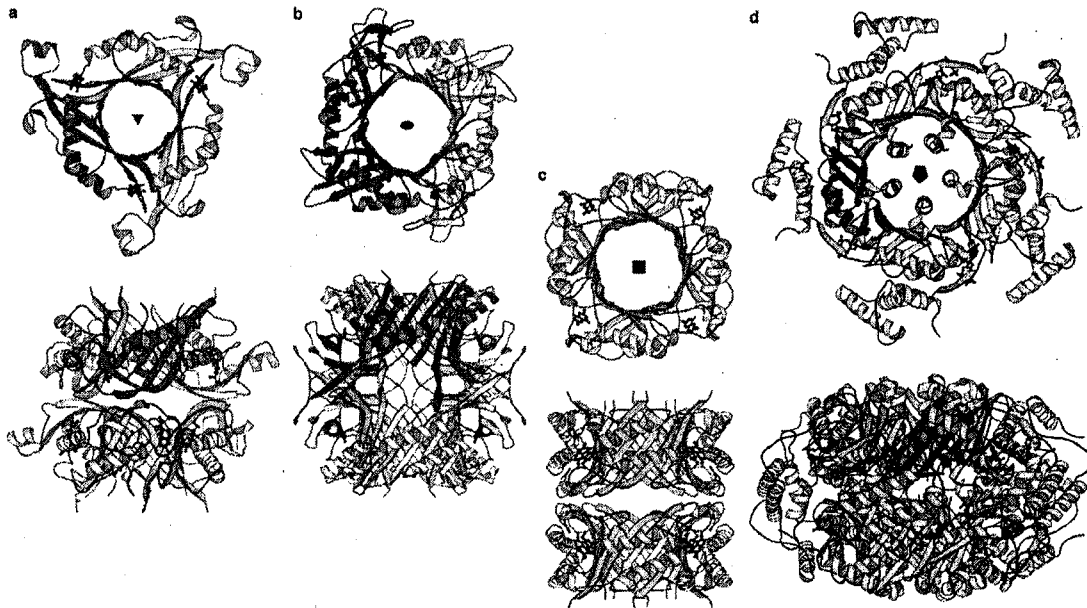


Figure 65. Representative Structures of T-fold proteins; (a) PTPS, (b) UOX, (c) DHNA, and (d) GCYH-I. Oligomerization entails the association of 2 multimeric barrels in a “head-to-head” fashion resulting in the formation of a tunnel-like center. Image taken from publish work of Colloc’h [139].

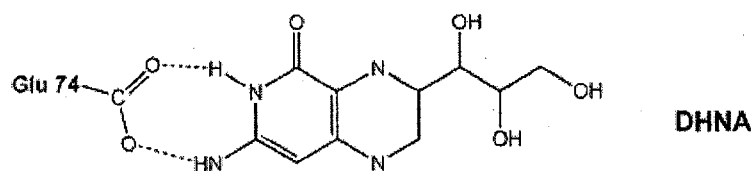
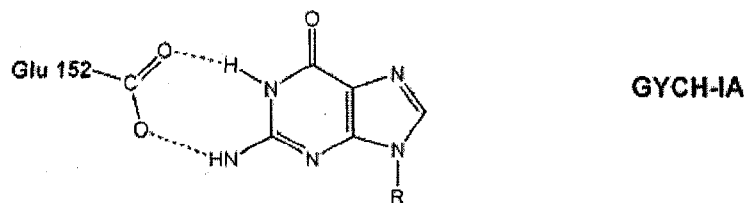
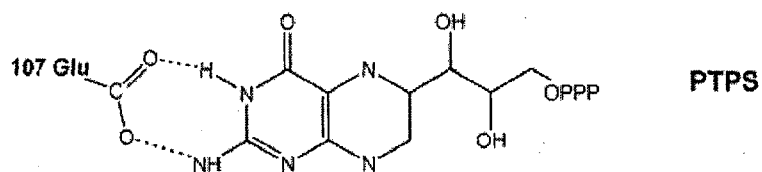
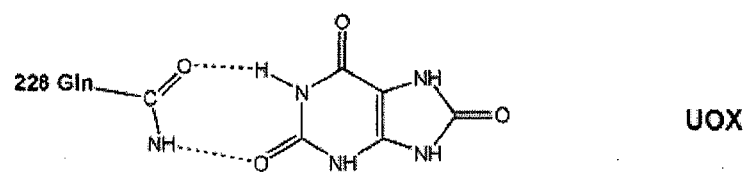


Figure 66. Substrate binding of T-fold proteins (UOX, PTPS, GYCH-IA and DHNA) with a conserved Gln or Glu residue.

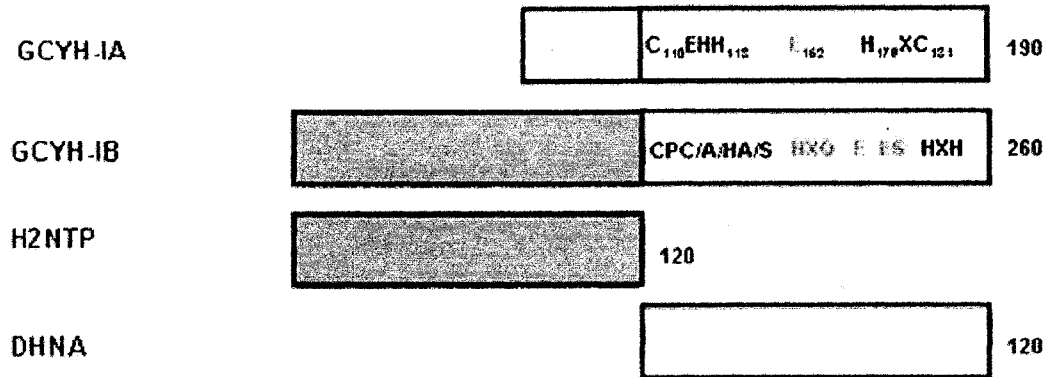


Figure 67. Organization of the T-fold domain region in GCYH-IA, GCYH-IB, 7,8-dihydroneopterin triphosphate epimerase (H2NTP), and 7,8-dihydroneopterin aldolase (DHNA). The substrate and metal binding residues in GCYH-IA along with putative metal coordinating and substrate binding domains of GCYH-IB are also displayed. Zinc binding and catalytic residues are represented in black and red, respectively. An additional conserved sequence found in GCYH-IB but not in GCYH-IA is represented in pink. Image taken from published work of El Yacoubi [123].

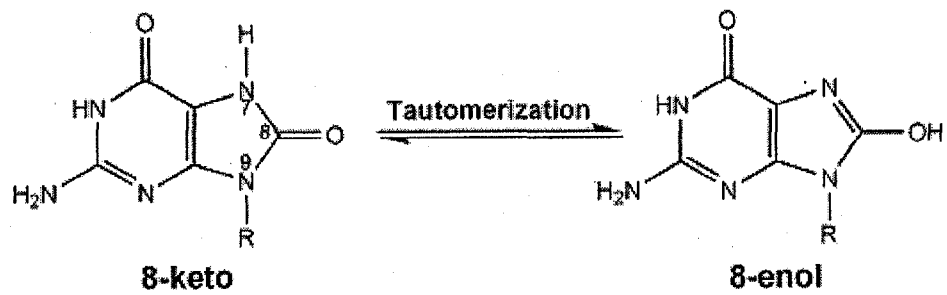


Figure 68. Tautomeric forms of 8-oxoGTP

Reference

1. Dunin-Horkawicz, S., et al., *MODOMICS: a database of RNA modification pathways*. Nucl. Acids Res., 2006. **34**(suppl_1): p. D145-149.
2. Bjork, G.R., *Biosynthesis and Function of Modified Nucleosides*, in *tRNA: Structure, Biosynthesis and Function*, D. Soll, RajBhandary, U.L., Editor. 1995, American Society for Microbiology: Washington D.C. p. 165-205.
3. Sprinzl, M. and K.S. Vassilenko, *Compilation of tRNA sequences and sequences of tRNA genes*. Nucl. Acids Res., 2005. **33**(suppl_1): p. D139-140.
4. Bjork, G.R., and Kohli, J., *In Chromatography and Modification of Nucleosides, Part B. Biological Roles and Function of Modification*, ed. C. Gehrke, and Kuo, K. 1990: Elsevier. B13-B67.
5. Muramatsu, T., et al., *Codon and amino-acid specificities of a transfer RNA are both converted by a single post-transcriptional modification*. J. Biol. Chem., 1988. **336**(6195): p. 179-181.
6. Muramatsu, T., et al., *A novel lysine-substituted nucleoside in the first position of the anticodon of minor isoleucine tRNA from Escherichia coli*. J. Biol. Chem., 1988. **263**(19): p. 9261-9267.
7. Gregson, J., et al., *Structure of the archaeal transfer RNA nucleoside G*-15 (2-amino-4,7-dihydro-4-oxo-7-beta-D-ribofuranosyl-1H-pyrrolo[2,3-d]pyrimidine-5-carboxamide (archaeosine))*. J. Biol. Chem., 1993. **268**(14): p. 10076-10086.
8. Kasai, H., et al., *Structure of the modified nucleoside Q isolated from Escherichia coli transfer ribonucleic acid. 7-(4,5-cis-dihydroxy-1-cyclopenten-3-ylaminomethyl)-7-deazaguanosine*. Biochemistry, 1975. **14**(19): p. 4198-4208.
9. Sprinzl, M., et al., *Compilation of tRNA sequences and sequences of tRNA genes*. Nucl. Acids Res., 1989. **17** (Suppl): p. r1-r172.
10. Kersten, H., *The nutrient factor queuine: Biosynthesis, occurrence in transfer RNA and function*. Biofactors, 1988. **1**(1): p. 27-29.
11. Katze, J., B. Basile, and J.A. McCloskey, *Queuine, a modified base incorporated posttranscriptionally into eukaryotic transfer RNA: Wide distribution in nature*. Science, 1982. **216**(4541): p. 55-56.
12. Carlson, B.A., et al., *Transfer RNA modification status influences retroviral ribosomal frameshifting*. Virology, 1999. **255**(1): p. 2-8.
13. Jacks, T., et al., *Signals for ribosomal frameshifting in the rous sarcoma virus gag-pol region*. Cell, 1988. **55**(3): p. 447-458.
14. Hatfield, D., et al., *Chromatographic analysis of the aminoacyl-tRNAs which are required for translation of codons at and around the ribosomal frameshift sites of HIV, HTLV-1, and BLV*. Virology, 1989. **173**(2): p. 736-742.
15. Durand, J., et al., *vacC, a virulence-associated chromosomal locus of Shigella flexneri, is homologous to tgt, a gene encoding tRNA-guanine transglycosylase (Tgt) of Escherichia coli K-12*. J. Bacteriol., 1994. **176**(15): p. 4627-4634.

16. Marks, T. and W.R. Farkas, *Effects of a diet deficient in tyrosine and queuine on germfree mice*. Biochemical and Biophysical Research Communications, 1997. **230**(2): p. 233-237.
17. Okada, N., et al., *Detection of unique tRNA species in tumor tissues by Escherichia coli guanine insertion enzyme*. PNAS, 1978. **75**(9): p. 4247-4251.
18. White, B.N., Tener, G.M., *Activity of a transfer RNA modifying enzyme during the development of Drosophila and its relationship to the su(s) Locus*. Journal of Molecular Biology, 1973. **74**(4): p. 635-651.
19. Reuter, K., Fichner, F, *Sequence Analysis and Overexpression of the Zymomonas mobilis tgt Gene Encoding tRNA-Guanine Transglycosylase: Purification and Biochemical Characterization of the Enzyme*. Journal of Bacteriology, 1995. **177**(18): p. 5284-5288.
20. Huang, B., R. Wu, and K. Chien, *Relationship of the queuine content of transfer ribonucleic acids to histopathological grading and survival in human lung cancer*. Cancer Res, 1992. **52**(17): p. 4696-4700.
21. Baranowski, W., et al., *Deficiency of queuine, a highly modified purine base, in transfer RNAs from primary and metastatic ovarian malignant tumors in women*. Cancer Res., 1994. **54**(16): p. 4468-4471.
22. Reuter, K. and F. Fichner, *Sequence analysis and overexpression of Zymomonas mobilis tgt gene encoding tRNA-guanine transglycosylase: purification and biochemical characterization of the enzyme*. J. Bacteriol., 1995. **177**(18): p. 5284-5288.
23. Langgut, W. and H. Kersten, *The deazaguanine-derivative, queuine, affects cell proliferation, protein phosphorylation and the expression of the proto oncogenes c-fos and c-myc in HeLa cells*. FEBS Letters, 1990. **265**(1-2): p. 33-36.
24. Langgut, W., et al., *Modulation of mammalian cell proliferation by a modified tRNA base of bacterial origin*. FEBS Letters, 1993. **336**(1): p. 137-142.
25. Reisser, T., W. Langgut, and H. Kersten, *The nutrient factor queuine protects HeLa cells from hypoxic stress and improves metabolic adaption to oxygen availability*. Eur. J. Biochem., 1994. **221**: p. 979-986.
26. Reisser T., Eicher A., and Langgut W., *Mitogenic stimulation of HeLa cells increases the activity of the anoxic stress protein, LDH 6/k: suppression by queuine*. Biochemical and Biophysical Research Communications, 1993. **197**(3): p. 1319-1325.
27. Kuchino, Y., et al., *Biosynthesis of the modified nucleoside Q in transfer RNA*. Nucl. Acids Res., 1976. **3**(2): p. 393-398.
28. Reader, J.S., et al., *Identification of four genes necessary for biosynthesis of the modified nucleoside queuosine*. J. Biol. Chem., 2004. **279**(8): p. 6280-6285.
29. Bai, Y., et al., *Hypermethylation of tRNA in thermophilic archaea. Cloning, overexpression, and characterization of tRNA-guanine transglycosylase from Methanococcus jannaschii*. J. Biol. Chem., 2000. **275**(37): p. 28731-28738.

30. Watanabe, M., et al., *Biosynthesis of archaeosine, a novel derivative of 7-deazaguanosine specific to archaeal tRNA, proceeds via a pathway involving base replacement on the tRNA polynucleotide chain.* J. Biol. Chem., 1997. **272**(32): p. 20146-20151.
31. Okada, N. and S. Nishimura, *Isolation and characterization of a guanine insertion enzyme, a specific tRNA transglycosylase, from Escherichia coli.* J. Biol. Chem., 1979. **254**(8): p. 3061-3066.
32. Slany, R.K., M. Bosl, and H. Kersten, *Transfer and isomerization of the ribose moiety of AdoMet during the biosynthesis of queuosine tRNAs, a new unique reaction catalyzed by the QueA protein from Escherichia coli.* Biochimie, 1994. **76**(5): p. 389-393.
33. Slany, R.K., et al., *A new function of S-adenosylmethionine: The ribosyl moiety of AdoMet is the precursor of the cyclopentenediol moiety of the tRNA wobble base queuine.* Biochemistry, 1993. **32**(30): p. 7811-7817.
34. Frey, B., McCloskey, J., Kersten, W., Kersten, H., *New Function of Vitamin B₁₂: Cobamide-Dependent Reduction of Epoxyqueuosine in tRNAs of Escherichia coli and Salmonella typhimurium.* Journal of Bacteriology, 1988. **170**(5): p. 2078-2082.
35. Gunduz, U., and Katze, J.R., *Queuine Salvage in Mammalian Cells; Evidence that Queuine is Generated from Queuosine 5'-Phosphate.* The Journal of Biological Chemistry, 1984. **259**(2): p. 1110-1113.
36. Shindo-Okada, N., et al., *Transfer ribonucleic acid guanine transglycosylase isolated from rat liver.* Biochemistry, 1980. **19**(2): p. 395-400.
37. Costa, A., et al., *Determination of queuosine derivatives by reverse-phase liquid chromatography for the hypomodification study of Q-bearing tRNAs from various mammal liver cells.* Journal of Chromatography B, 2004. **801**(2): p. 237-247.
38. Blaise, M., et al., *A minimalist glutamyl-tRNA synthetase dedicated to aminoacylation of the tRNA^{Asp} QUC anticodon.* Nucl. Acids Res., 2004. **32**(9): p. 2768-2775.
39. Frey, P.A., *S-Adenosylmethionine: A Wolf in sheep's clothing, or a rich man's adenosylcobalamin?* Chem. Rev., 2003. **103**: p. 2129-2148.
40. Tabor, C.W. and H. Tabor, *Polyamines.* Annual Review of Biochemistry, 1984. **53**(1): p. 749-790.
41. Lu, S.C., *S-Adenosylmethionine.* The International Journal of Biochemistry & Cell Biology, 2000. **32**: p. 391-395.
42. Frey, P.A., *Radical mechanisms of enzyme catalysis.* Annual Review of Biochemistry, 2001. **70**(1): p. 121-148.
43. Van Lanen, S.G. and D. Iwata-Reuyl, *Kinetic mechanism of the tRNA-modifying enzyme S-adenosylmethionine:tRNA ribosyltransferase-isomerase (QueA).* Biochemistry, 2003. **42**(18): p. 5312-5320.
44. Kinzie, S.D., Thern, B., Iwata-Reuyl, D., *Mechanistic Studies of the tRNA-Modifying Enzyme QueA: A Chemical Imperative from the Use of AdoMet as a Ribosyl Donor.* Organic Letters, 2000. **2**(9): p. 1307-1310.

45. Krumdieck, C.L., E. Shaw, and C.M. Baugh, *The Biosynthesis of 2-Amino-4-hydroxy-6-substituted Pteridines. The origin of carbon atoms 6, 7, and 9 of folic acid.* J. Biol. Chem., 1966. **241**(2): p. 383-387.
46. Uematsu, T. and R.J. Suhadolnik, *Nucleoside antibiotics VI. Biosynthesis of the pyrrolopyrimidine nucleoside antibiotic toyocamycin by Streptomyces rimosus.* Biochemistry, 1970. **9**: p. 1260-1266.
47. Suhadolnik, R.J. and T. Uematsu, *Biosynthesis of the pyrrolopyrimidine nucleoside antibiotic, toyocamycin. VII. Origin of the pyrrole carbons and the cyano carbon.* J. Biol. Chem., 1970. **245**(17): p. 4365-4371.
48. Smulson, M.E. and R.J. Suhadolnik, *The Biosynthesis of the 7-deazaadenine ribonucleoside, tubercidin, by Streptomyces tubercidicus.* J. Biol. Chem., 1967. **242**(12): p. 2872-2876.
49. Graham, D.E., H. Xu, and R.H. White, *A Member of a new class of GTP cyclohydrolase produces formylaminopyrimidine nucleotide Monophosphate.* Biochemistry, 2002. **41**: p. 15074-15084.
50. Foor, F. and G.M. Brown, *Purification and properties of guanosine triphosphate cyclohydrolase II from Escherichia coli.* J. Biol. Chem., 1975. **250**(9): p. 3545-3551.
51. Burg, A.W. and G.M. Brown, *The Biosynthesis of folic acid.* J. Biol. Chem., 1968. **243**(9): p. 2349-2358.
52. Nar, H., et al., *Active site topology and reaction mechanism of GTP cyclohydrolase I.* PNAS, 1995. **92**: p. 12120-12125.
53. Schramek, N., et al., *Reaction mechanism of GTP cyclohydrolase I: single turnover experiments using a kinetically competent reaction intermediate.* Journal of Molecular Biology, 2002. **316**(3): p. 829-837.
54. Slany, R.K. and H. Kersten, *Genes, enzymes and coenzymes of queuosine biosynthesis in procaryotes.* Biochimie, 1994. **76**(12): p. 1178-1182.
55. Ki W. Cha, W.P., Jeongbin J. Yim, *Pteridines. Part CVI. Isolation and characterization of limipterin (1-O-(2'-L-erythro-biopterin-2'-yl)-N-acetylglucosamine) and its 5,6,7,8-tetrahydro derivative from green sulfur bacterium Chlorobium limicola f. thiosulfatophilum NCIB 8327.* Helvetica Chimica Acta, 1995. **78**(3): p. 600-614.
56. Chung, H.J., et al., *Purification and characterization of UDP-glucose:tetrahydrobiopterin glucosyltransferase from Synechococcus sp. PCC 7942.* Biochimica et Biophysica Acta, 2000. **1524**(2-3): p. 183-188.
57. Cho, S.-H., et al., *Tepidopterin, 1-O-(3-threo-biopterin-2'-yl)-[beta]-N-acetylglucosamine from Chlorobium tepidum.* Biochimica et Biophysica Acta, 1998. **1379**(1): p. 53-60.
58. Nar, H., et al., *Atomic structure of GTP cyclohydrolase I.* Structure, 1995. **3**(5): p. 459-466.
59. Bracher, A., et al., *Histidine 179 Mutants of GTP cyclohydrolase I catalyze the formation of 2-Amino-5-formylamino-6-ribofuranosylamino-4(3H)-pyrimidinone triphosphate.* J. Biol. Chem., 1999. **274**(24): p. 16727-16735.

60. Bracher, A., N. Schramek, and A. Bacher, *Biosynthesis of pteridines. Stopped-flow kinetic analysis of GTP cyclohydrolase I*. *Biochemistry*, 2001. **40**(26): p. 7896-7902.
61. Auerbach, G., et al., *Zinc plays a key role in human and bacterial GTP cyclohydrolase I*. *PNAS*, 2000. **97**(13567-13572).
62. Nichol, C.A., G.K. Smith, and D.S. Duch, *Biosynthesis and metabolism of tetrahydrobiopterin and molybdopterin*. *Annual Review of Biochemistry*, 1985. **54**(1): p. 729-764.
63. Howell, D. and R. White, *D-erythro-neopterin biosynthesis in the methanogenic archaea Methanococcus thermophila and Methanobacterium thermoautotrophicum ΔH* . *J. Bacteriol.*, 1997. **179**(16): p. 5165-5170.
64. Lucock, M., *Folic acid: biochemistry, molecular biology and role in disease processes*. *Molecular Genetics and Metabolism*, 2000. **71**(1-2): p. 121-138.
65. Achari, A., et al., *Crystal structure of the anti-bacterial sulfonamide drug target dihydropteroate synthase*. *Nat. Struct. Mol. Biol.*, 1997. **4**(6): p. 490-497.
66. Chio, L., et al., *Identification of a class of sulfonamides highly active against dihydropteroate synthase from Toxoplasma gondii, Pneumocystis carinii, and Mycobacterium avium*. *Antimicrob. Agents Chemother.*, 1996. **40**(3): p. 727-733.
67. Hughes, W. and J. Killmar, *Monodrug efficacies of sulfonamides in prophylaxis for Pneumocystis carinii pneumonia*. *Antimicrob. Agents Chemother.*, 1996. **40**(4): p. 962-965.
68. Klaus, S.M.J., et al., *A Nudix enzyme removes pyrophosphate from dihydroneopterin triphosphate in the folate synthesis pathway of bacteria and plants*. *J. Biol. Chem.*, 2005. **280**(7): p. 5274-5280.
69. De Saizieu, A., P. Vankan, and A. Van Loon, *Enzymatic characterization of Bacillus subtilis GTP cyclohydrolase I. Evidence for a chemical dephosphorylation of dihydroneopterin triphosphate*. *Biochem. J.*, 1995. **306**: p. 371-377.
70. Known, N.S., C.F. Nathan, and D.J. Stuehr, *Reduced biopterin as a cofactor in the generation of nitrogen oxides by Murine Macrophages*. *J. Biol. Chem.*, 1989. **264**: p. 20469-20501.
71. Kaufman, S., et al., *Dependence of alkyl glycerol-ether monooxygenase activity upon tetrahydropterins*. *Biochimica et Biophysica Acta*, 1990. **1040**: p. 19-27.
72. Duch, D.S. and G.K. Smith, *Biosynthesis and function of tetrahydrobiopterin*. *Journal of Nutr. Biochem.*, 1991. **2**: p. 441-423.
73. Kaufman, S., *Metabolism of the phenylalanine hydroxylation cofactor*. *J. Biol. Chem.*, 1967. **242**(17): p. 3934-3943.
74. Takikawa, S.I., et al., *Biosynthesis of tetrahydrobiopterin. Purification and characterization of 6-pyruvoyl-tertrahydropterin synthase from human liver*. *Eur. J. Biochem.*, 1986. **161**(2): p. 295-302.

75. Thony, B., Gunter, A., Blau, N., *Tetrahydrobiopterin biosynthesis, regeneration and functions*. *Biochem. J.*, 2000. **347**: p. 1-16.
76. Skold, O., *Sulfonamide resistance: Mechanisms and trends*. *Drug Resistance Updates*, 2000. **3**(3): p. 155-160.
77. Doublie, S., *Preparation of selenomethionyl proteins for phase determination*. *Methods Enzymology*, 1997. **276**: p. 523-530.
78. Van Lanen, S.G., et al., *tRNA modification by S-adenosylmethionine:tRNA ribosyltransferase-isomerase. Assay development and characterization of the recombinant enzyme*. *J. Biol. Chem.*, 2003. **278**(12): p. 10491-10499.
79. Chomczynski, P., Sacchi, N., *Single-step method of RNA isolation by acid guanidinium thiocyanate-phenol-chloroform extraction*. *Analytical Biochemistry*, 1987. **162**(1): p. 156-159.
80. Nishimura, S., *Purification of methionine, valine, phenylalanine and tyrosine specific tRNA from Escherichia coli*. *Biochimica Et Biophysica Acta*, 1967. **142**(1): p. 133-148.
81. Nishimura, S., et al., *Purification of methionine-, valine-, phenylalanine-, and tyrosine- specific tRNA from Escherichia coli*. *Biochimica et Biophysica Acta*, 1967. **142**(1): p. 133-148.
82. Gillam, I., et al., *The Separation of soluble ribonucleic acids on benzoylated dithylaminoethylcellulose*. *Biochemistry*, 1967. **6**(10): p. 3043-3056.
83. Thompson, J.A., et al., *Purification of nucleic acids by RPC-5 analog chromatography: peristaltic and gravity-flow applications*. *Methods Enzymology*, 1983. **100**: p. 368-399.
84. Tanner, N.K., *Purifying RNA by column chromatography*. *Methods Enzymology*, 1989. **180**: p. 25-41.
85. Alfonzo, J.D., A. Sahota, and M.W. Taylor, *Purification and characterization of adenine phosphoribosyltransferase from Saccharomyces cerevisiae*. *Biochimica et Biophysica Acta*, 1997. **1341**(2): p. 173-182.
86. Alfonzo, J.D., et al., *APT1, but not APT2, codes for a functional adenine phosphoribosyltransferase in Saccharomyces cerevisiae*. *J. Bacteriol.*, 1999. **181**(1): p. 347-352.
87. Hochstadt, J., *Adenine phosphoribosyltransferase from Escherichia coli*. *Methods in Enzymology*, 1978. **51**: p. 558-567.
88. Braven, J., et al., *A Spectrophotometric assay of phosphoribosyl pyrophosphate pyntetase*. *Annals of Clinical Biochemistry*, 1984. **21**(Pt 5): p. 366-71.
89. LoBrutto, R., *5'-Deoxyadenosine contacts the substrate radical intermediate in the active site of ethanolamine ammonia-Lyase*. *Biochemistry*, 2001. **40**(1): p. 9-14.
90. Parkin, D., H. Leung, and V. Schramm, *Synthesis of nucleotides with specific radiolabels in ribose. Primary ¹⁴C and secondary ³H kinetic isotope effects on acid-catalyzed glycosidic bond hydrolysis of AMP, dAMP, and inosine*. *J. Biol. Chem.*, 1984. **259**(15): p. 9411-9417.

91. Markham, G.D., et al., *S-Adenosylmethionine synthetase from Escherichia coli*. J. Biol. Chem., 1980. **255**(19): p. 9082-9092.
92. Graham, D.E., Bocks, C.L., Schalk-Hihi, C., Lu, Z.J., Markham, G.D., *Identification of a Highly Diverged Class of S-Adenosylmethionine Synthetases in the Archaea*. The Journal of Biological Chemistry, 2000. **275**(6): p. 4055-4059.
93. Park, J., Tai, J., Roessner, C.A., Scott, I.A., *Enzymatic Synthesis of S-Adenosyl-L-Methionine on the Preparative Scale*. Bioorganic & Medicinal Chemistry, 1996. **4**(12): p. 2179-2185.
94. Iwig, D.F. and S.J. Booker, *Insight into the polar reactivity of the onium chalcogen analogues of S-adenosyl-L-methionine*. Biochemistry, 2004. **43**: p. 13496-13509.
95. Lu, Z.J. and G.D. Markham, *Enzymatic properties of S-adenosylmethionine synthetase from the archaeon Methanococcus jannaschii*. J. Biol. Chem., 2002. **277**(19): p. 16624-16631.
96. Graham, D.E., et al., *Identification of a highly diverged class of S-adenosylmethionine synthetases in the archaea*. J. Biol. Chem., 2000. **275**(6): p. 4055-4059.
97. Shapiro, S.K., and Mather, A. N., *The Enzymatic Decomposition of S-Adenosyl-L-Methionine*. The Journal of Biological Chemistry, 1958. **233**(3): p. 631-633.
98. Craig SP, I., et al., *High level expression in Escherichia coli of soluble, enzymatically active schistosomal hypoxanthine/guanine phosphoribosyltransferase and trypanosomal ornithine decarboxylase*. PNAS, 1991. **88**(6): p. 2500-2504.
99. Allen, T.E. and B. Ullman, *Cloning and expression of the hypoxanthine-guanine phosphoribosyltransferase gene from Trypanosoma brucei*. Nucl. Acids Res., 1993. **21**(23): p. 5431-5438.
100. Allen, T.E. and B. Ullman, *Molecular characterization and overexpression of the hypoxanthine-guanine phosphoribosyltransferase gene from Trypanosoma cruzi*. Molecular and Biochemical Parasitology, 1994. **65**(2): p. 233-245.
101. Jardim, A. and B. Ullman, *The conserved serine-tyrosine dipeptide in Leishmania donovani hypoxanthine-guanine phosphoribosyltransferase Is essential for catalytic activity*. J. Biol. Chem., 1997. **272**(14): p. 8967-8973.
102. Gill, S.C. and P.H. von Hippel, *Calculation of protein extinction coefficients from amino acid sequence data*. Analytical Biochemistry, 1989. **182**(2): p. 319-326.
103. Ferre, J., *Purification of guanosine triphosphate cyclohydrolase I from Escherichia coli*. Journal of Chromatography, 1986. **357**: p. 283-292.
104. Pfleiderer, W., *Chemistry of naturally occurring pterins*, in *Folates and Pterins*, R.L. Blakley, Benkovic, S.J., Editor. 1985, John Wiley & Sons, Inc: New York. p. 43-114.

105. Yim, J.J. and G.M. Brown, *Characteristics of guanosine triphosphate cyclohydrolase I purified from Escherichia coli*. J. Biol. Chem., 1976. **251**(16): p. 5087-5094.
106. Fish, W., *Rapid colorimetric micro-method for the quantitation of complexed iron in biological samples*. Methods in Enzymology, 1988. **158**: p. 357-364.
107. Percival, M., *Human 5-lipoxygenase contains an essential iron*. J. Biol. Chem., 1991. **266**(16): p. 10058-10061.
108. Burg, A.W. and G.M. Brown, *The biosynthesis of folic acid. VIII. Purification and properties of the enzyme that catalyzes the production of formate from carbon atom 8 of guanosine triphosphate*. J. Biol. Chem., 1968. **243**(9): p. 2349-2358.
109. Chomczynski, P. and N. Sacchi, *Single-step method of RNA isolation by acid guanidinium thiocyanate-phenol-chloroform extraction*. Analytical Biochemistry, 1987. **162**(1): p. 156-159.
110. Parkin, D.W., Leung, H.B., Schramm, V.L., *Synthesis of Nucleotides with Specific Radiolabels in Ribose. Primary 14C and Secondary 3H Kinetic Isotope Effects on Acid-Catalyzed Glycosidic Bond Hydrolysis of AMP, dAMP and Inosine*. Journal of Biological Chemistry, 1984. **259**(15): p. 9411-9417.
111. Shapiro, S.K. and A.N. Mather, *The enzymatic decomposition of S-adenosyl-L-methionine*. J. Biol. Chem., 1958. **233**(3): p. 631-633.
112. Basset, G., et al., *Folate synthesis in plants: The first step of the pterin branch is mediated by a unique bimodular GTP cyclohydrolase I*. PNAS, 2002. **99**(19): p. 12489-12494.
113. Cone, J. and G. Guroff, *Partial purification and properties of guanosine triphosphate cyclohydrolase, the first enzyme in pteridine biosynthesis, from Comamonas sp. (ATCC 11299a)*. J. Biol. Chem., 1971. **246**(4): p. 979-985.
114. Plowman, J., J.E. Cone, and G. Guroff, *Identification of d-erythro-dihydroneopterin triphosphate, the first product of pteridine biosynthesis in Comamonas Sp. (ATCC 11299a)*. J. Biol. Chem., 1974. **249**(17): p. 5559-5564.
115. Iwig, D.F., et al., *Isotope and elemental effects indicate a rate-limiting methyl transfer as the initial step in the reaction catalyzed by Escherichia coli cyclopropane fatty acid synthase*. Biochemistry, 2004. **43**: p. 13510-13524.
116. Walsh, C., *Enzymatic Reaction Mechanisms*, ed. W.H. Freeman. 1979, New York: W.H. Freeman.
117. Versees, W., et al., *Enzyme-substrate Interactions in the purine-specific nucleoside hydrolase from Trypanosoma vivax*. J. Biol. Chem., 2002. **277**(18): p. 15938-15946.
118. Gordon, R.K., et al., *Anti-HIV-1 Activity of 3-deaza-adenosine Analogs; Inhibition of S-adenosylhomocysteine hydrolase and nucleotide congeners*. Eur. J. Biochem., 2003. **270**(17): p. 3507-3516.
119. Backlund, P.S., D. Carotti, and G.L. Cantoni, *Effects of the S-adenosylhomocysteine hydrolase inhibitors 3-deazaadenosine and 3-deazaaristeromycin on RNA methylation and synthesis*. Eur. J. Biochem., 1986. **160**(2): p. 245-251.

120. Parkin, D., et al., *Nucleoside hydrolase from Crithidia fasciculata. Metabolic role, purification, specificity, and kinetic mechanism.* J. Biol. Chem., 1991. **266**(31): p. 20658-20665.
121. Estupinan, B. and V. Schramm, *Guanosine-inosine-preferring nucleoside N-glycohydrolase from Crithidia fasciculata.* J. Biol. Chem., 1994. **269**(37): p. 23068-23073.
122. Katze, J.R., Simonian, M.H., Mosteller, R.D., *Role of Methionine in the Synthesis of Nucleoside Q in Escherichia coli Transfer Ribonucleic acid.* Journal of Bacteriology, 1977. **132**(1): p. 174-179.
123. El Yacoubi, B., et al., *Discovery of a new prokaryotic type I GTP cyclohydrolase family.* J. Biol. Chem., 2006. **281**(49): p. 37586-37593.
124. Switchenko, A.C., J.P. Primus, and G.M. Brown, *Intermediates in the enzymic synthesis of tetrahydrobiopterin in Drosophila melanogaster.* Biochemical and Biophysical Research Communications, 1984. **120**(3): p. 754-760.
125. Grochowski, L.L., et al., *Characterization of an Fe²⁺-Dependent Archaeal-Specific GTP Cyclohydrolase, MptA, from Methanocaldococcus jannaschii.* Biochemistry, 2007. **46**(22): p. 6658-6667.
126. Kobashi, M. and K. Iwai, *Isolation and characterization of cyclic phosphate of neopterin and other 6-alkylpterin compounds enzymatically synthesized from GTP by cell free extracts of Serratia indica.* Agr. Biol. Chem, 1972. **36**: p. 1685.
127. Nathalie Colloc'h, A.P., Jean-Paul Mornon,, *Sequence and structural features of the T-fold, an original tunnelling building unit.* Proteins: Structure, Function, and Genetics, 2000. **39**(2): p. 142-154.
128. Maier, J., et al., *Homology cloning of GTP-cyclohydrolase-I from various unrelated eukaryotes by reverse-transcription polymerase chain-reaction using a general set of degenerate primers.* Biochemical and Biophysical Research Communications, 1995. **212**(2): p. 705-711.
129. Van Lanen, S.G., et al., *From cyclohydrolase to oxidoreductase: Discovery of nitrile reductase activity in a common fold.* PNAS, 2005. **102**(12): p. 4264-4269.
130. Lee, S., et al., *Biochemical characterization of oligomerization of Escherichia coli GTP cyclohydrolase I.* Journal of Biochemistry and Molecular Biology, 2002. **35**(3): p. 255-261.
131. Boyd, J.M., H. Ellsworth, and S.A. Ensign, *Bacterial acetone carboxylase Is a manganese-dependent metalloenzyme.* J. Biol. Chem., 2004. **279**(45): p. 46644-46651.
132. Crowley, J.D., D.A. Traynor, and D.C. Weatherurn, *Enzymes and proteins containing manganese: An overview,* in *Metals ions in biological systems: manganese and its role in biological processes*, A.a.S. Sigel, H., Editor. 2000, Marcel Dekker: New York. p. 209-277.
133. Bock, C.W., et al., *Manganese as a replacement for magnesium and zinc: Functional comparison of the divalent ions.* J. Am. Chem. Soc., 1999. **121**(32): p. 7360-7372.

134. Wilkins, P.C., and Wilkins, R.G., *Inorganic Chemistry in Biology*. Oxford Chemistry Primers, ed. J. Evans. 1997, New York: Oxford University Press.
135. Bock, C.W., et al., *Manganese as a replacement for magnesium and zinc: Functional comparison of the divalent Ions*. J. Am. Chem. Soc., 1999. **121**: p. 7360-7372.
136. Tanaka, Y., et al., *Novel reaction mechanism of GTP cyclohydrolase I. high-resolution X-Ray crystallography of Thermus thermophilus HB8 enzyme complexed with a transition state analogue, the 8-oxoguanine derivative*. J. Biochem. (Tokyo), 2005. **138**(3): p. 263-275.
137. Culp, S.J., et al., Structural and conformational analyses of 8-hydroxy-2'-deoxyguanosine. Chem. Res. Toxicol., 1989. 2(6): p. 416-422.
138. Iwata-Reuyl, D., Biosynthesis of the 7-deazaguanosine hypermodified nucleosides of transfer RNA. Bioorganic Chemistry, 2003. 31(1): p. 24-43.
139. Colloc'h, N., A. Poupon, and J.-P. Mornon, Sequence and structural features of the T-fold, an original tunnelling building unit. Proteins: Structure, Function, and Genetics, 2000. 39(2): p. 142-154.

Appendix A. Plasmids and Proteins

Plasmid	<i>E. coli</i> Expression Cell Line	Expression Product
pGEX-QA	DH5 α	<i>E. coli</i> GST-QueA
pET30-EcqueA	BL21(DE3)	<i>E. coli</i> His ₆ -QueA
pQEAPTI	DH5 α	<i>E. coli</i> APRTase
pK8	DH5 α	<i>E. coli</i> MAT
pMJ1208	BL21(DE3)	<i>M. jannaschii</i> MAT
pBRS11R	DH5 α	<i>S. typhimurium</i> PRPP synthetase
pTRC99B-Tyr	K12QueA	<i>E. coli</i> tRNA ^{Tyr} specific I
pBAC-HGPRTase-LD	SØS6	<i>L. donovani</i> HGPRTase
pET30-EcribA	BL21(DE3)	<i>E. coli</i> His ₆ -RibA
pET30-EcfolE	BL21(DE3)	<i>E. coli</i> His ₆ -FolE
pET30-BsfolE2	BL21(DE3)	<i>B. subtilis</i> His ₆ -FolE2
pET30-NgfolE2	BL21(DE3)	<i>N. gonorrhoeae</i> His ₆ -FolE2
pET30-TmfolE2	BL21(DE3)	<i>T. maritima</i> His ₆ -FolE2

Appendix B. Primer sequences

Sequence Name	Sequence (5'→3')
Bs-foIE2-s	GGTATTGAGGGTCGCATGAATCAACATACGCTGCTCCCG
Bs-foIE2-as	AGAGGAGAGTTAGAGCCTCATATTTTATCCAC
Ng-foIE2-s	GGTATTGAGGGTCGCATGAACGCCATTGCAG
Ng-foIE2-as	AGAGGAGAGTTAGAGCCCTACGGGTAGGCGATATAG
Tm-foIE2-s	GGTATTGAGGGTCGCTTGAAGGATGTTCAGAAC
Tm-foIE2-as	AGAGGAGAGTTAGAGCCTCATCCCTCCAGAACG
Ng-foIE2-H245K-s	CGAGTCTATCAAGAACCATTCCGG
Ng-foIE2-H245K-as	GCTCAGATAGTTCTTGGTAAGCC
Ng-foIE2-H245N-s	CGAGTCTATCCAGAACCATTCCGG
Ng-foIE2-H245N-as	GCTCAGATAGTTGTTGGTAAGCC
Ng-foIE2-H245Q-s	CGAGTCTATCCAGAACCATTCCGG
Ng-foIE2-H245Q-as	GCTCAGATAGGTCTTGGTAAGCC
Ng-foIE2-H245D-s	CGAGTCTATCGCAACCATTCCGG
Ng-foIE2-H245D-as	GCTCAGATAGCTGTTGGTAAGCC

Appendix C. Buffer designation and components

Buffer Designation	Components
A	50 mM Tris-Acetate (pH 8.0), 100 mM KCl, 2 mM CaCl ₂
B	20 mM sodium acetate (pH 4.5), 10 mM MgCl ₂ , 0.5 M NaCl
C	Buffer B + 1M NaCl
D	10 mM sodium acetate (pH 4.5), 10 mM MgCl ₂ , 0.2 M NaCl
E	100 mM Tris-HCl (pH 7.5), 300 mM KCl, 2 mM β -mercaptoethanol, 1% Triton X-100, 1 mM PMSF, 10% glycerol
F	Buffer E + 20 mM imidazole
G	Buffer F without Triton X-100 and PMSF
H	Buffer G + 200 mM imidazole
I	50 mM Tris-HCl (pH 8.0), 1 mM PMSF, 1 mM DTT, 0.5 mM EDTA
J	Buffer I + 10% glycerol
K	50 mM Tris-HCl (pH 7.8), 100 mM KCl, 10 mM MgCl ₂ , 1 mM PMSF, 2 mM DTT, 10% glycerol
L	Buffer K + 1% Triton X-100, 2 mM PMSF
M	Buffer K + 2 mM PMSF
N	Buffer K + 2 mM PMSF and 20 mM reduced glutathione
O	20 mM Tris-HCl (pH 8.0), 10 mM MgCl ₂ , 2 mM DTT, 10% glycerol
P	200 mM Tris-Acetate (pH 8.0), 1.2 M KCl, 8 mM β -mercaptoethanol, 4 mM PMSF and 40% glycerol
Q	100 mM Tris-Acetate (pH 8.0), 300 mM KCl, 2 mM β -mercaptoethanol, 1% Triton X-100, 1 mM PMSF, 10% glycerol
R	Buffer Q + 20 mM imidazole
S	Buffer R without Triton X-100 and PMSF
T	Buffer S + 250 mM imidazole
U	100 mM gly-gly (pH 8.7), 100 mM EDTA (pH 8.7), 100 mM KCl, 0.5 mM DTT
V	50 mM Tris-HCl (pH 8.0), 100 mM EDTA (pH 8.0), 100 mM KCl and 0.5 mM DTT
W	100 mM Tris-HCl (pH 8.0) and 300 mM KCl
X	Buffer W + 250 mM imidazole
Y	50 mM Tris-HCl (pH 8.0), 50 mM KCl, 1 mM DTT